# Parametric study regarding the influence of preliminary design parameters of a long-span timber footbridge on the human-induced dynamic behaviour

Romée van Es | June 30, 2022

ARUP | TUDelft

# Parametric study regarding the influence of preliminary design parameters of a long-span timber footbridge on the human-induced dynamic behaviour

by

Romée van Es

to obtain the degree of

**Master of Science**

in Civil Engineering

at the Delft University of Technology

to be publicly defended on June 30, 2022 at 9:30

| | | |
|---|---|---|
| Student number | 4364805 | |
| Project duration | September 1, 2021 - June 30, 2022 | |
| | | |
| Thesis committee | Prof. dr. ir. J.G Rots | TU Delft, chair |
| | Dr. ir. E. Lourens | TU Delft |
| | Ir. M. P. Felicita | TU Delft |
| | Ir. F. de Meijier | Arup |
| | Ir. L.F.M. Koning | Arup |

# Preface

In front of you or on your screen is the product of the master thesis project I have worked on for the past months. Even though it was an individual project, I could not have accomplished this without the help of many great people. Therefore I would like to express my gratitude to those who have helped me during the process, with their expertise on the topic as well as helping me manage the ups and downs that come along with writing a master thesis.

First of all Laetitia and Felix. Owing to a miscommunication I was lucky enough to have you both as daily supervisors from Arup. Whereas the intention was that one of you would leave the train at some point, I am very happy this didn't happen. You were always there for me and your expertise, ideas and experience were of invaluable help. Thank you so much.

I would also like to thank Arup for giving me the opportunity do to this project. I have met many helpful people who readily answered my page-long lists of questions. Roel, Edwin, thank you for dedicating your time to explaining the design calculations of the Dafne Schippers bridge. Specifically I would like to thank Dirk, without your help I would still be figuring out how to make a node in gsapy and I would never have understood the code of the optimisation algorithm.

And then of course my family and friends. Mom, dad, I am grateful you always supported me in the sometimes drastic and study-prolonging decisions I have made. My dear housemates and Joep, thanks for enduring my short temper in some of the more stressful weeks and let me see the temporary hiccups in the project in a broader perspective. My friends at the faculty, the lunch breaks (preferably outside) with you were one of the main reasons I kept motivated till the end.

Last, but not least, I would like to thank the committee, Maria Felicita, Eliz-Mari Lourens and Jan Rots for your comments, input and questions during the meetings and for actually taking the time to read this thesis.

I hope you will enjoy.

*Romée van Es*
*Delft, June 2022*

# Summary

Dynamic behaviour often is a topic of concern in the design of long-span pedestrian bridges. It is time-consuming to assess and little is known about the way it is influenced by the characteristics of a bridge. In many cases, a bridge needs testing after is has been finished to determine the specifications of a damper.

Striving to reduce the environmental impact of bridges, there lies a great potential in using materials with a low environmental impact, such as timber. This research combined the lack of knowledge about dynamic behaviour of footbridges with the need for using timber instead of other materials.

It served two main goals. One was to increase knowledge about the influence of three preliminary design parameters on the human-induced dynamic behaviour of a long-span timber footbridge. The second was to investigate to what extent it is possible to design a long-span timber footbridge that does not need dampers to control excessive vibrations. With this, advice might be given to bridge designers on how to deal with dynamic behaviour in the early stage of a design process.

To limit the scope of the research, it was performed as a case study on the design brief of Dafne Schippers bridge. The span, the width, the loads and the serviceability requirements were used as boundary conditions for the new design in timber. This new design was based on a literature study summarising good design practice of timber footbridges, and reference projects, particularly the Älvsbacka bridge.

A parametric model for an early-stage design was developed, which was used to answer the two research goals. The python package *gsapy* was used to build a finite element (FE) model in the FE program GSA. The results from the static and dynamic analyses were processed using python.

The *parameter study* was used to study the first research goal, which was to investigate the influence of three early-stage design parameters on the human-induced dynamic behaviour of a long-span timber footbridge. These parameters, named *studied parameters*, were the height of the pylons, the shape of the pylons and the amount of cables. To improve the dynamic behaviour, in general an increase in the natural frequencies is desired, which can be accomplished by a higher stiffness to mass ratio. The parameters were selected since they were expected to influence this ratio. The pylon height was chosen because literature suggests it increases the vertical stiffness, without changing the vibrating mass, provided the dimensions of the deck are not adjusted based on the pylon height. The same applies to the relation between the pylon shape (A-, H- or V-shape, see figure 1) and the torsional stiffness. The number of cables was chosen since an increased number of cables can affect both the material use and stiffness of the bridge.
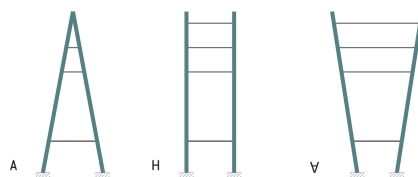


**Figure 1:** Pylon shapes, varying from A-shape to V-shape

The parameter study was done by varying the values of the studied parameters and subsequently examine the dynamic behaviour of the model. To be able to make a fair comparison between the variants, a mass optimisation was done in each step. It was chosen to optimise for mass because it is a measure for the amount of material, constant in time and straightforward to interpret.

The optimisation was done using the Artificial Bee Colony algorithm, which is beneficial for the type of problems where the evaluation of the objective function (to minimise the mass) is computationally cheap, while the evaluation of the behavioural constraints (create and analyse the model of a design variant) is not. The static verifications were done based on the relevant Eurocode norms and the

dynamic verifications were done using the method outlined in the JRC guideline for the assessment of human-induced vibrations. It consists of a modal analysis and an evaluation of the maximum acceleration.

The parametric model consists of four types of parameters. The three *studied parameters*, the pylon height, the pylon shape and the amount of cables were mentioned before. In the parameter study, they were varied in order to evaluate their effect on the dynamic behaviour.

The *optimisation parameters* are the values optimised in the optimisation process. The diameter of the cables, the section dimensions of the pylons, the height of the main beams and the height of the cross beams in the deck were chosen as optimisation parameters since they were expected to have the biggest influence on the mass and stiffness of the structure.

To limit the computation time, *dependent parameters* and *fixed values* were introduced. As the name suggests, dependent parameters depend on the values of the studied and optimisation parameters based on predefined rules, and the fixed values do not change during the optimisation process.

The parameter study gave insight into the way the dynamic behaviour is influenced by the characteristics of a bridge. To be able to explain the results, the effect of only changing the optimisation parameters and only changing the studied parameters (without the mass optimisation in each step) was examined. Interpreting the results, the $\psi$-factor is of importance, which reflects the critical range of frequencies for pedestrian loading. As a consequence of changing parameters, the natural frequencies of the governing mode change. When the $\psi$ becomes lower than 1, other modes can become governing which often causes a 'kink' in the results.

Increasing the pylon height has an increasing effect on the vertical accelerations, although the results did not show a clear correlation. The effect is mainly explained by the changing optimisation parameters. These also explain the increasing effect on the lateral accelerations.

Varying the shape of the pylons shows the highest vertical accelerations for a modest A-shape. This peak is explained by the changing governing modes. V-shaped pylons result in lower lateral accelerations than A-shaped pylons, explained by the way the deck rotates in the lateral vibration.

In general, increasing the amount of cables has an increasing effect on both the vertical and lateral accelerations, although the results do show some deviations from the trend. The effect can be explained by the changing optimisation parameters, because the accelerations decrease when cables are added without running optimisations in each step.

To give more insight in the results of the parameter study, a set of verification studies was performed. One outcome was that when investigating one studied parameter (e.g. the pylon shape), varying the other studied parameters (e.g. the pylon height and the amount of cables), can overrule the previously found effect. Another outcome was that the influence of changing the damping value or the traffic class has a bigger impact than varying the studied parameters. Lastly, the effect of the connection stiffness in the deck was examined. It was found that it only affects the vertical vibrations, changing the type of governing mode.

To research the second research goal, which was to examine to what extent it is possible to design a footbridge that does not need dampers to control excessive vibrations, two optimisation runs were carried out. In this optimisation study, the studied parameters (the pylon height, pylon shape and amount of cables) were treated as optimisation parameters. To be able to take into account dynamic behaviour in an automatic optimisation process, a python script was written to automatically determine the type of modes. This script consists of a set of if-statements that categorise the mode shapes based on the modal displacements.

In the model where dynamic behaviour was taken into account, a damping value of 1.2% was used, which was deemed the most realistic value based on literature, together traffic class 2 and comfort class 2, which were also deemed most realistic.

The optimisation study showed that for the case study, a design variant that does not need dampers can be obtained when an increase in mass is accepted. Compared to a standard model, where dynamic behaviour was not taken into account in the optimisation process, a 14% increase in mass was found. This additional mass is comprised of a 17% increase in timber and a 10 % increase in steel. Depending on the chosen damping value, traffic class and comfort class, these numbers are expected to vary.

Since the influence of changing a parameter depends on many factors, advice that is valid in all situations (e.g. always aim for higher pylons) can not be given for the early stage of a design process. When aiming to avoid the need of dampers, the design can be adjusted in a later stage in a way that the $\psi$-factors of the governing modes become lower than 1. Depending on the mode and frequency, this could imply trying to increase or decrease the frequency of the mode. As found in the optimisation study, the new design is likely to have a higher mass. However, the result will heavily depend on the damping value, the traffic class and the comfort requirements. The exact damping value will remain uncertain until the bridge has been built, which is why a conservative damping value would need to be assumed in the design. To be able to judge whether adding material to obtain a design without the need of dampers is a sensible option, a life cycle assessment and an investigation of the costs is advised.

# Contents

<div align="right">

# 1

</div>

# Introduction

## 1.1. Research context

The building industry is responsible for more than a quarter (26%) of the worldwide man-made greenhouse gas emissions. This number excludes transport of building materials, so one could argue that the percentage is actually even higher [51]. Striving to reduce emissions, there lies a great potential in using materials that have a smaller environmental impact than the ones that are commonly used. Most modern pedestrian bridges are made of concrete, steel, or a combination of the two. Studies have shown that applying timber instead of these materials significantly reduces the environmental impact.

A study by O'Born [36] involved a Life Cycle Assessment (LCA) of two variants of a 1650m long highway bridge in Norway. The first variant was entirely made of concrete. In the second, the superstructure was replaced by a timber truss. O'Born showed that the timber alternative had significantly lower emissions than the concrete alternative across the regarded categories. The total amount of $CO_2$ equivalent emissions of the two bridges is compared in figure 1.1.

Another study, carried out under guidance of Beco [21], compared the LCA of four pedestrian bridges, each with a different main construction material: one in concrete, one in steel, one in timber and one in composite. The study showed that the environmental impact of a timber footbridge is lower than the impact of bridges in other materials and that it even has a negative component in three of the effect categories. The outcome, split up per category, is shown in figure 1.2.

Whereas in terms of environmental impact, the use of timber has obvious benefits, it is often not yet the first choice in bridge design. Research about the behaviour of timber bridges might encourage the application of timber.
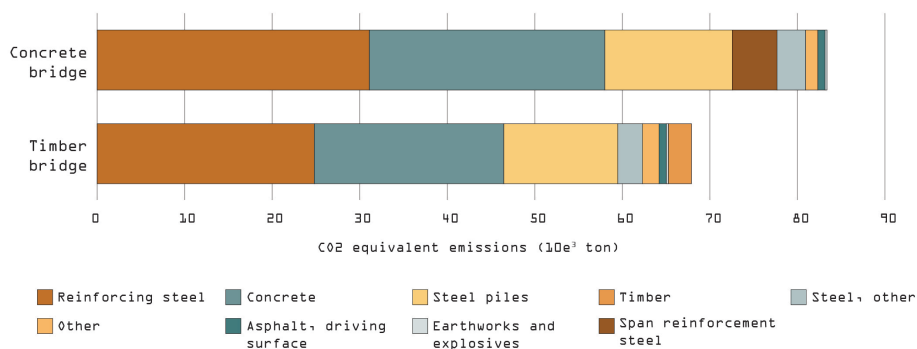


**Figure 1.1:** Contribution to the total amount of $CO_2$ equivalent emissions per bridge component, adjusted from [36]

Because of technical developments, there is a trend of bridges becoming more slender over the past years [42]. Slender structures tend to be more susceptible to vibrations because of their relatively low stiffness. This problem is extra pronounced in pedestrian bridges since they are subjected to harmonic loading. As a consequence they frequently require a more thorough dynamic analysis in order to ensure vibrations stay within acceptable limits. The dynamic behaviour of timber pedestrian bridges differs from concrete or steel pedestrian bridges because of the lower mass and stiffness and higher structural damping [23].

If the dynamic requirements cannot be fulfilled by the bridge itself, additional damping devices can be added. Although it should be taken into account in the design of the bridge, they are usually added
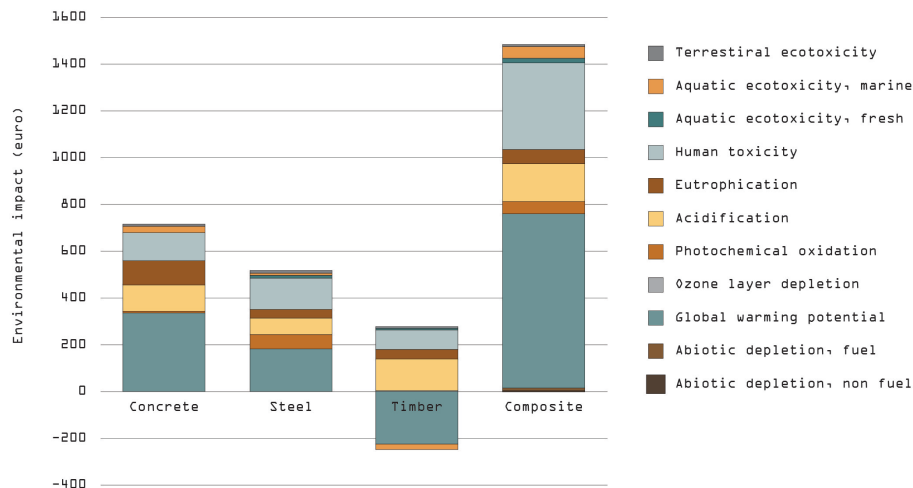
**Figure 1.2:** Environmental impact of four bridge designs, adjusted from [21]

after construction since they mostly have to be tuned to a specific frequency.

Some research has been done on human induced vibrations in timber footbridges, yet the amount is limited and the studies are carried out on specific bridges, without drawing more general conclusions. Examples are dynamic investigations of the timber Alvsbacka bridge [6, 25], the steel/timber footbridge in Pribor and timber bridge in Armentia [29]. These studies have investigated the natural frequencies, mode shapes and damping of the bridges. However, little is known about the effect of design parameters on the dynamic behaviour of a bridge.

## 1.2. Problem definition

The dynamic behaviour of a structure is quantified by the acceleration as a result of harmonic loading and is dependent on the mass, the stiffness and the structural damping. During the preliminary design phase, choices are made that might influence the dynamic properties of the system, such as the type of structure, the type of connections and the dimensions of the members. However, it is not known to what extent these choices influence the dynamic behaviour. In a design process, this could be determined by analysing different variants in a finite element software, but making a sufficiently accurate model is time consuming and often not feasible during the initial design phase. Studying the influence of initial design choices on the dynamic behaviour of timber pedestrian bridges can provide useful insight for structural designers to avoid problems with dynamic behaviour.

## 1.3. Research goals and question

This research serves two main goals. One is to increase knowledge about the influence of three preliminary design parameters on the dynamic behaviour of a long-span timber footbridge. The second is to investigate to what extent it is possible to design a long-span timber timber footbridge that does not need dampers to control excessive vibrations. The research goals lead to the following research question:

*What is the influence of preliminary design parameters on the human-induced dynamic behaviour of a long-span timber footbridge and to what extent is it possible to design a long-span timber footbridge that does not need dampers to control excessive vibrations?*

The choice for a long span was made because it was expected to be more interesting in terms of dynamic behaviour compared to a short span. The preliminary design parameters that are studied in this research are the height of the pylons, the shape of the pylons and the amount of cables. The motivation of this selection is set out in chapter 5.

## 1.4. Research approach

The research presented in this thesis consists of different parts, which are briefly described below.

**Literature review**

A literature review was carried out to make an overview about the state of the art in timber bridge design and to get informed about what is known regarding dynamic behaviour in pedestrian bridges. Since an optimisation was needed for a fair comparison between design variants, a literature study about a suitable optimisation method was done as well. The results of these studies are presented in chapter 2 to 4.

**Case study**

To narrow down the scope of the research, it was carried out as a case study on the design brief of the Dafne Schippers bridge (DSB). This bridge was chosen for several reasons. First of all, it has a span in the order of magnitude of the longest timber bridges, which was a requirement to answer the research question. Secondly, it is a cyclist/pedestrian bridge, which makes it fit for the intended research too. Lastly, the structural design of the bridge was done by Arup, so all documentation was available for reference.

The DSB, shown in figure 1.3, connects Leische Rijn with Oog in Al, crossing the Amsterdam Rijnkanaal near Utrecht. It is an asymmetrical suspension bridge with a span of 110m, two steel pylons and a concrete deck. As mentioned before, only the design brief of the bridge were be used to make a new design in timber. This means the main span, the width, the loads and the serviceability requirements were taken as boundary conditions for a new design in timber.



**Figure 1.3:** The Dafne Schippers bridge [49]

**Design and modelling and assessment**

A parametric model for an early-stage design was made in the programming language python linked with the finite element program GSA. The design and the parametric model, together with the assessment of the design variants are explained in chapter 5.

**Parameter study**

In this part of the research the influence of the three preliminary design parameters was researched by varying the values and subsequently examine the dynamic behaviour. To be able to make a fair comparison between each variant, a mass optimisation was done in each step. This process is described in chapter 6, the results are presented in chapter 7.

**Optimisation study**

In this last part of the research, an attempt was made to optimise the model taking into account dynamic behaviour in order to learn to what extent it is possible to avoid the need of dampers and examine the influence on the design of the bridge. This is described in chapter 8.

# 2

# Timber bridge design

In this chapter the most important aspects of timber bridge design are explained. It starts with the structural system, followed by wood products, durability, design choices and connections.

## 2.1. Structural system

There is a wide variety of structural systems for bridges, the most common ones being the suspension bridge, the cable-stayed bridge, the arch bridge, the truss bridge and the girder bridge. To get an idea of what is possible in timber bridge design, an overview with the spans of different types of timber bridges is presented in figure 2.1. Due to the amount of timber bridges a selection needed to be made, which was done based on the following considerations. There are at least three examples per type of structural system, per structural system there is a focus on the longest spans and mostly pedestrian bridges were included although there are some remarkable highway bridges.
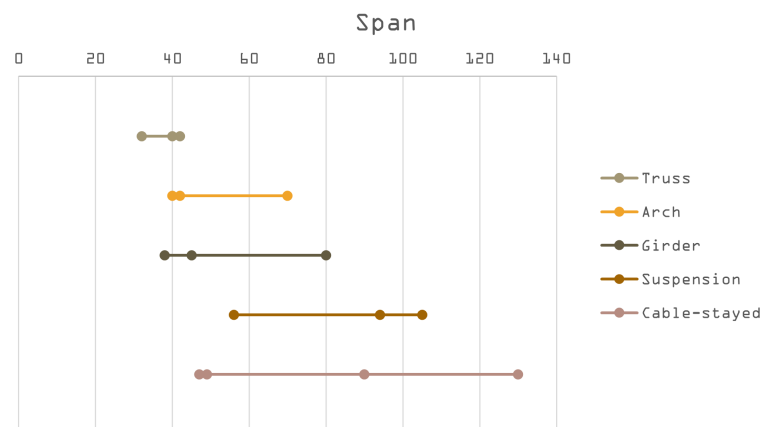


**Figure 2.1:** Overview bridge spans

In the figure it can be seen that there is a certain hierarchy in the type of structure used for increasing spans, although there is a considerable amount of overlap. For short spans, truss structures are used, in the order or increasing span followed by arch, girder, suspension and cable-stayed bridges. Yet drawing definite conclusions about the fitness of different types for specific spans is hard because it also depends on the use and whether or not timber is combined with other building materials. With a span of 130 m, the longest bridge fit for modern use is the cable-stayed Älvsbacka bridge in Sweden. Since the span of the case study is 110 m and since the bridge is also intended for cyclists and pedestrians, a cable-stayed structure was chosen for the case study. A suspension bridge was considered too, but since no recent examples of long-span timber suspension bridges were found and since a suspension bridge was thought to be less promising in terms of dynamics, the cable-stayed bridge was preferred over the suspension bridge. Therefore the rest of this literature review will focus on cable-stayed bridges.

For each type of bridge, an example is shown in figure 2.2. The complete overview including usage, span and construction year can be found in appendix A.1.

4
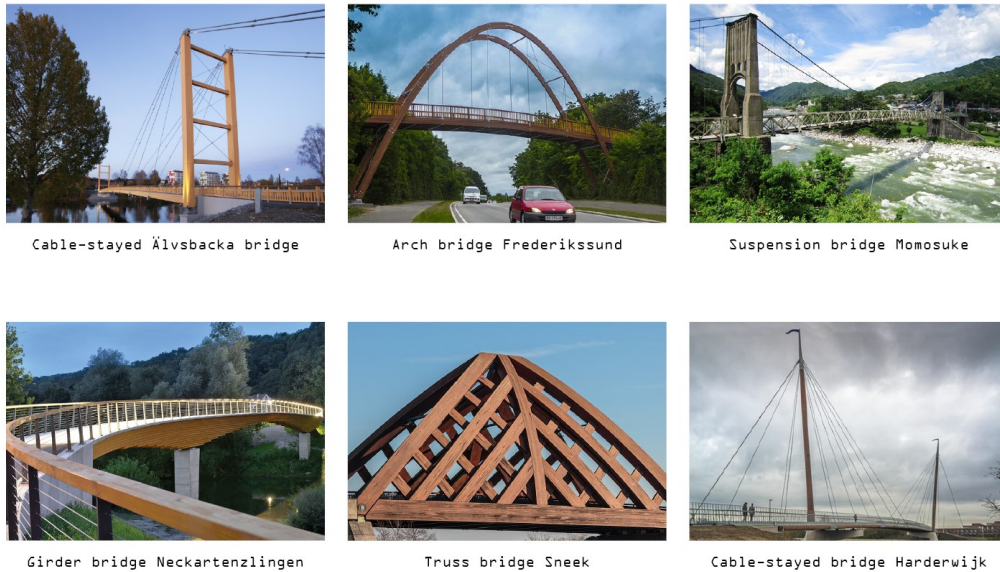
**Figure 2.2:** Examples of timber bridges [5, 56, 40, 45, 25, 30]

## 2.2. Wood products in timber footbridges

Wood products can be divided in traditional wood products and engineered wood products. Traditional wood products are solid members sawn from logs, whereas engineered wood products are man-made timber products optimised in terms of mechanical properties and material efficiency [51]. In structural applications they are replacing the use of solid timber because of the need for more homogeneous and high-performance properties. Generally, engineered wood products consist of layers of timber glued together in different ways. As a result, irregularities are spread, increasing the overall quality of an element. In addition, the direction of the grain can be adjusted in order to make it suitable for different load-bearing directions. There is a wide variety of engineered wood products, the ones relevant for timber bridges are shown in figure 2.3.
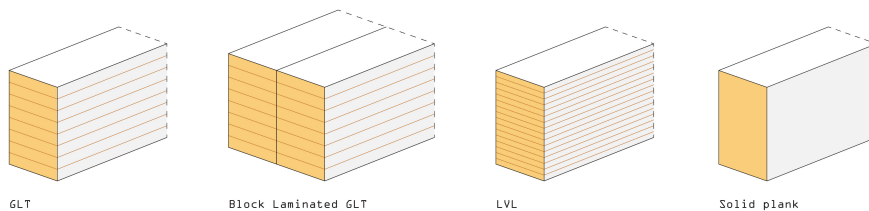


**Figure 2.3:** Timber products

Glue-laminated timber, commonly known as glulam or GLT, consists of timber parts of up to a few centimeters thickness glued together with all grains in longitudinal direction, resulting in a high strength in that direction. Therefore it is most often used for the main structural parts such as girders, crossbeams and pylons. Long elements can be obtained by finger-jointing individual pieces. The common wood species used for glulam are spruce, pine, fir and larch [51]. The width of regular glulam is limited by the width of raw timber. When greater widths are desired, this can be overcome by gluing timber pieces together in horizontal direction too, resulting in block-glued glulam. The application and timber species used for block-glued glulam are the same as for regular glulam.

Laminated Veneer Lumber, known as LVL, consists of veneers of up to a few millimeters thickness glued on top of each other to make beams or panels. The direction of the grain depends on the intended use; for beams the grains are placed in longitudinal direction, in panels some of the layers are placed crosswise. LVL can be used for structural purposes, however in bridges it is mostly used in the deck to carry the finishing layer.

Solid planks belong to the category of traditional wood products but they are relevant in this overview

5

because they are commonly used as cladding on bridges or for handrails. Many timber species can be used depending on the desired specifications.

## 2.3. Durability and protection of timber

Left untreated or unprotected, timber is prone to biological attack from fungi, insects and termites, which has a detrimental effect on the quality [51]. In an outdoor environment, fungi are the main source of concern. The level of resistance to fungi is reflected in durability classes, which are shown in table 2.1. When the moisture level in timber rises above 20%, fungi become active. Since this happens regularly in an outdoor environment, measures are needed to protect the timber from decay. Various old-growth tropical hardwoods have naturally occurring extractives which provide a natural resistance up to durability class 1. An example is the tropical hardwood Azobé which is among others used in the main structural parts of the bridge in Harderwijk and Oirschot. However, most softwoods from Northern regions - which are most commonly used in European timber construction - only reach durability class 5 up till 3 [51].

| 1 | Very durable |
|---|---|
| 2 | Durable |
| 3 | Moderately durable |
| 4 | Slightly durable |
| 5 | Non-durable |

**Table 2.1:** Durability classes

Approaches to protect timber in a bridge can be aimed either at keeping the timber dry or preventing decay when wet. The latter means that the moisture content needs to be under 20 % for the great majority of time.

**Preventing timber to get wet**
One way of making sure the structural timber stays dry is to apply an external protection layer in the form of a coating. However, these coatings can make it harder to reuse the timber later and are therefore not always the preferred option [51]. The other way to ensure structural parts stay dry is by means of the geometry of the design, which is shown in figure 2.4. Option *a* and *b* reflect the cladding of structural parts. This can be done in various ways, for example with timber planks in combination with a watertight membrane. When a non-durable specie is used, these might need several replacements during the lifetime of a bridge. Option *c* shows it is also possible to create an overhang in order to prevent rain from hitting the load-bearing parts. The angle should be maximum 30°.
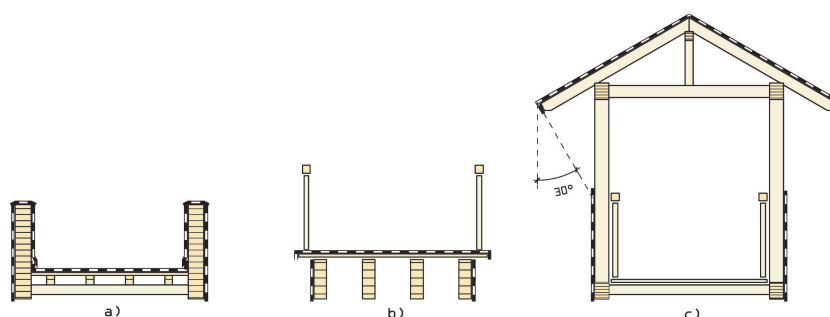


**Figure 2.4:** Options to keep the structural timber dry. Adjusted from [17]

**Wood modification**
In case keeping the structural timber in bridges dry is undesirable or hard to obtain, timber can be modified. In modified wood the hygroscopicity, i.e. the ability to bind water, is reduced, ensuring the moisture content stays below the limit of 20%. This is done by targetting the OH-groups in cellulose and hemicellulose, which are responsible for binding water [7]. There are various ways to modify

wood, each with it's own (dis)advantages. The ones most commonly used for application in bridges are described in appendix B.

## 2.4. Design choices for cable-stayed timber footbridges

In this section an overview is given of some important design choices in the design of a cable-stayed timber footbridge. In section 2.2 and 2.3 different wood products and ways to protect the timber have been discussed. The aspects covered in this section are the structural system, the deck, the railing, the pylons and the cables.

### What parts belong to main structural system

An important choice for a cable-stayed bridge is whether the deck parts outside the main span belong to the structural system. Including the deck parts outside the main span (figure 2.5) in the structural system comes with the advantage that there is horizontal force equilibrium in the deck, reducing the load on the pylon. In addition, there will be no tension forces in the foundation because of the absence of anchor cables. However, this is not always possible due to the location.
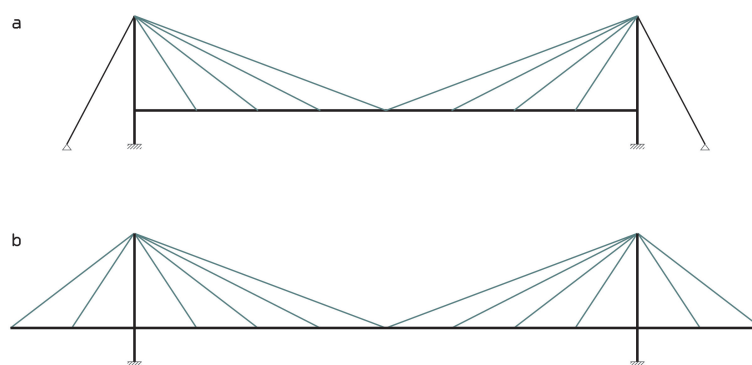


**Figure 2.5:** Include outer deck parts

### Deck types

The second topic is the way the deck is built. There are as many ways to build the deck as there are timber bridges, so for this research the options are narrowed down to two characteristics which are though to be most fundamental. The first characteristic is the way the deck is connected to the cables. This can be done either with steel beams integrated in the deck (figure 2.6a) or with steel beams under the deck (figure 2.6b). When the steel beams are integrated in the deck, the deck is split in segments. When the steel beams are under the deck, the deck can be continuous.



**(a)** Steel parts integrated in deck [38]



**(b)** Steel parts under deck [17]

**Figure 2.6:** Connection deck to cables

The second characteristic is the way the deck is built up. Block laminated timber can be used to form a solid deck (figure 2.7a). The other option is to use main girders, crossbeams and lateral bracing as shown in figure 2.7b and 2.7c. In the latter one, the main girders are used as railings. This is often done when the bridge deck is relatively narrow, whereas option b) is used for wider bridges. Naturally, many variations are possible.

7

a) Block laminated deck      b) Main girders and crossbeams      c) Load-bearing railing
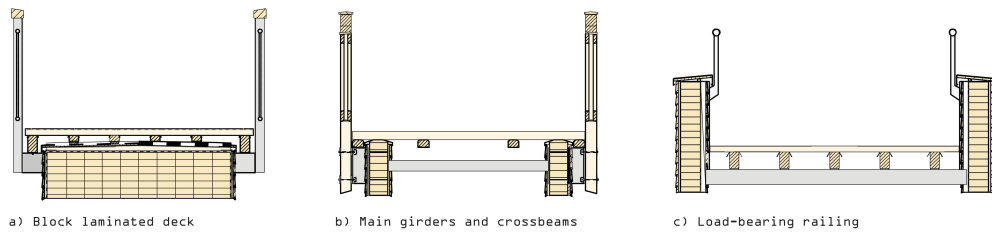
**Figure 2.7:** Deck types Adjusted from [17]

**Railing**

The third choice for the design of a timber bridge is whether or not to include the railing as a structural element. A stiff railing contributes to the stiffness of the deck, which might have a positive influence on the dynamic behaviour [23]. On the other hand, a stiff railing comes at the expense of the openness, which is needed to reduce the effects of wind loading.

**Pylons**

The next choice is the shape and the height of the pylons. There are two basic types of pylons, double and single pylons. Single pylons usually used for relatively short spans, while double pylons are used for longer span. Double pylons can be subdivided in A-shaped, H-shaped and V-shaped pylons, as seen in figure 2.8. H-shaped pylons consist of two parallel pylons connected by cross beams, an example of which is the Älvsbacka bridge. A-shaped pylons consist of two non-parallel pylons connected by cross beams. From the bottom they can incline towards each other, while in a V-shaped pylon they incline away, which can be seen in the two pylons of the Dafne Schippers bridge. According to Schlaich [41], A-shaped pylons are better for the torsional stiffness compared to H-shaped pylons.

Pylons can also be tilted around the lateral axis. This is usually done for aesthetic reasons because it is not the preferred solution from a structural point of view.

The height of the pylons needs to be chosen too. Literature suggests that a higher pylon increases the vertical stiffness of the bridge [41], but there might be limitations due to material use or buckling.
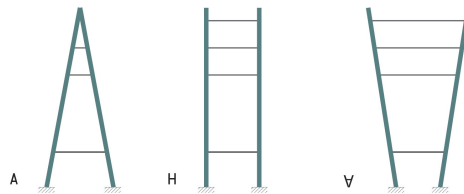


**Figure 2.8:** Pylon shapes

**Cables**

The last major choice is the amount and arrangement of the cables. There are two configurations in which the cables can be connected to the pylons; the harp and the fan configuration, which are shown in figure 2.9, though mixes exist too. If it is possible, a fan configuration is chosen because it is more efficient in transferring forces and results in a stiffer bridge. Crossing the cables from two sides can be beneficial, although this is most often done in road bridges [2]. Literature suggests that the stiffness of the bridge increases with increasing cables sections, but Schlaich [41] points out this is uneconomical.

harp
configuration

fan
configuration
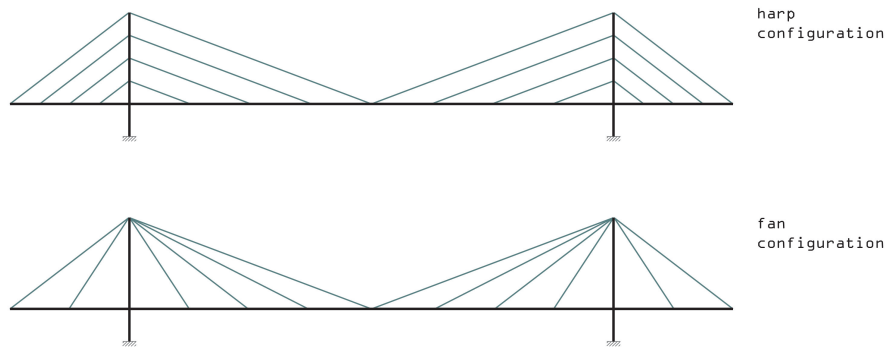
**Figure 2.9:** Cable configuration

## 2.5. Connections in cable-stayed timber footbridges

Since timber is an orthotropic material, it has different strength properties depending on the direction of the load. In fact, the tensile and compression strength differ a factor 10 and 40 respectively, if the load changes from parallel to perpendicular to the grain. In connections, forces are transferred from one element to another, whereby often forces are applied perpendicular to the grain. Therefore connections are usually the weakest link in a timber structure and become the critical point in a design. As a result the connection design rather than the stresses in the members itself, often determines the size of the members.

**Types of connections**
Blass [7] distinguishes three types of connections between structural members; glued joints, carpentry joints and joints with metal fasteners. Whereas in timber bridges glue is used within members to connect different timber parts, it is not common to use glue as a way to connect different members. Carpentry joints are contact joints working in compression and are uncommon in bridge design as well. This leaves us joints with metal fasteners that can be subdivided into dowel-type fasteners and surface-type fasteners. Of these two, dowel type connections are most often applied in timber bridges.

Examples of surface-type metal fasteners are split ring connectors, toothed plate connectors and punched metal plate fasteners. Dowel-type fasteners include nails, staples, bolts, screws, dowels and threaded rods.

**Connections in cable-stayed timber footbridges with steel beams integrated in the deck**
Which connections are of importance in a cable-stayed timber bridge, depends on the specific structure, and the choices described in section 2.4. In figure 2.10, some locations of possible critical connections that are relevant for the case study are indicated. These are connections between:

- The pylon and the cables
- The pylon and its crossbeams
- The deck and the steel beam
- The main girder and the crossbeams in the deck
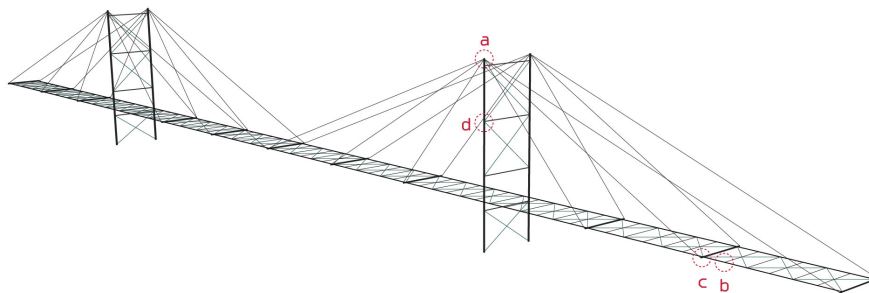


**Figure 2.10:** Connections in a timber cable-stayed bridge

9

For each connection a common type is shown in figure 2.11. In figure 2.11a it can be seen that the tension forces from the cables are transferred to the pylon via a steel cap, making sure the load is spread over the full cross-sectional area of the pylon. Figure 2.11c shows that the main beam can be connected to the steel beam by means of shear plates that are welded to the steel beam. The actual connection is made by dowels. Although there is a small arm to take up some moment, the rotational stiffness is very low, so the connection is regarded as a hinge. By enlarging the connection and adding more dowels it is possible go create more rotational stiffness. Figure 2.11b shows a common connection between the timber cross beam and the timber main beam. The joist hanger is connected to the main beam by screws. As with the main beam - steel beam connection it goes that the rotational stiffness so low that is is negligible, resulting in a hinged connection.



**(a)** Pylon - cable connection



**(b)** Cross beam - main beam connection



**(c)** Main beam - steel beam connection



**(d)** Crossbeam - pylon connection
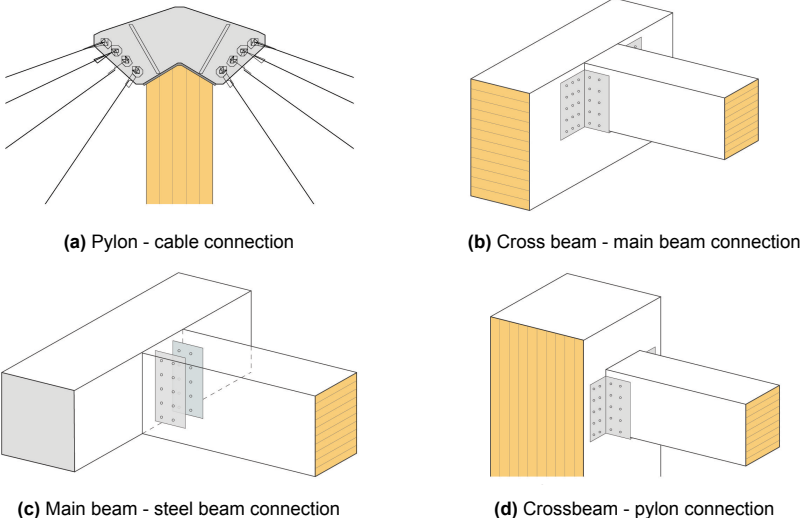
**Figure 2.11:** Details

# 3

# Human-induced vibrations in footbridges

In this chapter the basic concepts of vibrations in relation to footbridges are explained. It starts with an introduction about vibrations, followed by an explanation about footfall loading, dynamic properties, damping, comfort and dynamic assessment of footbridges.

## 3.1. Introduction

The Merian-Webster definition of a vibration is *a periodic motion of the particles of an elastic body […] in alternately opposite directions from the position of equilibrium when that equilibrium has been disturbed*. In other words, a vibration is a phenomenon whereby oscillations occur around an equilibrium point. A single degree of freedom oscillator displaying a harmonic vibration is shown in figure 3.1.
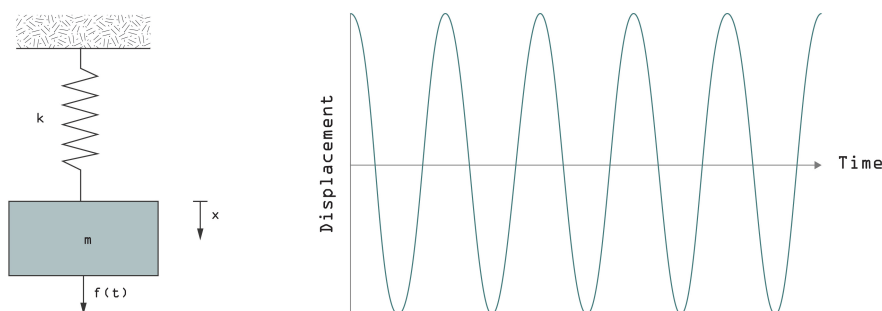


**Figure 3.1:** Harmonic vibration

There are several phenomena that can cause a structure to vibrate, namely earthquakes, wind, waves, traffic loading and pedestrian loading. In the case of the Dafne Schippers Bridge (DSB), only wind and pedestrian loading are relevant because of the absence of earthquakes, waves and road traffic. To limit the scope of this thesis, only pedestrian loading will be regarded.

Very large vibrations can cause a structure to fail, but in most cases and especially for pedestrian loading, it is a comfort issue rather than a structural safety issue. The element that has a negative influence on the comfort level of people is the acceleration of the bridge deck, which is a consequence of vibrations. Figure 3.1 shows the sinusoidal variation of the displacement over time, implying the presence of accelerations.

## 3.2. Footfall loading

Figure 3.2 shows the dynamic component of four measured footfall force time histories caused by different persons on the same location [57]. Note that there is a great variety in frequency, amplitude and shape. Willford points out that factors that contribute to this variation include weight, height, gender, footwear, walking speed and walking surface. Typically, when walking, a person takes between 1.25 and 2.3 steps second (1.25 - 2.3 Hz) [23].

To be able to perform calculations with footfall loading, the load is often divided into different sinusoidal oscillations called *harmonics* by a Fourier transformation shown in equation 3.1 [41].

$$F(t) = F_0 + \sum_i F_i \cdot \sin\left(2\pi \cdot i \cdot f_s \cdot t - \varphi_i\right) \tag{3.1}$$
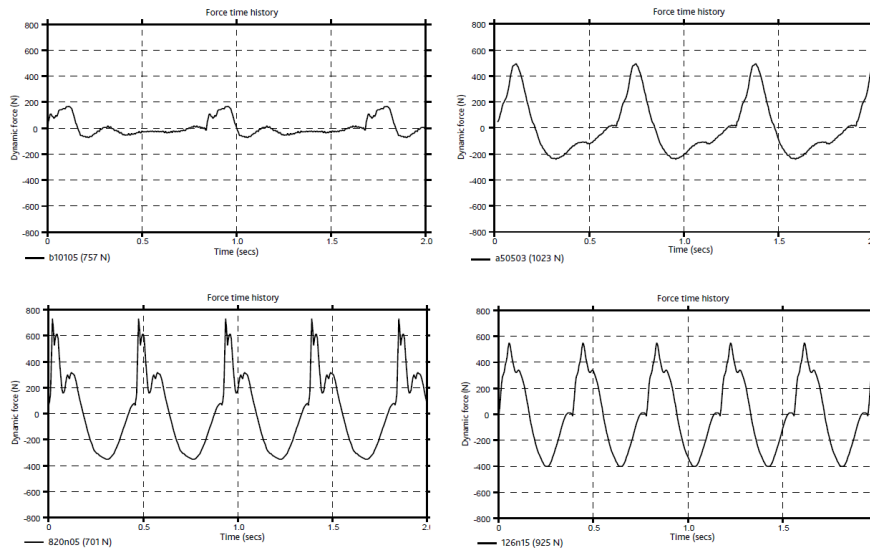
**Figure 3.2:** Footfall time histories [57]

$F_0$ is the mean or static load

$F_i$ is the load component for frequency i · f$_s$

$f_s$ is the step frequency

$\varphi_i$ is the phase angle of load component F$_i$

From the formula one can see that the total load is the sum of all harmonics. If the system is assumed to be linear, the response of the system can be calculated as the sum of the responses to these different harmonics. According to Willford [57], only the first three or four harmonics are of importance for pedestrian loading on footbridges. In practice the first harmonic is the governing one. An example of how two subsequently recorded footfalls can be decomposed into three harmonics is shown in figure 3.3. One can see that the frequency of the second harmonic is twice the ground frequency and that the frequency of the third harmonic is three times the ground frequency.
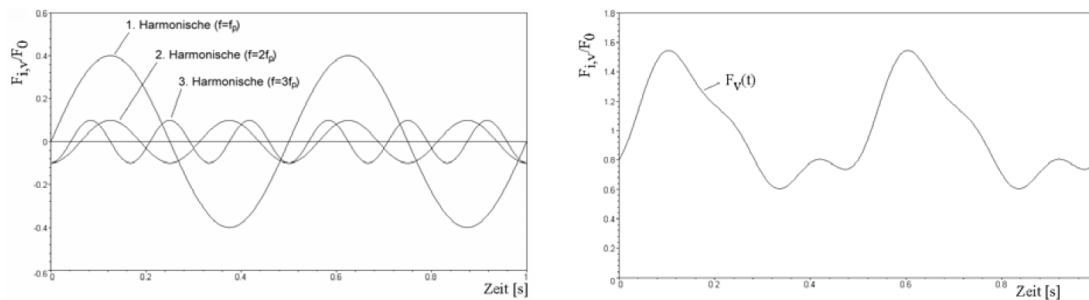


**Figure 3.3:** Three harmonics [41]

## 3.3. Dynamic properties

To predict the response of the structure to dynamic loading, four dynamic properties have to be known, being the mode shapes, the natural frequencies, the modal mass and the modal damping.

**Mode Shapes**

Mode shapes are also known as the *natural modes of vibration* and can be described as the structure's preferred patterns of vibration when excited by a sudden impact [57]. The amount of modes in a

structure is equal to it's degrees of freedom, which goes to infinity for continuous systems. On a global level of the structure, there are vertical, lateral and torsional mode shapes. In a dynamic assessment, only the modes with natural frequencies in the range of the loading frequency are investigated, which comes down to roughly 10 modes for pedestrian bridges. The first three vertical modes of a simply supported idealised bridge are shown in figure 3.4a. When a dynamic force is applied to the bridge, it starts vibrating in a pattern that is a combination of all modes that have a non-zero displacement in the mode shape at the point of excitation. For example, if a person jumps in the middle of the bridge, modes 1 and 3 are excited. The resulting vibration pattern could look like 3.4b, depending on the frequency of the jumping.



**(a)** Three modes of a simply supported bridge deck      **(b)** Excitation of mode 1 and 3
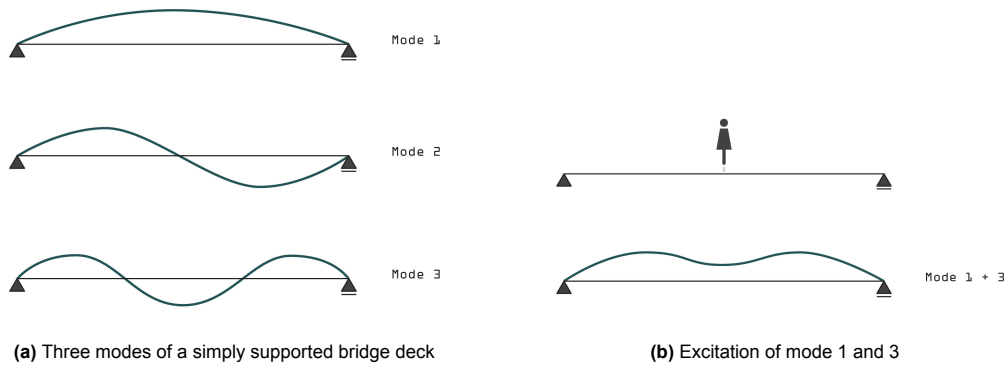
**Figure 3.4:** Modes

**Natural frequency**

A natural frequency is the frequency in which a structure vibrates after a sudden impact and is determined by the stiffness and the mass. Each mode shape is connected to a natural frequency. When a structure is excited in one of its natural frequencies, resonance occurs. Resonance is the phenomenon in which the vibrations of each load cycle reinforce the vibrations generated before, whereas normally in the steady state the amplitude of the response remains constant with a constant amplitude of the force [57]. As an illustration, the development of resonance of a single degree of freedom (SDOF) oscillator is shown in figure 3.5.
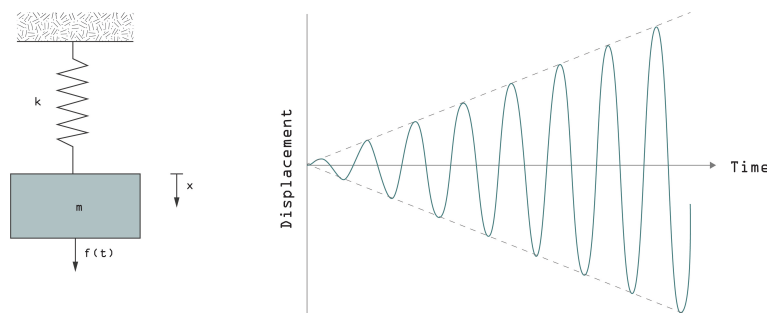


**Figure 3.5:** Resonance in the time domain for a SDOF oscillator

In a pedestrian bridge, resonance occurs when one of the harmonics of the footfall loading approaches a natural frequency of a mode. Since almost all energy goes to that mode, the contribution of other modes to the total response of the bridge is negligible.

Figure 3.6 depicts the averaged peak velocity for 882 footfall force time histories against the ratio $r$ of the first natural frequency over the forcing frequency [57]. It shows that in general the vibration response decreases for higher values of $r$. However, there are peaks around round values of $r$. The high peak at $r = 1$ is caused by resonance to the first harmonic of the footfall loading, the peak at $r = 2$ is caused by the second harmonic of the loading, etc. The sharp decrease in magnitude of the peaks explains why in most cases only the first harmonic is taken into account in a dynamic assessment.

13
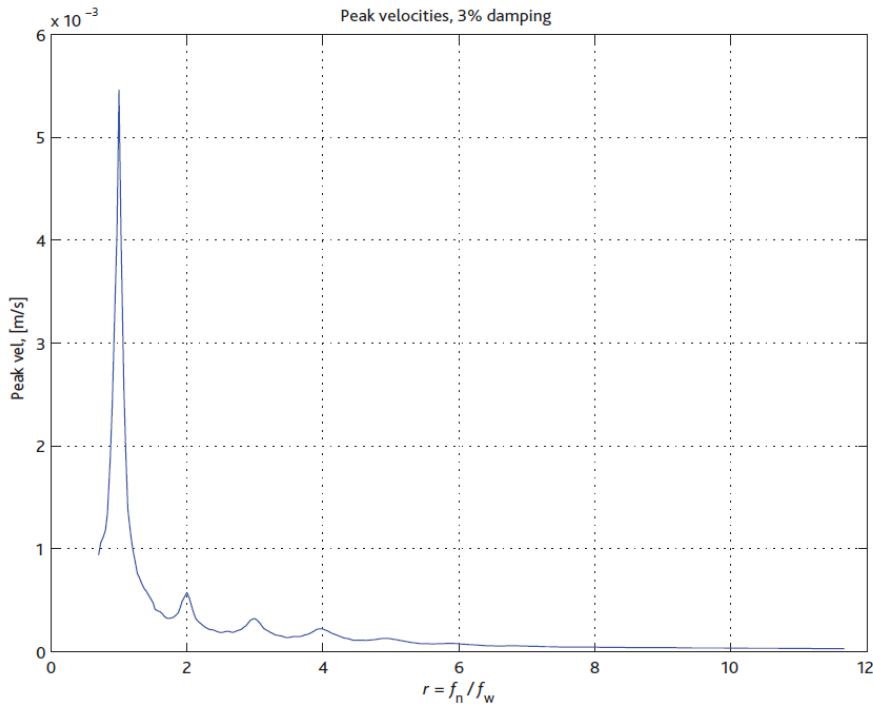
**Figure 3.6:** Resonance in the time domain for a SDOF oscillator [57]

Since the amplitude of a vibration at resonance is significantly higher than non-resonant vibration, the dynamic response of a pedestrian bridge is only checked at forcing frequencies that are natural frequencies of the bridge.

**Modal damping and modal mass**
The modal damping is the damping active in a certain mode. The concept of damping is further explained in paragraph 3.4. The exact definition of modal mass is unclear because the technique used to normalise the mode shapes determines the units and the magnitude depends on the number of degrees of freedom used to discretise a problem [1]. To grasp the concept, it can be interpreted as the mass activated in a particular mode of vibration [23]).

## 3.4. Damping

The accelerations caused by a certain loading are greatly influenced by the amount of damping. Damping is the decrease of amplitude of a vibration caused by the dissipation of energy. That is to say, it causes a vibration to gradually stop when no loading is present anymore, see figure 3.7.
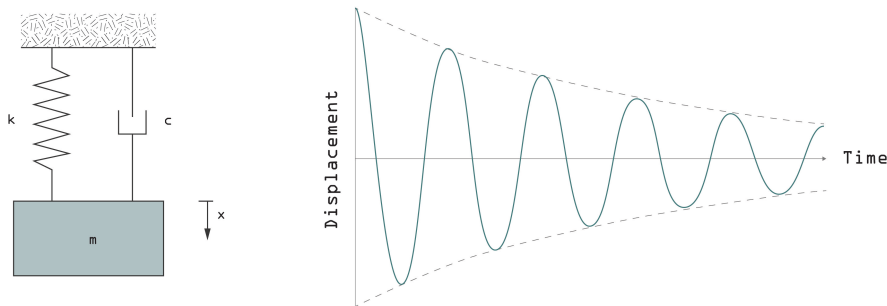


**Figure 3.7:** Harmonic vibration with damping

Figure 3.8 shows the damping in three types of systems: an under-damped system, an over-damped system and a critically-damped system. In an under-damped system, there are one or more oscillations

14
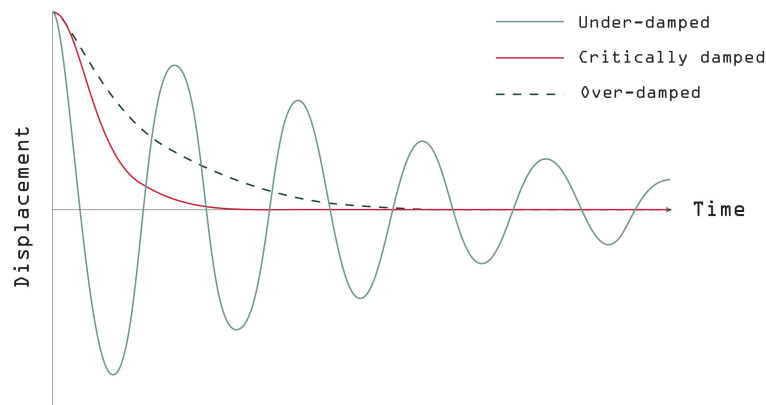
**Figure 3.8:** Types of damping

after the loading stops before the systems returns to its equilibrium position. This is the case for virtually all bridges. Critical damping is defined as the threshold between under-damping and over-damping. When a system is critically damped, it returns to the equilibrium position as quickly as possible [54]. If a system is over-damped there is more damping than the critical damping, so it takes longer to go back to the equilibrium state.

## Types of damping

Damping is a complicated phenomenon that can be caused by different mechanisms. A distinction can be made between material and non-material damping. Next to that, additional damping devices can be installed.

**Material damping**

Material damping is caused by the deformation of the material, which can occur in many forms [37]. For bridge structures it is useful to understand the difference between elastic and plastic damping, caused by elastic and plastic deformation respectively. The effect of elastic deformation is called 'internal friction' and is induced by friction between molecules and slip of micro-cracks. Internal friction damping is generally small [44]. The effect of plastic deformation is called 'plastic hysteresis'. It involves a change of the microscopic structure of the material and is larger than internal friction. However, in the case of pedestrian loading it is not relevant since linear elastic behaviour is assumed.

**Non-material damping**

Non-material damping is caused by interaction between parts of the structure or between the structure and its surroundings. Just as with material damping, there are many forms of non-material damping [37]. The types that are important for pedestrian bridges are external friction damping and aerodynamic damping. External friction damping is defined as energy dissipation due to friction between solids [48]. It occurs mainly in the joints, but also in the interface between structural and non-structural elements of a structure, such as the load-bearing beams and the cladding. Aerodynamic damping is caused by the interaction between the structure and the air. For bridges it plays a role in wind-induced vibrations because it increases with increasing wind velocity. However, when assessing pedestrian-induced vibrations, aerodynamic damping cannot be taken into account because wind is not always present [23].

## Additional damping devices

If the damping naturally present in the structure is insufficient, additional damping devices can be installed. There are several types, the most popular of which are viscous dampers and tuned mass dampers [23].

**Viscous dampers**

Viscous dampers dissipate vibrations by means of the deformation of a viscous fluid or by letting a fluid flow through calibrated openings. When impacted by a sudden vibration, they dissipate energy by

converting kinetic energy to heat or by volume variation. The damping capacity of a viscous damper is proportional to the relative velocity of both ends. Therefore they only are an efficient solution if the ends can be connected to locations in the structure with significant relative displacement (larger than +/- 10 mm) [31]. The advantage of viscous dampers is that they enable simultaneously controlling several vibration modes since they are not tuned to a specific frequency. A piston inside a cylinder is the most common viscous damper, as shown in figure 3.9a.



**(a)** Viscous damper
**(b)** Tuned mass damper
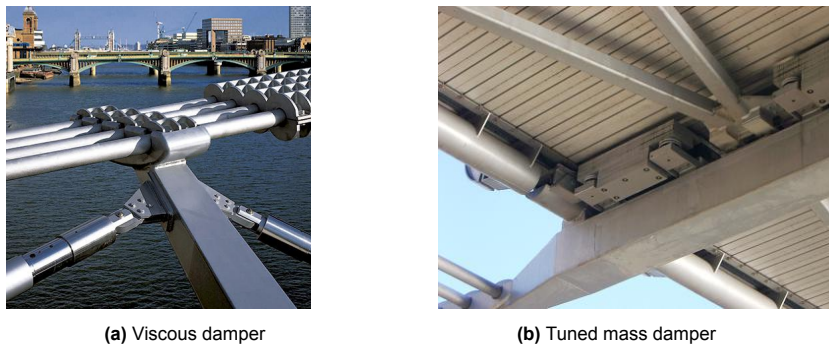
**Figure 3.9:** Dampers in the Milenium bridge London [58]

### Tuned mass dampers

A tuned mass damper (TMD) consists of a moving mass, a spring/stiffness element and a damping element, which are placed at the location of greatest vibration amplitude of a certain mode [31]. An example is shown in figure 3.9b. The natural frequency of the TMD tuned to the natural frequency of the considered mode. Without a damper, the structure would start resonating when excited in that frequency. If a damper is added, the device starts resonating, dissipating the energy that would otherwise cause the structure to resonate. The principle of a vertical TMD is shown in figure 3.10.

## Influence on damping

In a pedestrian bridge under pedestrian loading, external friction is the most important source of damping when no additional damping devices are installed. The amount of external friction is influenced by the type of connections, the non-structural elements, the considered mode shape and the level of vibration.

The type of connections has influence on the amount of external friction because bolted connections have more friction – so more damping – than connections that are for example welded or glued [41].

Non-structural elements such as the deck finish, cladding, bridge furniture and, if not included in the structural system, the railing, influence the amount of damping by friction as well [44].

If the bridge vibrates in lateral direction, deformations occur in different parts of the structure than when it vibrates in e.g. vertical direction. This is why the level of damping is influenced by the considered mode shape [23].
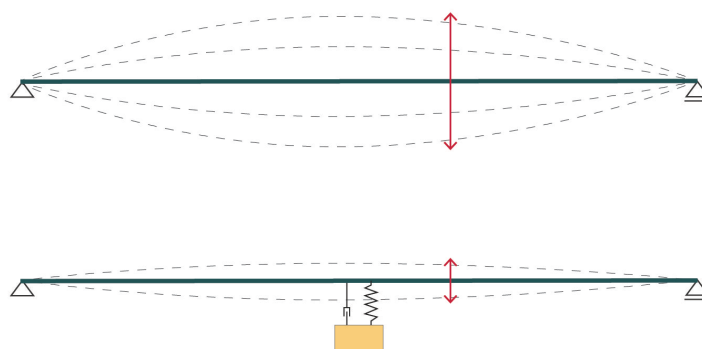


**Figure 3.10:** Tuned mass damper

16

Higher levels of vibrations, so higher deformations, cause more friction, which is the reason that damping is dependent on the level of vibration [23].

## Quantifying damping

Considering the complexity of damping, it is not possible to accurately obtain the damping value of a structure based on a model, unless a detailed non-linear model is made containing values for all possible material and non-material friction coefficients. This is infeasible for the intended optimisation. In engineering practice, one damping value is assumed for the entire structure, regardless of the mode or level of vibration [57]. This value is based on measurements done on similar structures. Since damping is highly dependent on how exactly the structure is build, it might be clear that this can never be accurate. Therefore it is important to check the sensitivity of the results to changing damping values.

### Values from Eurocode and guidelines

In calculations, damping is most often assumed to be viscous damping because it is related to velocity and is therefore applicable in a linear analysis. A viscous damping value can be presented as a percentage of the critical damping or as a logarithmic decrement of the damping. They are related as in equation 3.2 in which $\Lambda$ is the logarithmic decrement of the damping and $\zeta$ is the damping ratio expressed as a percentage of the critical damping.

$$\Lambda = 2\pi\xi \tag{3.2}$$

In table 3.1 damping values for timber bridges recommended in different codes and guidelines are presented. No specification for the type of bridges is given, except in the EN1995 draft. It can be noticed that differences between the values is quite high. As a reference, recommended values for steel pedestrian bridges are given in table 3.2. It can be seen that in general, the recommended values for steel bridges are lower that the ones for timber. This is due to the fact that there is more friction in timber joints and to a lesser extend because timber has more material damping.

| | Lower limit | Upper limit | Average |
|---|---|---|---|
| *Guidelines for the design of footbridges* [41] | 1.1% | 1.5% | 1.3% |
| *European design guide for footbridge vibrations* [22] and *Footbridges* [42] | 1.5% | – | 3.0% |
| *British national annex* [43] | 0.95% | 1.91% | – |
| *Design of lightweight footbridges for human induced vibrations* [23] | 1.0% | – | 1.5% |
| EN1995-2 | – | – | 1.5% |
| EN1995 draft (cable-stayed bridges) | – | – | 0.5% |

**Table 3.1:** Damping values from guidelines - Timber footbridges

| | Lower limit | Upper limit | Average |
|---|---|---|---|
| *Guidelines for the design of footbridges* [41] | 0.7% | 1.2% | 0.9% |
| *European design guide for footbridge vibrations* [22] and *Footbridges* [42] | 0.2% | – | 0.4% |
| *British national annex* [43] | – | – | 0.48% |
| *Design of lightweight footbridges for human induced vibrations* [23] | 0.2% | – | 0.4% |

**Table 3.2:** Damping values from guidelines - Steel footbridges

### Damping in literature

The amount of literature about structural damping in timber bridges is limited. Kliger [25] describes the case of the Älvsbacka bridge in Sweden, which is a 130 meter long cable-stayed timber bridge. After measurements the researchers found a damping ratio of 1.2% for a group of walking pedestrians.

Magdaleno [29] describes a timber arch-girder bridge in Spain, which has a 2.91% damping in the lateral mode and a 2.85% damping in the vertical mode. The frequencies of these modes fall outside the critical range for pedestrian loading. In a graph with measured damping ratios of footbridges, Heinemeyer [23] shows two timber bridges with a span of around 70 and 90 meter, with a 3.5% and 1.2% damping ratio respectively, see figure 3.11 and 3.12. The structural system of these bridges is unknown. The graph also shows measured damping ratios of bridges made of other materials.

A part of the literature about damping in timber structures focuses on buildings or specific joints and is thus less relevant for this thesis. An example is the research carried out by Labonnote [26], that showed an attempt to get the total damping value for floor vibrations of a building based on the construction material, the type of furniture and the type of finish. Another example is the research by Feldmann [18], who investigated the damping ratios tall timber structures under wind-induced vibrations. They found a modest positive correlation between the first natural frequency and the damping ratio. There is also some literature about viscous damping in timber buildings under seismic loading, but since that involves plastic deformation it is not relevant for this thesis. Finally research done by Awaludin [3] showed that pretensioning of fasteners results in more damping because forces are transferred through friction, although the results are not directly applicable on this thesis since this also involved plastic deformation. The literature about damping in steel and/or concrete pedestrian bridges is more extensive, the majority of which include testing on existing structures [4, 14, 11, 28, 53]. An overview of measured damping values in pedestrian bridges can be found in appendix A.2.
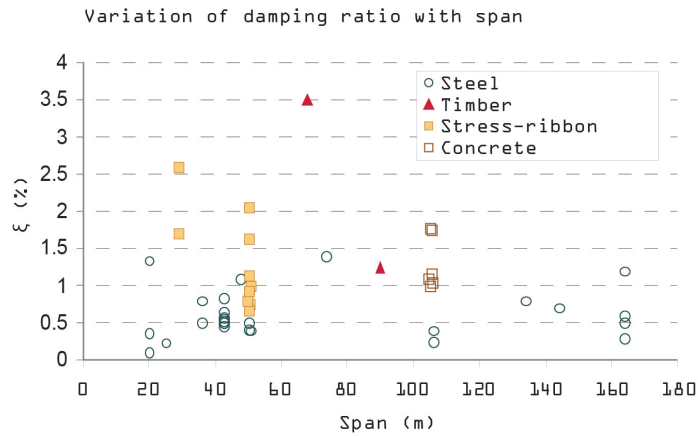


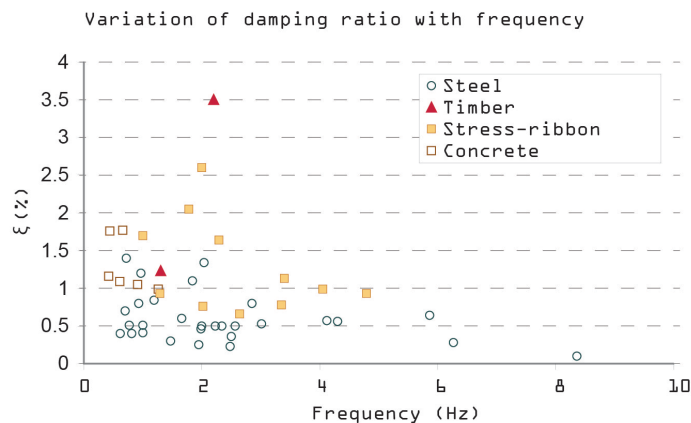**Figure 3.11:** Measured damping ratios of footbridges under service loads. Adjusted from [23]



**Figure 3.12:** Measured damping ratios of footbridges under service loads. Adjusted from [23]

## 3.5. Comfort

In the context of structural dynamics, comfort is defined as *a state of physical ease*. As mentioned before, accelerations have a negative impact on the comfort level of people. However, since comfort is a highly subjective concept, there are many aspects influencing the acceptance of a certain acceleration. They are listed below.

- The frequency. People are most sensitive to vibrations at frequencies between 4Hz and 8Hz [57, 23].
- The location. Outdoors, people accept more vibrations [57] and if there is traffic running under the bridge, people accept less vibrations according to Setra [42]. Setra is not explicit as to whether this also applies to ship traffic.
- The design. The higher people walk above the ground and the more transparent the deck and railing are, the less comfortable people are [22]. The expectations based on the appearance of the bridge have an influence too. A good example is a comparison study done on a suspension bridge versus an arch bridge with the same dynamic properties. People felt less at ease on the arch bridge because they expected it to be sturdier [23].
- The state of people. It matters if a person is sitting, standing or walking. In a study, the same vibration judged by standing person was unacceptable, whereas for a walking person it was fine [41]. In addition, a person just out of a hospital is more sensitive to vibrations than someone hiking a trail in the mountains [23].
- The orientation of the vibration relative to the axes of the human body. Pedestrians are more easily brought off balance by horizontal vibration than by vertical ones [42, 57].
- The frequency of use. The more a bridge is used by a person, the more the acceptance of vibrations increases [41].
- The effects of a vibration on a bridge. Sound and visual influences may provoke discomfort [41].
- The type of vibration. Stochastic vibrations cause more discomfort than periodic ones [41] and long vibrations cause more discomfort than short ones [22].
- The number of people on a bridge. The more people, the more discomfort [22].

**Lateral lock-in effect**

Compared to vertical vibrations, people are more sensitive to lateral vibrations, because unlike the former, lateral vibrations cannot be absorbed by the body. On a laterally vibrating bridge, pedestrians intuitively try to compensate the vibrations by slight lateral motions to keep their balance. This change in movement involves a widening of the gait, increasing lateral ground reaction forces, and an adaptation of the walking frequency to the natural frequency of the bridge. Since the increased forces are in resonance with the structure, energy is put into the system and the structure starts vibrating even more. This is called the lock-in effect [41, 22]. The lock-in effect can be coupled to either the lateral accelerations or the number of pedestrians on a bridge. Based on tests, Heinemeyer [22] writes that the effect can occur with accelerations starting from 0.1 to 0.15 m/s², these accelerations being the values from which people start to compensate the movement. Based on research of Arup, Schlaich [41] gives a formula to calculate the critical number of pedestrians above which the lock-in effect can be triggered, see expression 3.3.

$$N_L = \frac{8\pi * \xi * m^* * f}{k} \tag{3.3}$$

In the equation, $\xi$ is the structural damping ratio, $m^*$ is the modal mass, $f$ is the natural frequency and $k$ is a constant that is usually taken as 300 $Ns/m$. Joggers are less affected because the contact with the deck is short and the higher speeds makes them more stable.

## 3.6. Dynamic assessment of footbridges

There are several ways to assess dynamic behaviour in structures, written down in different guidelines. For timber footbridges, Eurocode 1995-2 refers to Eurocode 1990-A1, which advices to use the method described in the JRC guideline for the assessment of human-induced vibrations [23]. The relevant steps of that document are described in appendix D. The outcome is a maximum acceleration which can be tested against comfort criteria.

**Comfort classes**

Due to the subjective nature of comfort, there are different ways to quantify comfort. Examples are comfort classes or a response factor, which are based on accelerations. If it is desired to take into account the duration of the exposure, the VDV (vibration dose value), can be used. The JRC document uses comfort classes, which are shown in table 3.3. There are four comfort classes, ranging from 'maximum comfort' to 'unacceptable discomfort', each coupled to vertical and lateral acceleration limits. The comfort classes used for a specific bridge project can be determined in the project specifications.

| Comfort class | Degree of comfort | Vertical $a_{\text{limit}}[m/s^2]$ | Lateral $a_{\text{limit}}[m/s^2]$ |
|---|---|---|---|
| CL1 | Maximum | $< 0.50$ | $< 0.10$ |
| CL2 | Medium | $0.50 - 1.00$ | $0.10 - 0.30$ |
| CL3 | Minimum | $1.00 - 2.50$ | $0.30 - 0.80$ |
| CL4 | Unacceptable discomfort | $> 2.50$ | $> 0.80$ |

**Table 3.3:** Comfort classes according to the JRC document [23]

<div align="right">

$4$

</div>

# Structural optimisation

In this chapter, the concept of structural optimisation is explained. The first section is about the formulation of an optimisation problem, followed by how to solve an optimisation problem. The chapter ends with an explanation about a specific solving algorithm that is relevant for this thesis.

## 4.1. Formulating the optimisation problem

### Forms of optimisation

Before parametric optimisation came into play, three distinct forms of structural optimisation could be identified, which are shown in the first three lines of figure 4.1 [13]. Sizing optimisation is the simplest form. In this type of optimisation, the shapes of structural members are predefined and only the size of the members change. Second comes shape optimisation, in which shapes can change but no new boundaries can be formed. Thirdly, topology optimisation determines where material is present. It is unrestricted by predefined boundaries or members, giving the widest range of possible outcomes.

Parametric design can be seen as a combination of these types. It resembles sizing optimisation most, but it adds the possibility to change the position of the members, material grades, amount of members etc. It does however not reach the freedom of typology optimisation since the design options are predefined with the parameters.
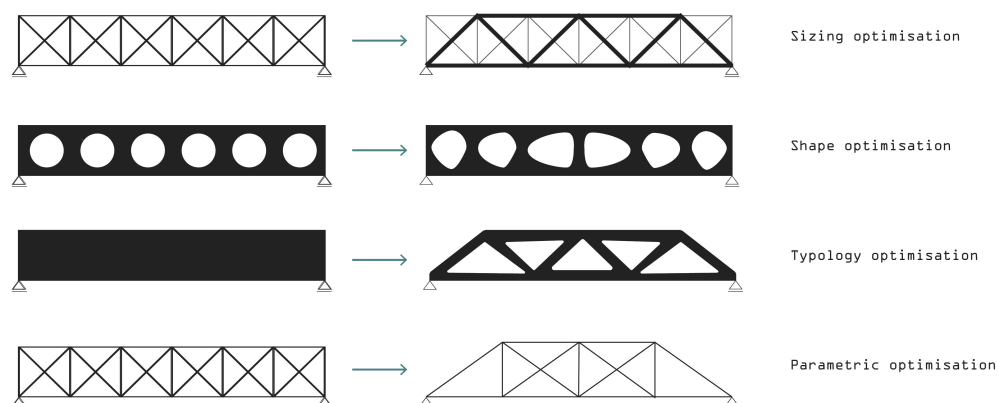


**Figure 4.1:** Forms of structural optimisation

### Single- and multi-objective optimisation

In optimisation problems there can be one or more objectives. Objectives are the goals for the optimisation, either minimising or maximising a certain quantity. Examples of single-objective problems are finding the top of a parabola function or the most cost-effective design of a truss.

As the name suggests, in multi-objective optimisations there are multiple goals to aim for. Examples are getting the highest grades with the least amount of effort or reducing material use in a truss while minimising the amount of different members.

In these types of problems no single solution exists that optimises both objectives simultaneously. In fact, multiple 'optimal' solutions exist, which are called Pareto optimal solutions. These are solutions

where none of the objective functions can be improved without worsening any of the other objective functions (wikipedia about multi-objective opt). The solutions on the green line in figure 4.2 are Pareto optimal.
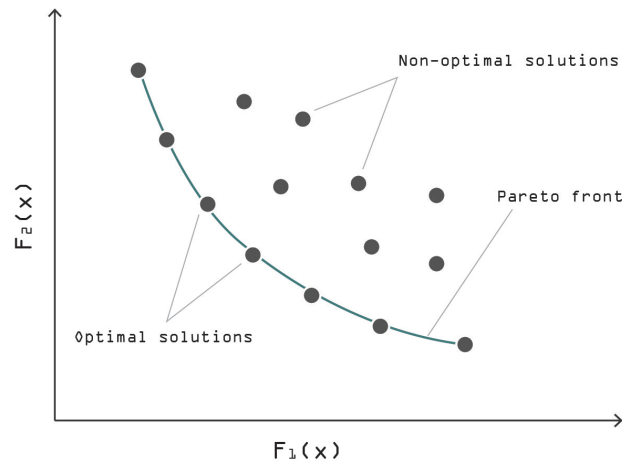


**Figure 4.2:** Pareto optimal solutions

Choosing the best solution of a multi-objective optimisation is not possible without subjective information about the relative importance of the objectives because there may exist a great number of solutions on the Pareto front which are all considered equally good. There are numerous ways to overcome this problem. The most widely used is turning the problem into a single-objective problem by linear scalarisation. Then the total objective function value is the sum of the two objective functions values multiplied by different scalars that are based on the preference of the decision maker. In the truss example, if the decision maker cares more about material use than about issues related to the amount of different members (affordability, reusability), the ratio could be 3:1. However, depending on the preferences it could as well be the other way around.

In practice, for bridges it is usually chosen to optimise for just one objective, like cost or material use, while implementing other objectives as constraints in the optimisation. To explain the concept of constraints, first the mathematical formulation of a structural optimisation problem is given in the following section.

## Mathematical formulation
Written in a mathematical way, a single-objective structural optimisation problem has the following form [13]. The parts of which it consists will be further explained below.

$$
\text{Structural Optimisation}
\begin{cases}
\text{minimize} & f(x,y) \text{ with respect to } x \text{ and } y \\
\text{subject to} &
\begin{cases}
\text{design constraint on } x \\
\text{behavioural constraint on } y \\
\text{equilibrium constraint}
\end{cases}
\end{cases}
\tag{4.1}
$$

### Objective function
$f(x,y)$ is the objective function. Usually it is written in such a way that a smaller value is better than a larger one. Hence the optimisation problem becomes a minimisation problem. $x$ are the design variables, the parameters that change. It may be a vector and can represent geometry or material choice. $y$ are the state variables, which represent the response of the structure. Examples are stresses, strains or accelerations.

### Constraints
As can be seen in expression 4.1, the objective function has to comply with constraints. There are three types of constraints in structural engineering problems, namely design constraints, behavioural

constraints and an equilibrium constraint. They are explained below with the simplified version of the truss example, which is minimising the material use of a truss bridge.

- **Design constraints.** The design space is the set of possible designs based on the range of values in which the parameters can vary. The limit values of $x$, the parameters, are called the design constraints. For example, the section height of the truss member can be defined to range between 500 and 800 mm.
- **Behavioural constraints.** The state variables $y$ are limited by behavioural constraints. In the setup of the problem, they make sure a solution would work. For example, limits can be set to the normal stress in a member or the deflection of the truss so that the design fulfills utility and serviceability requirements.
- **Equilibrium constraint.** As in all structural engineering problems, the equilibrium condition needs to be satisfied, which is expressed in the equilibrium constraint. In discrete or discretised problems, the equilibrium constraint looks like $\boldsymbol{K}(x)\boldsymbol{u} = \boldsymbol{F}(x)$, where $\boldsymbol{K}(x)$ is the stiffness matrix, $\boldsymbol{u}$ is the displacement vector and $\boldsymbol{F}(x)$ is the force vector [13].

**Penalty function**
Behavioural constraints can be implemented by means of a penalty function. This function can be included in the objective function by multiplying its value with or adding its value to the original objective function value. For instance, when the normal stress in a truss member exceeds the tensile strength, the penalty function will have a high value, resulting in a high value of the objective function. Since the goal is to minimise the objective value, design variants which don't fulfil the behavioural constraints are less likely to end up in the final result of the optimisation.

## 4.2. Solving the optimisation problem

To find a solution to the optimisation problem, a solving strategy is needed. There is a wide range of strategies available and new possibilities are still being developed [50]. An important topic to consider when choosing a solving strategy, is the convexity of the problem because it effects the applicability of the strategy as well as the reliability of the result.

A problem is convex if both the objective function and the constraints are convex. A set is convex if any point on a line connecting two points of the set is also in that set [13], otherwise, the set is called concave. This is illustrated by figure 4.3. The dotted part of the line in figure 4.3a is not in the set, implying the set is concave, whereas the line in figure 4.3b is entirely in the set, suggesting the set can be convex.
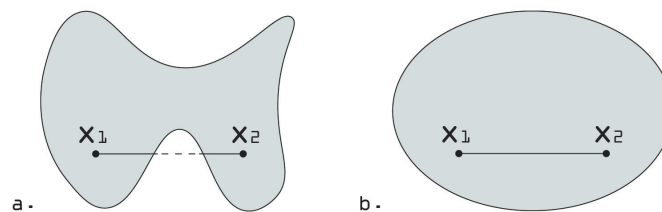


**Figure 4.3:** A concave and a convex set

A convex optimisation problem enables the use of highly efficient solving procedures and guarantees finding the global optimum [50, 13]. The solving procedures used for convex problems are *gradient-based*, meaning they search the design space based on the derivatives of the objective and constraint functions. This causes the process to converge in a relatively low number of iterations. However, these algorithms only work efficiently if the gradients can be calculated without high computational cost and when there are no local optima other than the global optimum.

Unfortunately, most structural engineering problems are concave [13]. Should one use a gradient-based solving strategy, chances are the solution gets stuck in a local optimum when the starting parameters are chosen with bad luck. This is illustrated in figure 4.4a. When starting in point A, the optimum can be found. However, starting in point B will result in the local optimum, which is undesired.

**(a)** Gradient-based optimisation                                        **(b)** Heuristic optimisation
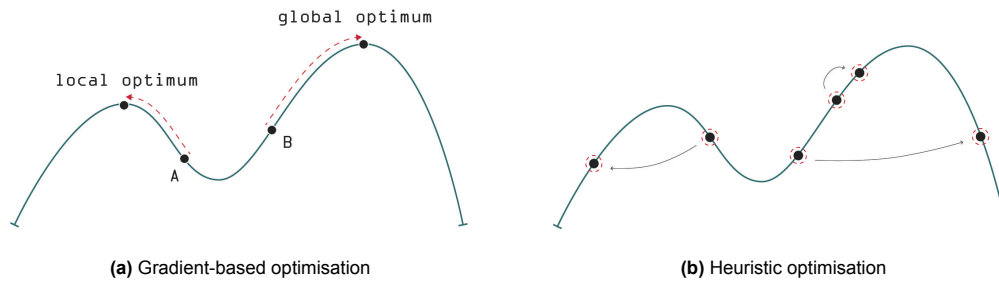
## Heuristic programming

A solution to this problem is the use of heuristic methods. A heuristic, or heuristic technique, is *any approach to problem-solving that uses a practical method or various shortcuts in order to produce solutions* [12]. When using these, finding the global optimum is not guaranteed. Yet heuristic methods are capable of finding good solutions and they overcome the main concerns one would have when using a gradient-based method on a concave problem. This is why they are commonly used in engineering practice [13, 20].

Whereas gradient-based methods start with one design variant and find a better solution in each iteration, heuristic methods try a set of variants simultaneously and find a next set partly random and party based on the performance of the variants. This means some variants can be worse than previous ones.

The feature of randomness holds both the advantages and disadvantages of heuristic methods. Because of the partly random search of the design space, the search can be inefficient and there is no guarantee to find the optimal solution. The main advantage is that it enables the escape of local mimima. On top of that, heuristic methods can be applied to discrete problems and are easy to implement, since no gradients are needed.

Schematically, a global search of the design space is shown in figure 4.4b. It can be seen that the method differs from the gradient based methods shown in figure 4.4a in that it might temporarily go to worse solutions. It can also be seen that variants in the entire design space can be investigated, with exploration around certain points. Note that a realistic visualisation depends on the specific heuristic method.

### Types of heuristic methods

There is a wide variety of heuristic methods described by Hare [20]. Hare distinguishes three categories, a short overview of which is given here.

The first and most commonly used category of heuristic methods are evolutionary algorithms. These methods are inspired by natural evolution and follow the concepts of selection, recombination, mutation and reproduction to come to an optimised solution. They have been found quick in finding good solutions and are fit for problems with many variables. The downside is that they have to maintain large populations of candidate solutions, which make them somewhat unfit for problems with a small amount of variables.

The second category are physical and stochastic algorithms, which are inspired by physical processes and the nature of stochastic processes. Examples of these processes are the transition of a light ray from one medium to another or the annealing process in material science. They have often been found successful in acquiring good solutions and are design to escape local minima. The latter characteristic however can cause difficulty in finding convergence. Hence stochastic algorithms are often used in combination with other algorithms.

The last category is the swarm algorithms. They are based on self-organising systems in nature, because often simple rules are employed to develop efficient system behaviour. Examples are a bee colony's search for food or the flocking behaviour of a group of birds.

### Artificial Bee Colony

Van der Laan [50] has done an extensive literature study about which method is best for structural optimisation. A definite conclusion was hard to draw because all methods have (dis)advantages and studies usually compare just a few methods on a specific application. For the optimisation of stiffened

24

plates in an orthotropic steel bridge deck, he has chosen the swarm-based Artificial Bee Colony algorithm (ABC). This method is suitable in the context of this thesis too, because of the following reasons.

- Even though it is a relatively new method, it has shown good results in comparative studies.
- It possesses the so-called elitism property, which means that it only remembers better problem solutions. This results in a large time reductions when the calculation of the objective function is computationally cheap, while the evaluation of the behavioural constraints is not. This is often the case in structural engineering problems, see for example the mass optimisation of a truss structure. In this example, the total mass simply follows from the element lengths and the sections, whereas for the behavioural constraints a finite element analysis is needed. If the algorithm finds a solution with a higher mass, it can skip the FE analysis and move on to a new variant.
- It requires less tuning parameters than other swarm-based methods. This is beneficial since finding good values for these can be time-consuming. Next to the usual population size and stopping criterion, it only needs a limit value, which will be explained in section 4.3.
- In each iteration there are several independent variants, which makes it possible to run the algorithm on several servers at the same time, reducing computation time. This benefit is not directly valuable for this thesis, though it can improve its future applicability.

In the next paragraph the Artificial Bee Colony algorithm is explained in more detail.

## 4.3. Principle of the Artificial Bee Colony algorithm

The Artificial Bee Colony (ABC) algorithm is inspired by the food foraging behaviour of honey bee swarms. In bee colonies, some bees look for food sources, while others wait for information on where to help searching and get the nectar. The swarm also shares information about whether or not a food source still contains nectar. In the ABC algorithm, a food source is a design variant and the amount of nectar stands for the performance of the design variant.

The method uses three types of bees; scout bees, employed bees and onlooker bees. Scout bees start the optimisation process by randomly flying in the design space in search for food sources. Then employed bees check how much food there is at a certain source. In other words, they check the performance of that design variant by evaluating the objective function. Based on this performance, the employed bees assign a probability to their food source with equation 4.2 [50].

$$p_i = \frac{f\left(x_i\right)}{\sum_{n=1}^{N} f\left(x_n\right)} \tag{4.2}$$

In this equation, $x_i$ is the considered food source, $f$ is the objective function and $N$ the number of food sources at that moment in the optimisation process.

The onlooker bees use this information to look in the neighbourhood of the food sources with high probabilities. That is to say, they explore the design space around a well-performing design variant. When they find a new source with a higher amount of nectar, the new variant replaces the one found by the employed bee in the collective memory of the bee colony. The employed bee then comes back and chooses a new variant in the neighbourhood.

If the onlooker bees fail to find a better solution within a certain number of attempts, the food source is abandoned and the employed be belonging to the food sources becomes a scout bee. This bee can then again fly to a random unexplored area in the design space. The number of attempts per food source is determined by the limit, which needs to be chosen when setting up the algorithm.

New food sources are chosen by the onlooker bees and the employed bees with equation 4.3.

$$v_{ij} = x_{ij} + \phi_{ij}\left(x_{ij} - x_{kj}\right) \tag{4.3}$$

In this equation, $v_{ij}$ is the new design variant, $\phi_{ij}$ is a random number between -1 and 1, $j$ a random design variable and where $k$ selects a random employed bee. [20] has summarised the procedure of the ABC in figure 4.5.

```
procedure ArtificialBeeColony
begin
  Initialize n, limit, food positions x_i for i = 1, …, n each with
    dimension d;
  Evaluate the fitness of each food position;
    while (not termination condition) do
    begin
      Employed phase:
        Produce new solutions with k ∈ {1, …, n}, j ∈ {1, …, d},
        ϕ ∈ [0, 1] at random according to υ_ij = x_ij + ϕ_ij · (x_ij − x_kj);
        Evaluate solutions;
        Apply greedy selection for employed bees;
      Onlooker phase:
        Calculate probability values for each solution x_i
        according to P_i = f_i / (Σ_{j=i}^{n} f_j);
        Produce new solutions from x_i selected using P_i;
        Evaluate these solutions;
        Apply greedy selection for onlooker bees;
      Scout phase:
        Find abandoned solution:
          if limit exceeds
            Replace with new random solution;
          end
        Update best solution;
    end
end
```

**Figure 4.5:** ABC procedure [20]

# 5

# Design, modelling and assessment of the case study

In this chapter the design of the timber Dafne Schippers bridge as well as the modelling and assessment is explained.

## 5.1. Design

A cable-stayed bridge was chosen because all modern long-span footbridges are cable-stayed and thus this type of structure seems to be the most feasible option. As the basis of a cable-stayed footbridge design, several design decisions can be made. These, as explained in section 2.4, are whether or not to include the parts outside the main span in the structural system, the type of deck, to what extend the railing has a load-bearing function, the height and shape of the pylons and the amount and configuration of the cables.

To improve the dynamic behaviour, in general an increase in the natural frequencies is desired, which can be accomplished by a higher stiffness to mass ratio [41]. In the parameter study, three parameters that were expected to influence this ratio were selected for studying their influence on the dynamic behaviour, namely the pylon height, the pylon shape and the amount of cables. The pylon height was chosen because it increases the vertical stiffness, without changing the vibrating mass, provided the dimensions of the deck are not adjusted based on the pylon height [41]. The same applies to the relation between the pylon shape and the torsional stiffness. The number of cables was chosen since an increased number of cables can affect both the material use and stiffness of the bridge.

The design of the bridge was made as shown in figure 5.1. Note that this design should be seen as a starter design in which the height and shape of the pylons, the cables, and the dimensions of the members are variable. The outside deck parts are included in the structural system because it enables a more efficient transfer of forces and reduces tension forces in the foundation and because it is possible on the location of the case study. The steel beams are integrated in the deck because this saves construction height and results in a more efficient transfer of forces, though it might compromise on the stiffness of the deck. The deck consists of two main girders and crossbeams because the spans are too big to be realistic for a mass timber deck, unless a high amount of cables is used. Double pylons are chosen because one pylon is difficult to achieve from a structural point of view and most likely not economically feasible. Finally, a fan cable configuration was chosen because all pedestrian bridges considered in this thesis are built this way since it is more efficient. For nearly all decisions it goes that the other options would be interesting to investigate too, though for the sake of time, the most interesting or feasible options were chosen for the starter design.

As explained in section 2.3, it is important to ensure durability of the timber. A softwood specie was chosen because of the availability in Europe. Since it does not have sufficient natural durability and since problems have been reported when using acelytated timber as construction material, it was chosen to ensure durability by cladding the main structural parts, namely the pylons and the main beams, as was done with the Älvsbacka bridge. The timber crossbeams are protected by the deck, which has a watertight layer.

## 5.2. Modelling

Two methods for making a parametric model were considered, namely the parametric modelling tool Grasshopper in combination with the finite element program GSA, and python in combination with GSA.

**Figure 5.1:** Starter design

Python was chosen in favour of the more intuitive Grasshopper, because the communication between the parametric model and GSA proved to be smoother and processing the results is easier in python. Also the script to automatically determine the type of modes, needed for calculating the maximum accelerations, was written in python. GSA was chosen since it is the FE package developed and used by Arup.

Table 5.1 shows the members of the bridge with the corresponding materials, sections, elements and element sizes. They will be explained in the following paragraphs. An overview of the different members is shown in figure 5.2.

| Member | Material | Material code | Section type | Element | Mesh size [m] |
|---|---|---|---|---|---|
| Main beam | Timber | GL32h | Rectangular | Beam | 3 |
| Cross beam | Timber | GL32h | Rectangular | Beam | deck width / 2 |
| Pylon | Timber | GL32h | Square | Beam | 3 |
| Cross beam pylon | Timber | GL32h | Rectangular | Beam | deck width / 2 |
| Pylon supportbeam | Timber | GL32h | Rectangular | Beam | deck width / 2 |
| Cable | Steel | S1860 | Round | Bar | - |
| Steel beam | Steel | S355 | SHS | Beam | deck width / 2 |
| Bracing deck | Steel | S355 | Round | Bar | - |
| Bracing pylon | Steel | S355 | Round | Bar | - |

**Table 5.1:** Member properties
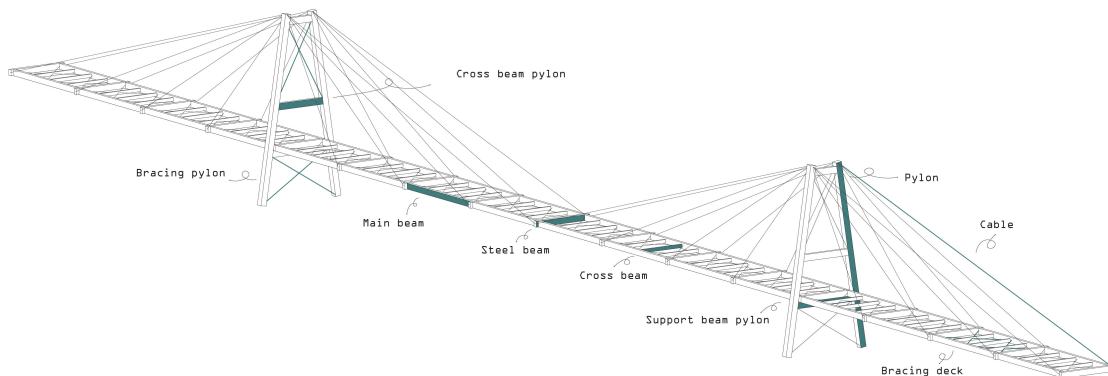


**Figure 5.2:** Names of the members in the model

28

**Materials**

To choose the glulam grade, the material properties of the Älvsbacka bridge were consulted. There, GL40c was applied, which is uncommon and therefore potentially expensive. Therefore, the more common GL32h was chosen for all timber members. A homogeneous section was selected because when using combined sections the strength of individual fasteners varies over the height of the sections, which results in difficulties when making a parametric model [46]. In the Bridon Structure Brochure [9], two possible types of cables for architectural footbridges are recommended: locked coil strand and spiral strand. The locked coil cables are chosen because they have good corrosion resistance and because they also have been used for the Dafne Schippers bridge. S355 was chosen for the steel beams and the bracing, since that is common in bridge design. Detailed material properties can be found in appendix C.1.

**Sections**

As can be seen in the table, the sections of the main beam and the cross beams are rectangular. The dimensions vary based on the optimisation, but the width is always half of the height to limit the amount of variables and thus computation time. It was checked that this way the width of the beam was not governing and still resulted in reasonable unity checks. In imitation of the Botterbrug in Harderwijk, a square hollow section with a wall thickness of 15 mm was chosen for the steel beams.

**Finite elements**

Timoshenko beam elements are used for all beams and columns of the bridge. When choosing the element size, several aspects need to be taken into consideration. First of all the accuracy of the results; halving the element size should not lead to significant changes in the results. Secondly the computational cost; both the time for running the analysis and saving the outputs increase exponentially when increasing the amount of elements. Thirdly, for finding reliable results in a modal analysis it is important to have approximately 10 nodes in each wave of a mode shape. And finally it is common practice in bridge modelling to have one element between each point where members meet. These considerations have led to the element sizes shown in table 5.1. More information about the influence of different element sizes on the model can be found in appendix G.3.

Bar elements are used to model the cables and the bracing because the use of nonlinear cable elements is not possible in a modal analysis. This simplification is possible under the assumption that the cables will always be in tension. For the cables it is reasonable to assume this is true. If the cables were in compression in some load cases, a pretension would be needed. With a form finding analysis the value of the pretension force was checked. The outcome was less than 1% of the force in the cable due to only it's own mass. Therefore it was concluded that the assumption is valid for the cables.

The assumption that the bar elements are always in tension, is not valid for the bracing elements. In load cases with vertical loading they were all in compression and in load cases with lateral wind loading, half of the bracing was in compression. In order to have a realistic distribution of forces, it was decided to exclude the compression elements from the analyses. As a result, no bracing elements are taken into account in vertical load cases and only the bracing elements in tension are taken into account in load cases with lateral loading. This is shown in figure 5.3.

Original situation with all bracing

Only tension elements in lateral load cases and modal analysis

No bracing elements in vertical load cases
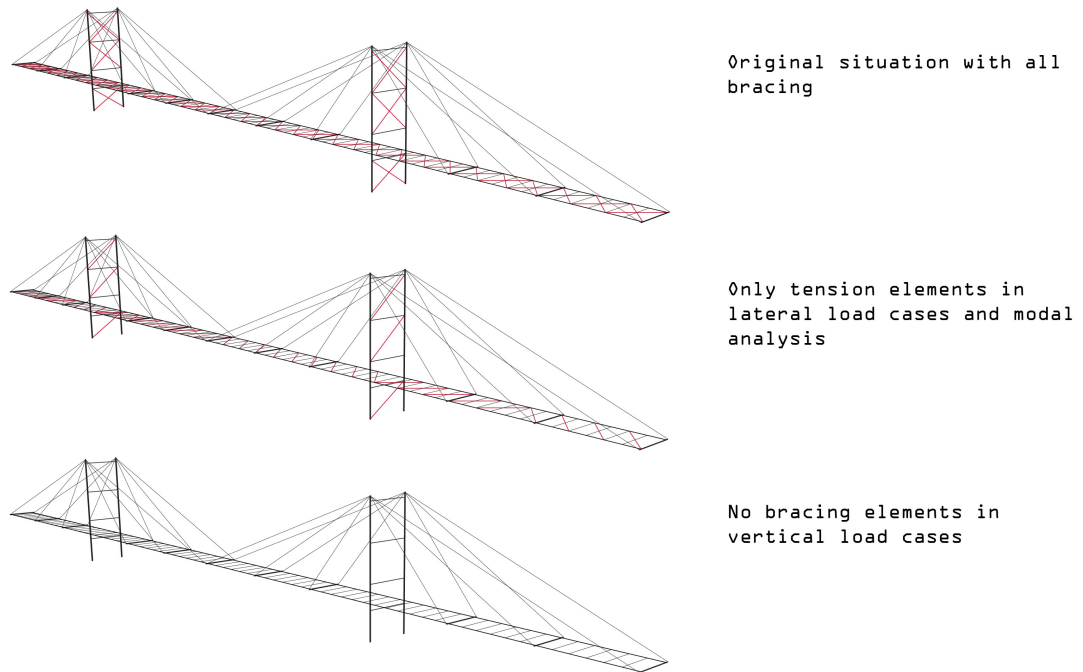
**Figure 5.3:** Modelling bracing elements in different load cases

**Boundary conditions**

The boundary conditions of the bridge are shown in figure 5.4. Since all pedestrian bridges with timber pylons consulted for this thesis, are hinged at the bottom (figure 5.5), this is done in the model too. The deck is supported by the foundations (location A and B) and by the supporting beam of the pylons (location C and D). At each location, the deck is supported on the left and the right hand side. In x-direction, the deck is restrained in location A and free in the other locations to allow for expansion due to moisture content and temperature changes. For the same reason, the deck is restrained in y-direction at the right hand side of the bridge and free at the left hand side. The connection between the deck and the pylon was modelled by spring elements with a different stiffness in different directions. A stiffness of 10 ($N/m$ or $Nm/rad$) represents a free direction, a stiffness of $1E+13$ represents a restrained direction. A summary of the boundary conditions is given in table 5.2 and 5.3. The stiffness of 10 ($N/m$ or $Nm/rad$) can be seen as zero, but was needed to avoid singularities.

In a later stadium, it was found that moment equilibrium around the x-axis was not satisfied with these springs because the difference in stiffness between the restrained and the free directions was too high. This could not be resolved by changing the stiffness of the springs. Therefore link elements with similar properties were used to evaluate the maximum accelerations in the parameter studies. In the optimisation study that included dynamic behaviour to obtain a design without the need of dampers, link elements were used.
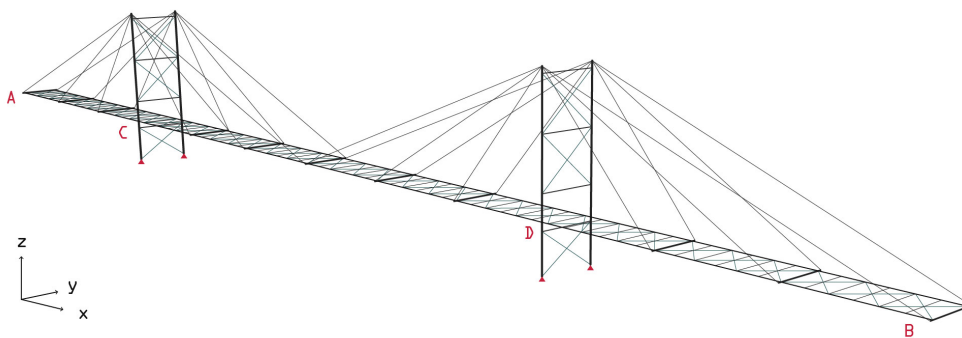


**Figure 5.4:** Boundary conditions

Cable-stayed bridge Älvsbacka   Cable-stayed bridge Neckarsteg

**Figure 5.5:** Hinged pylons

| Location | Restrain in x | Restrain in y | Restrain in z |
|---|---|---|---|
| Pylon foot | yes | yes | yes |
| A right | yes | yes | yes |
| A left | yes | no | yes |
| B right | no | yes | yes |
| B left | no | no | yes |

**Table 5.2:** Boundary conditions in location A and B and the pylon foot

| Location | $k_x$ [N/m] | $k_y$ [N/m] | $k_z$ [N/m] | $k_{xx/yy/zz}$ [Nm/rad] |
|---|---|---|---|---|
| C right | 10 | $1E+13$ | $1E+13$ | 10 |
| C left | 10 | 10 | $1E+13$ | 10 |
| D right | 10 | $1E+13$ | $1E+13$ | 10 |
| D left | 10 | 10 | $1E+13$ | 10 |

**Table 5.3:** Boundary conditions at location C and D

## 5.3. Assessment

**Static assessment**

For the static assessment, the self-weight, the permanent load, the pedestrian load and the wind load were taken into account. Member checks are performed on the main beams, the cross beams, the pylons and the cables. In each design variant it is checked whether it is possible to design a connection between the main beams and the steel beams and between the cross beams and the main beams. How this is done exactly can be consulted in appendix C, together with more information about the exact loads, load combination and checks.

**Dynamic assessment**

The dynamic assessment assesses the effect of groups of people walking along the bridge. Loading by joggers is not taken into account. With the type of assessment used for groups of people, this often gives a conservative result, which would make the results less realistic. To realistically assess the influence of jogger loading, an analysis with a moving load would be needed, which was outside the scope of this thesis.

The dynamic assessment of the bridge consists of a modal analysis, a script that determines the type of each mode and the computation of the maximum accelerations in lateral and vertical direction. The first and the third step are explained in detail in appendix D. The second step is explained here.

**Mode shape determination**

The outcome of a modal analysis by GSA consists of modal displacements and a dynamic summary, including the natural frequencies and modal mass per mode. To be able to calculate maximum accelerations, the type of mode needs to be known as well. In the range of frequencies relevant for the dynamic

analysis, four basic types of modes occur: lateral, vertical, torsion and pylon modes. Combinations of these are possible too.

Usually, the classification of modes happens by hand, but to include dynamic behaviour in an optimisation process, this needs to happen automatically. Therefore a script was written to automatically determine the type of mode. The input is a file with the modal displacements of the calculated modes. For each mode, the script determines the type of mode and whether or not it should be taken into account in the calculation. This procedure is visualised in figure C.10.
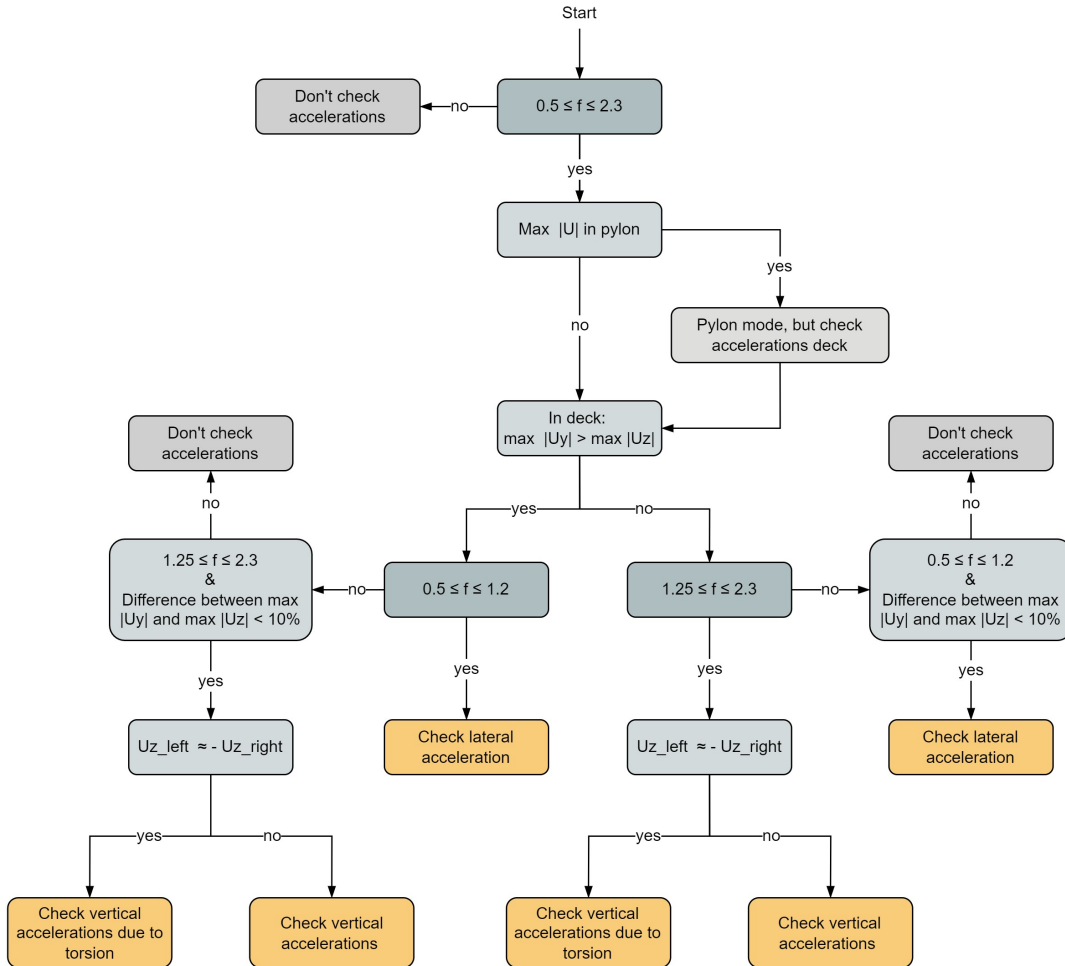


**Figure 5.6:** Determination of mode types in the python script

A mode is classified based on the maximum displacement. If the maximum displacement is in the pylon, it is considered a pylon mode. If the deck has modal displacements too, a pylon mode can still be induced by pedestrian loading. This is why they are treated the same way as deck modes. In the deck, the mode can be lateral, vertical or torsion. The maximum displacement is either in y- or in z-direction. If the displacement in z-direction is larger than the displacement in x-direction, it can be a vertical or a torsion mode, otherwise the mode is lateral. If the left and the right side of the deck have more or less opposite displacements, the mode is classified as torsion.

As mentioned before, combined modes exist too. However, one direction will be the leading direction, meaning that it is the direction in which the load is applied. The vibration in the other direction is seen as a result of the first. Therefore only the leading direction (the direction with the largest modal displacement) is taken into account in the calculation. However, if the difference between the two directions is less than 10%, both directions will be checked, to prevent unconservative results. If the frequency of the mode falls outside the range that needs to be checked, the mode isn't considered in the calculation. A few examples of modes are given in appendix D.

# 6

# Parameter study

As explained before, the research in this paper consists of two parts, the parameter study and the optimisation that takes into account dynamic behaviour. This chapter deals with the former. The parameters are explained, followed by the set-up of the optimisation problem and a description of the different parts of the parameter study. The results are presented in the next chapter.

## 6.1. Introduction

In chapter 5 it was explained that the three parameters that are studied in this thesis, are the height of the pylons, the shape of the pylons and the amount of cables.

These three parameters, the *studied parameters*, are shown in figure 6.1. The amount of cables is defined as the amount of cables on half of the main span, so a cable number of 3 actually represents 12 cables on the left and right side of the bridge (24 in total). The pylon height is defined as the height above the deck. Since the height of the deck is set to 6.63 m, a pylon height of 20 m represents a total pylon height of 26.73 m. The shape of the pylon is defined as the distance the top of the pylon has moved inwards or outwards compared to the straight version, when the pylon column rotates around the point where it connects to the deck. An inwards movement is represented by a positive number, while a negative number represents an outward movement.
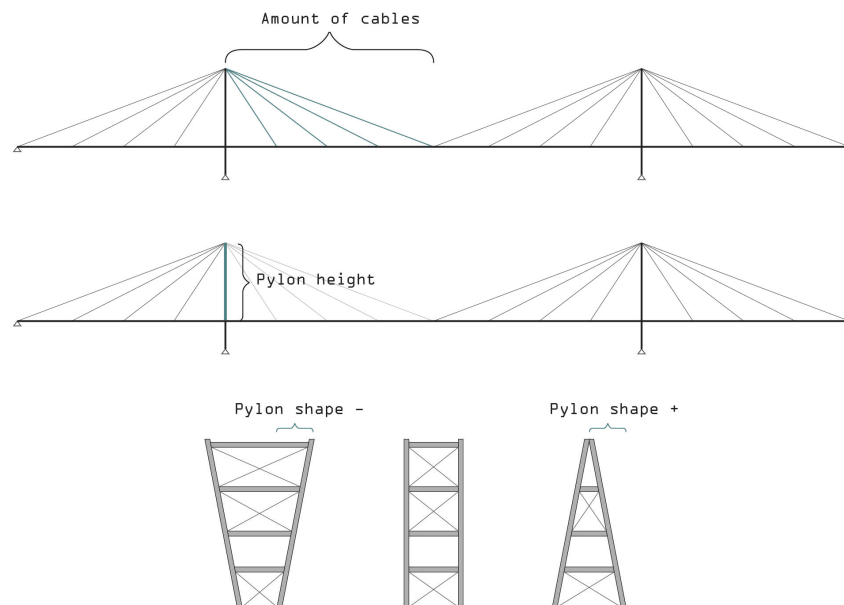


**Figure 6.1:** Studied parameters

All studied parameters are evaluated at different values. In the example of the cables, there can be 2, 3, 4, 5 or 6 cables. Just varying a parameter (e.g. increasing the amount of cables from 3 to 4), without changing other dimensions of the bridge, would lead to an unfair comparison between the two options. That is, it is not realistic to keep the same cable diameter when increasing the amount of cables, because they carry less load. To obtain reasonably realistic variants, the bridge model is

optimised for each value. The results of these optimisations are subsequently used to investigate the dynamic behaviour. This procedure is explained in more detail in section 6.4.

## 6.2. Types of parameters

In the optimisations, there are different types of parameters, which together form the parametric model, see figure 6.2. The *studied parameters* have been discussed above. We are interested in their influence on the dynamic behaviour of the bridge. How this is done exactly is explained in section 6.4.

*Optimisation parameters* are varied between a lower and a upper limit by the optimisation algorithm in order to find an optimised design after one of the studied parameters has been changed. The optimisation parameters chosen for the parameter study are the diameter of the cables, the section dimensions of the pylons, the height of the main beams and the height of the cross beams in the deck, because they are expected to have the biggest influence on the total mass and stiffness of the structure. The upper and lower limit values the optimisation parameters can differ per set of runs. Note that the columns of the pylon have a square section, inspired by the geometry of the Älvsbacka bridge in Sweden. This implies that a pylon dimension of 500 mm represents a 500 x 500 section.

As the name suggests, *dependent parameters* depend on the other parameters. They were introduced to limit the amount of variables and with that the time needed for an optimisation. The dependence, shown with the dashed arrows in figure 6.2, is defined in the python script by set expressions. The expressions are based on common practice or on the logic of the geometry. For example, the width of the main beam is always half of its height and the amount of bracings in the deck follows the amount of cables in the bridge. The dependencies are given in appendix F.

Finally, there are *fixed values*. They are either dictated by the design brief (e.g. the span) or expected to have a limited influence on the result (e.g. the height of the cross beams of the pylon). The values of the fixed values can be found in appendix F as well.
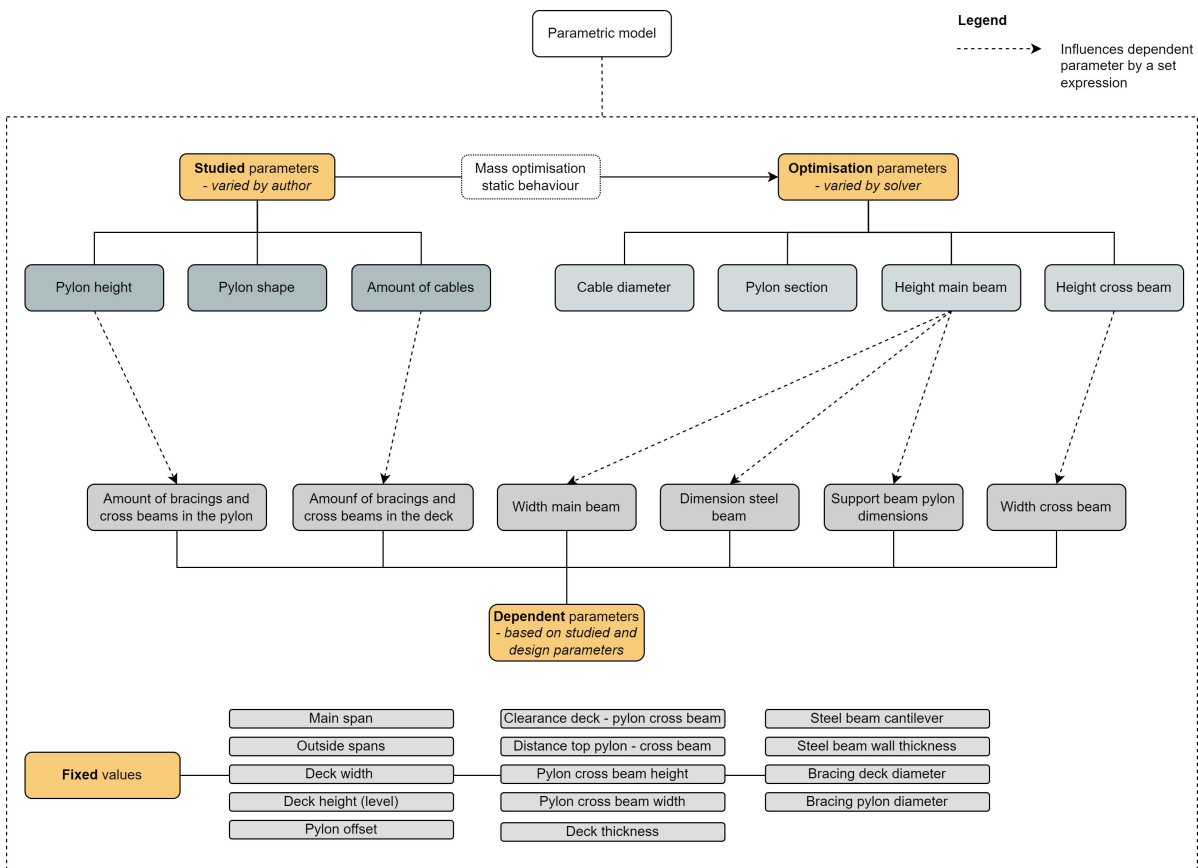


**Figure 6.2:** Parameters in the parameter study

## 6.3. Set-up of the optimisation problem

**Objective function**

Optimising the design of a bridge can have several meanings. It can for example involve minimizing the volume or mass of the materials, the costs or the environmental impact. In other words, several 'objectives' can be imagined, each with their own (dis)advantages.

The total volume of materials is straightforward to calculate. However, steel would be favoured over timber since it has more structural capacity per volumetric unit. In addition, labour cost, material cost or environmental impact would not be taken into account. Minimising the mass of the structure has the same (dis)advantages as the volume, except that it is more favourable for timber since steel has a higher density. If done well, minimising the cost can be a good option because it is a substantial factor in decision making. Yet, prices fluctuate, so the outcome of the analysis would depend on the time. On top of that, construction costs are hard to determine because they depend on many factors and no environmental impact is considered. Minimising the environmental impact serves a good purpose, but it is hard to determine, for example because the impact of transportation needs to be taken into account as well.

Ideally all aspects should be taken into account, weighed by their relative importance. However, within the scope of this thesis, it is not feasible to find meaningful values for all aspects and incorporate them well. Therefore it was chosen to optimise for mass since it gives an outcome that is easy to interpret, in contrast to for example cost or environmental impact.

The objective to minimise the mass is reflected in the objective function. As explained in chapter 4, the objective function consists of a value that needs to be minimised and a penalty function that accounts for the behavioural constraints. The objective function used in this research is as shown in equation 6.1, where $x$ are the optimisation parameters. The total mass is calculated with equation 6.2. The penalty function will be discussed below.

$$f_{\text{obj}}(x) = m_{\text{total}}(x) + f_{\text{pen}}(x) \tag{6.1}$$

$$m_{\text{total}}(x) = V_{timber}(x) * \rho_{\text{timber}} + V_{steel}(x) * \rho_{\text{steel}} \tag{6.2}$$

**Penalty function**

The penalty function is used to incorporate the behavioural constraints of the optimisation problem. The term decreases the performance of a variant that does not comply with these constraints. In this way, the total performance of the variant becomes such that it is very unlikely it will end up in the final solution.

In the parameter study, the behavioural constraint for the optimisation of the bridge is that the design should comply with ULS and SLS requirements. Thus, for each variant that is considered by the optimisation algorithm, unity checks (UCs) are calculated. The exact loads and checks can be found in appendix C.

The value of the penalty function is based on the UCs. For each UC that is higher than 1, the mass is increased by a high number and a value based on how high the UC is. By including this last term, the algorithm will favour a variant with a UC of 1.01 over a variant with a UC of 3, which helps searching the design space. The 'high number' is based on the order of magnitude of the total mass, which is $10e8$ kg. To make sure a variant with unity checks above 1 does not end up in the final result, the high number is set to 10.000.000.000, which is a factor 100 higher than the order of magnitude of the mass. The resulting penalty function is shown in equation 6.3, where $n$ is the amount of UCs.

$$f_{\text{penalty}} = \sum_{i=1}^{n} (10000000000 + (UC_i - 1) * 10000000000)_{\text{if UC}>1} \tag{6.3}$$

## 6.4. Parameter study

The parameter study is carried out in different parts.

- Part 1: In the first part, only the *optimisation parameters* are varied to evaluate their influence on the maximum accelerations. This was done to be able to explain variations in accelerations in later parts. Note that no optimisation takes place.

- Part 2: The second part is the main part. Here the influence of the *studied parameters* is investigated by varying a parameter (for example the amount of cables) and performing a mass optimisation in each step (part 2a). In order to understand the results better, the study is also done without optimising the models (part 2b). This gives insight in to what extent the results should be explained by the varying studied parameter or by the resulting change in dimensions.
- Part 3: In the last part, a set of verification studies is presented that investigate the influence of certain aspects on the results. These are the influence of other parameters, the influence of the damping value and the traffic class and the effect of connection stiffness.

The workflow part 2a is shown in figure 6.3. One can see that it starts by varying one of the studied parameters. The other studied parameters are kept at a fixed value. This is done in order to increase the chance of obtaining ease to interpret results. Then the optimisation of the model starts, using the Artificial Bee Colony (ABC) algorithm (section 4.3). The solver generates a set of optimisation parameters and based on these, the dependent parameters are calculated. With this, the entire model is defined and the mass can be calculated. If the mass is the lowest mass so far found at a certain food source, a GSA model is generated. Based on the outputs of the static analysis, the objective function is evaluated, which forms the basis for a new iteration. Once the optimisation is finished, a modal analysis is performed on the optimised model to calculate the accelerations. The settings of the algorithm were determined in a set of test runs, which is described in appendix G.
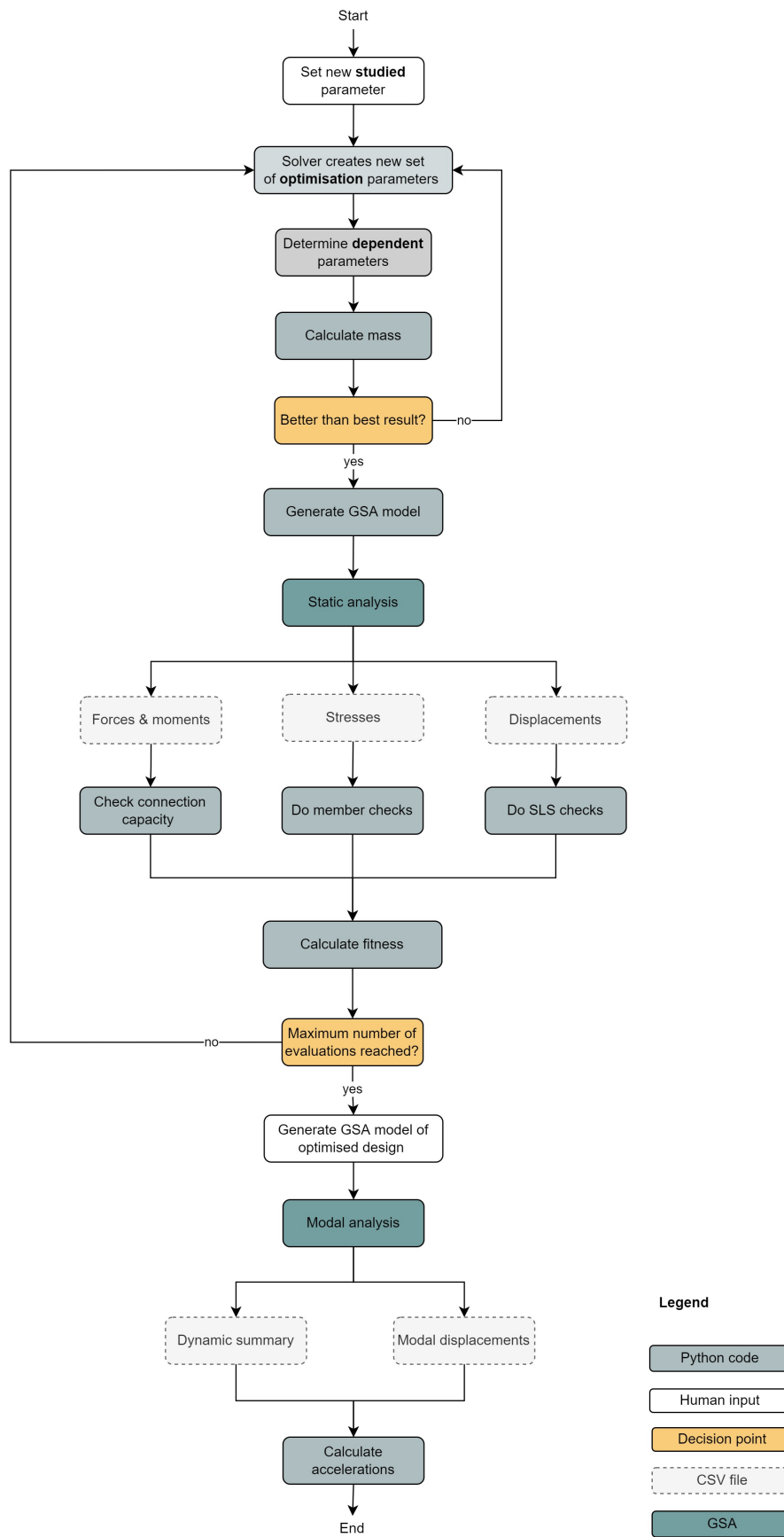
**Figure 6.3:** Overview parameter study - part 2a

A condensed version of the workflow of part 1 and part 2b are shown in figure 6.4. Since no optimisation takes place, a model that was the result of an optimisation in part 2a is taken as a basis. The process starts by setting a new parameter; an optimisation parameter in part 1 and a studied parameter in part 2b. With that, the entire model is defined and a modal analysis can be performed to calculate the accelerations in the final step.
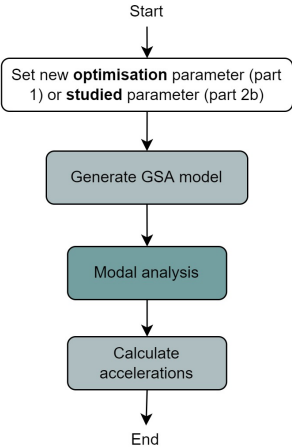


**Figure 6.4:** Overview parameter study - part 1 and part 2b

**Damping**

To calculate the maximum accelerations, a damping value is needed. Based on section 3.4, a damping value of 1.2% was deemed most realistic since it is just below the average value recommended in most codes and guidelines and it corresponds with the measured value of the Älvsbacka bridge which is similar in design to the bridge of this thesis. However, given the large uncertainty, the calculations are performed with a range of damping values. The lower bound of this range, 0.5%, is the lowest value found in literature and the upper bound, 3.0% is the highest value recommended in codes and guidelines.

# Results parameter study

In this chapter the results of the parameter study are presented. As explained in chapter 6, the parameter study consists of three parts. The first section of this chapter deals with part 1, the second with part 2 and the third section with part 3.

The results are presented as graphs, containing maximum accelerations on the y-axis and the varied parameter on the x-axis. The tables below each figure describe the type of the governing modes, which were explained in section 5.3, together with the natural frequency of that mode. The different mode types are given in table 7.1.

| Direction | Pylon mode | Name |
|---|---|---|
| Lateral | No | Lateral |
| Lateral | Yes | Pylon lateral |
| Vertical | No | Vertical |
| Vertical | Yes | Pylon vertical |
| Torsion | No | Torsion |
| Torsion | Yes | Pylon torsion |

**Table 7.1:** Mode names

To be able to understand the results, the $\psi$-factor is of importance, shown in figure 7.1. As explained in appendix D, this reduction factor reflects the critical range of vertical and lateral frequencies and is applied to the maximum acceleration of a mode. In the middle of the range, the value is 1, at the edge it goes linearly to zero. As a consequence of changing parameters, the natural frequencies of the governing mode change. When the $\psi$ becomes lower than 1, an other mode can become the governing mode which often causes a 'kink' in the results. Where relevant, the result with a constant reduction factor over the critical range of frequencies is shown in the graphs too.



**(a)** Vertical

**(b)** Lateral
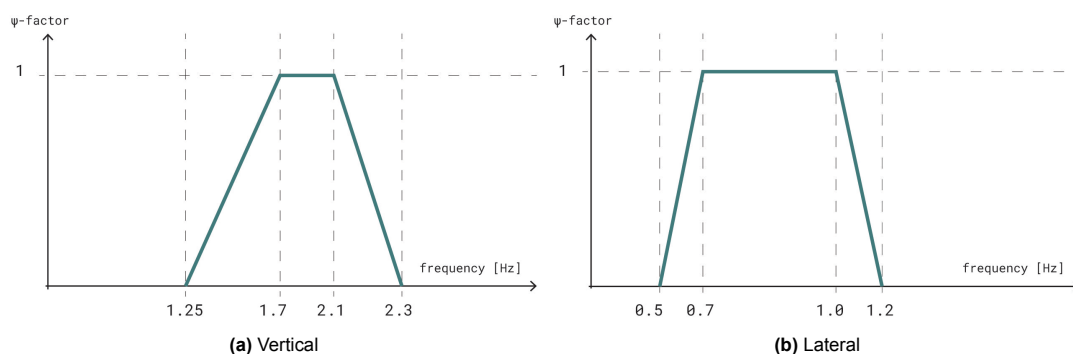
**Figure 7.1:** Reduction coefficient $\psi$ [23]

## 7.1. Part 1 - Influence of optimisation parameters

In this section the influence of only the optimisation parameters is investigated. These results are used later to find explanations for varying maximum accelerations in the parameter studies. Per optimisation parameter, the maximum vertical and lateral accelerations are shown for different values. These values

are selected such that they cover the range in which they appear in the optimisations of part 2a of the parameter study. For the different models, a basic model with the characteristics that were expected to be the most realistic after the optimisation runs of part 2 has been used. These are displayed in table 7.2.

| | Parameter | Value | Unit |
|---|---|---|---|
| Studied parameters | Pylon height | 15 | m |
| | Pylon shape | -1 | m |
| | Cables | 5 | - |
| Optimisation parameters | Cable diameter | 74 | mm |
| | Pylon dimension | 680 | mm |
| | Main beam height | 720 | mm |
| | Cross beam height | 400 | mm |

**Table 7.2:** Parameters in the standard model

**Cable diameter**
Figure 7.2 shows the vertical accelerations for cable diameters varying from 50 to 90 mm. In general a downward trend can be observed, though some results are higher than expected. Since treating torsion modes as vertical modes, which is done in this research, can be seen as conservative, the red line shows the results where the torsion modes are excluded. In this graph, the trend is clearer, although the higher values around 66 mm remain. When running the analysis on other basic models (different pylon height and pylon shape), higher values around some cable diameters were found too.
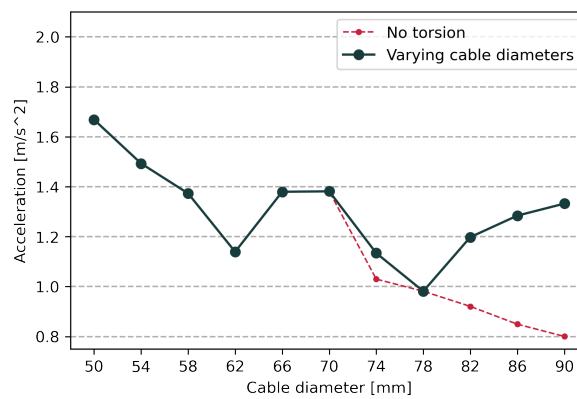


**Figure 7.2:** Vertical accelerations

| Diameter | 50 | 54 | 58 | 62 | 66 | 70 | 74 | 78 | 82 | 86 | 90 |
|---|---|---|---|---|---|---|---|---|---|---|---|
| Frequency | 1.99 | 2.12 | 1.84 | 1.73 | 2.01 | 2.08 | 1.69 | 1.89 | 1.95 | 1.99 | 2.04 |
| Type | vertical | vertical | vertical | vertical | vertical | vertical | torsion | vertical | vertical | torsion | torsion |

**Table 7.3:** Mode shape types. Examples of different types of modes are shown in appendix D.

Figure 7.3 displays the lateral accelerations for cable diameters varying from 50 to 90 mm. From the figure the conclusion can be drawn that a higher cable diameter has a diminishing effect on the lateral accelerations. The effect is most pronounced in diameters above 70 mm. This is because the natural frequencies drop below 0.7Hz, which causes the $\psi$-factor to become lower than 1. The red line in the graphs shows the result had the reduction factor been constant over the entire critical range of frequencies.
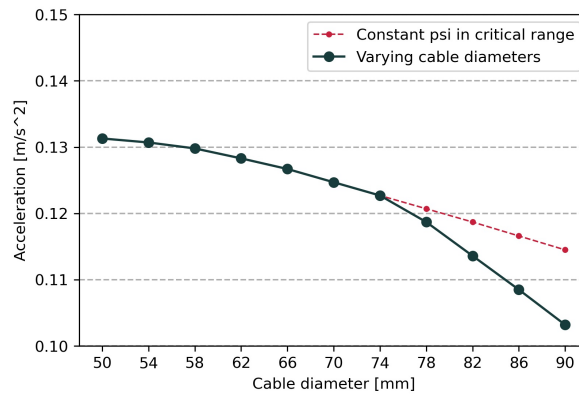
**Figure 7.3:** Lateral accelerations

| Diameter | 50 | 54 | 58 | 62 | 66 | 70 | 74 | 78 | 82 | 86 | 90 |
|---|---|---|---|---|---|---|---|---|---|---|---|
| Frequency | 0.73 | 0.72 | 0.72 | 0.71 | 0.71 | 0.71 | 0.70 | 0.70 | 0.69 | 0.69 | 0.68 |
| Type | lateral | lateral | lateral | lateral | lateral | lateral | lateral | lateral | lateral | lateral | lateral |

**Table 7.4:** Mode shape types

**Pylon dimension**

Figure 7.4 shows the effect of varying the pylon dimension on the vertical accelerations. Increasing the dimension of the pylon increases the maximum vertical accelerations, although the effect is small. A possible explanation is that with an increasing pylon section, the difference in stiffness between the pylon and the deck is enlarged, resulting in higher accelerations in the deck. The effect is most visible in smaller pylon sections. This is because for the lower dimensions, the frequency of the torsion mode becomes too low, causing the vertical mode to become governing.

Figure 7.5 shows that the dimension of the pylon has hardly any effect on the lateral accelerations, only a very small increase in natural frequency can be observed in the table, which corresponds to a very small decrease in accelerations.
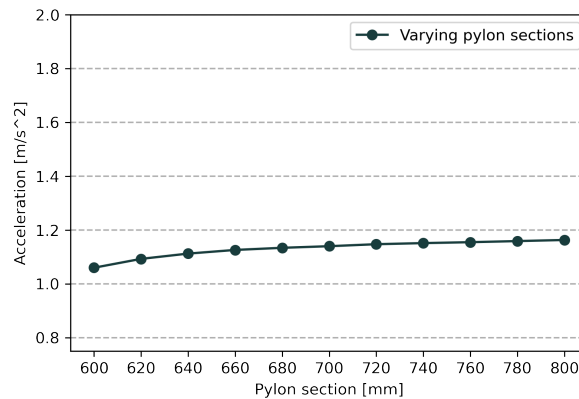


**Figure 7.4:** Vertical accelerations

| Dimension | 600 | 620 | 640 | 660 | 680 | 700 | 720 | 740 | 760 | 780 | 800 |
|---|---|---|---|---|---|---|---|---|---|---|---|
| Frequency | 2.143 | 1.685 | 1.686 | 1.687 | 1.687 | 1.687 | 1.688 | 1.688 | 1.688 | 1.688 | 1.688 |
| Type | vertical | torsion | torsion | torsion | torsion | torsion | torsion | torsion | torsion | torsion | torsion |

**Table 7.5:** Mode shape types
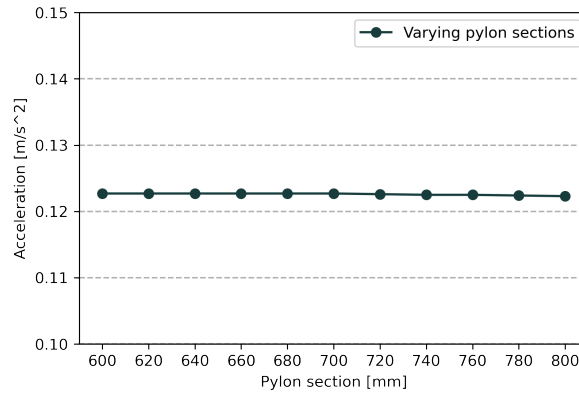
**Figure 7.5:** Lateral accelerations

| Dimension | 600 | 620 | 640 | 660 | 680 | 700 | 720 | 740 | 760 | 780 | 800 |
|-----------|-----|-----|-----|-----|-----|-----|-----|-----|-----|-----|-----|
| Frequency | 0.700 | 0.701 | 0.701 | 0.701 | 0.702 | 0.702 | 0.702 | 0.703 | 0.703 | 0.704 | 0.704 |
| Type | lateral | lateral | lateral | lateral | lateral | lateral | lateral | lateral | lateral | lateral | lateral |

**Table 7.6:** Mode shape types

**Main beam height**

In figure 7.6 it can be observed that the maximum vertical accelerations decrease with increasing main beam height and that the effect is most pronounced for smaller beam dimensions. This is because at beam height 660, the frequency of the governing vertical mode becomes larger that 2.1 Hz, causing the $\psi$-factor to become lower than 1. With higher beams, the torsion mode becomes governing, which results in lower accelerations. The result for a constant $\psi$-factor is shown in the graph too. Here the same vertical modes are governing.

In figure 7.7 the results for the lateral accelerations are shown. These increase slightly when the height of the main beam is increased from 600 to 690 mm. This is because the frequency of the first lateral mode approaches 0.7Hz, increasing the $\psi$-factor to 1. The overall decreasing effect of the height of the main beam is explained by the fact that the width of the main beam is dependent on the height, so that an increased main beam height also gives an increased lateral stiffness.
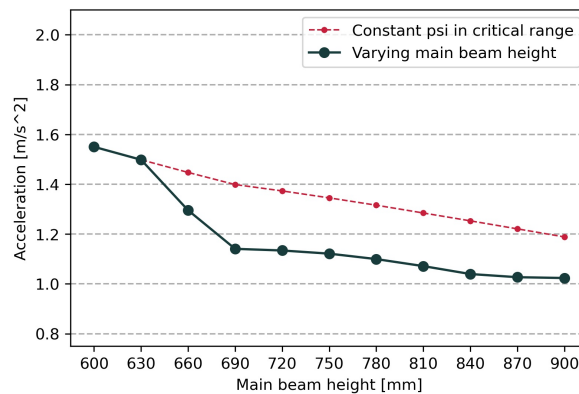


**Figure 7.6:** Vertical accelerations

| Main beam height | 600 | 630 | 660 | 690 | 720 | 750 | 780 | 810 | 840 | 870 | 900 |
|---|---|---|---|---|---|---|---|---|---|---|---|
| Frequency | 2.07 | 2.10 | 2.12 | 1.69 | 1.69 | 1.69 | 1.68 | 1.68 | 1.67 | 1.94 | 1.94 |
| Type | vertical | vertical | vertical | torsion | torsion | torsion | torsion | torsion | torsion | vertical | vertical |

**Table 7.7:** Mode shape types
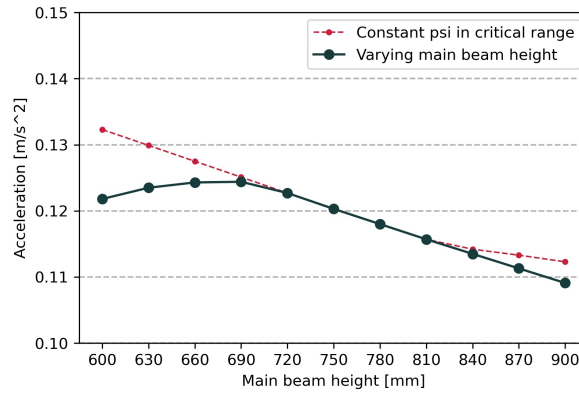


**Figure 7.7:** Lateral accelerations

| Main beam height | 600 | 630 | 660 | 690 | 720 | 750 | 780 | 810 | 840 | 870 | 900 |
|---|---|---|---|---|---|---|---|---|---|---|---|
| Frequency | 0.684 | 0.690 | 0.695 | 0.699 | 0.702 | 0.704 | 0.705 | 0.706 | 0.706 | 0.705 | 0.704 |
| Type | lateral | lateral | lateral | lateral | lateral | lateral | lateral | lateral | lateral | lateral | lateral |

**Table 7.8:** Mode shape types

**Cross beam height**

Figure 7.8 shows that increasing the cross beam height has a very modest decreasing effect on the vertical accelerations. The same can be said about the lateral accelerations, shown in figure 7.9.
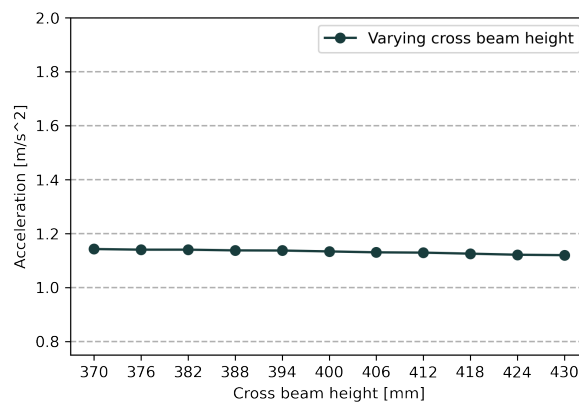


**Figure 7.8:** Vertical accelerations

| Cross beam height | 370 | 376 | 382 | 388 | 394 | 400 | 406 | 412 | 418 | 424 | 430 |
|---|---|---|---|---|---|---|---|---|---|---|---|
| Frequency | 1.690 | 1.689 | 1.689 | 1.688 | 1.688 | 1.687 | 1.686 | 1.686 | 1.685 | 1.684 | 1.684 |
| Type | torsion | torsion | torsion | torsion | torsion | torsion | torsion | torsion | torsion | torsion | torsion |

**Table 7.9:** Mode shape types
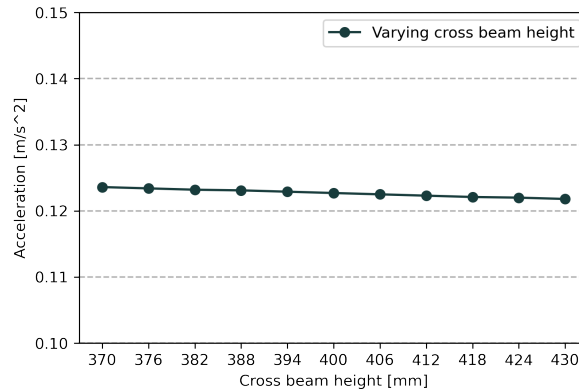


**Figure 7.9:** Accelerations lateral

| Cross beam height | 370 | 376 | 382 | 388 | 394 | 400 | 406 | 412 | 418 | 424 | 430 |
|---|---|---|---|---|---|---|---|---|---|---|---|
| Frequency | 0.703 | 0.703 | 0.703 | 0.702 | 0.702 | 0.702 | 0.701 | 0.701 | 0.701 | 0.700 | 0.700 |
| Type | lateral | lateral | lateral | lateral | lateral | lateral | lateral | lateral | lateral | lateral | lateral |

**Table 7.10:** Mode shape types

## 7.2. Part 2 - Influence of studied parameters

In this section the results of part 2 of the parameter study are shown. To make a fair comparison between each design variant, the model is optimised in each step. More information about the optimisations can be found in appendix F. In order to gain more insight in the results, the maximum accelerations without optimising the model in each step are shown too. For this, a standard model is used that was obtained with the optimisation.

### Pylon height

In table 7.11 the values of the studied parameters in the height runs are shown. The pylon height is varied between 13 and 23 meters, while the other two parameters have a constant value. The pylon shape of 0 was chosen because it is the middle value of the considered pylon shapes. The 4 cables were selected because it was deemed the most realistic based on the geometry of the Älvsbacka bridge. For the study without optimisation, the optimisation parameters of the optimised model with pylon height 15 have been used as a basic model.

Figure 7.10 shows how the distribution of cross beams and bracing in the pylon changes with the height.

| Studied parameter | Value | Unit |
|---|---|---|
| Pylon height | 13, 14, 15, 16, 17, 18, 19, 20, 21, 22, 23 | m |
| Pylon shape | 0 | m |
| Amount of cables | 4 | - |

**Table 7.11:** Studied parameters in height study
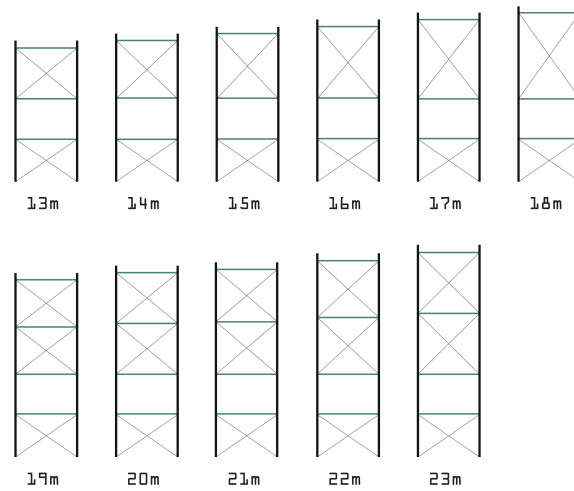
**Figure 7.10:** Heights pylons

**Result optimisation runs**

In figure 7.11 the total mass after the optimisation process is shown. Table 7.12 shows the corresponding values of the optimisation parameters. Note that in the optimisation runs a mistake was made in the calculation of the mass, so the values in the graph below do not correspond to the values shown in appendix F. However, since it was still a useful measure for the fitness of the design variants, it is deemed not to have influenced the results. In general, the mass increases with increasing pylon height. This is caused by a higher pylon in combination with an increasing pylon section and a higher main beam. The diameter of the cable decreases too, though it has a limited influence on the total mass. The height of the cross beams remain approximately constant. The exceptions are the mass of the models with pylon height 13, 14 and 15. This is caused by the higher main beam dimensions.
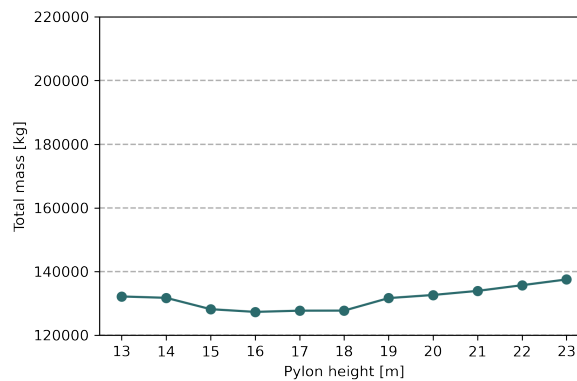


**Figure 7.11:** Total mass of models with different heights

| Pylon height [m] | Total mass [kg] | Cable diameter [mm] | Pylon dimension [mm] | Main beam height [mm] | Cross beam height [mm] |
|---|---|---|---|---|---|
| 13 | 132180 | 90 | 664 | 752 | 399 |
| 14 | 131754 | 81 | 672 | 756 | 400 |
| 15 | 128183 | 74 | 688 | 737 | 401 |
| 16 | 127334 | 69 | 703 | 731 | 400 |
| 17 | 127720 | 65 | 718 | 726 | 400 |
| 18 | 127736 | 60 | 736 | 721 | 399 |
| 19 | 131669 | 58 | 749 | 717 | 401 |
| 20 | 132646 | 54 | 763 | 715 | 400 |
| 21 | 133933 | 52 | 778 | 711 | 399 |
| 22 | 135717 | 49 | 792 | 710 | 399 |
| 23 | 137526 | 47 | 806 | 707 | 399 |

**Table 7.12:** Parameter results - height runs

**Accelerations**

Figure 7.12a shows the maximum vertical accelerations as a result of varying the height of the pylons. The results without optimisations do not show a clear trend. Trying find an explanation, the analysis was run with other basic models, in which other unclear graphs were obtained. An explanation could be that the height of the pylon has a big influence on the natural frequencies, causing several changes in the governing mode. An other explanation was sought in the distribution of cross beams and bracing in the pylon (figure 7.10). However, this can not explain the seemingly random shape of the graph, since the only abrupt change in the configuration of the pylon cross beams is between 18 and 19 meters, whereas the jump in the graph is just one amongst many. Using a constant reduction factor also does not help explaining the results.

With a few exceptions, the maximum vertical accelerations increase for the results with optimisations when increasing the height of the pylons. This might be explained by the decreasing cable diameters and the decreasing main beam heights. Also the height itself might increase the accelerations. The deviations from the trend might partially be explained by the big influence on the natural frequencies and with that the governing mode. Another explanation might be the changing cable diameter and main beam height, that cause higher accelerations around certain values. Whereas in the results without optimisations, the distribution of the cross beams in the pylon could not explain the results, here the jump becomes visible when the $\psi$-factor is 1 over the entire range of critical frequencies. This is shown in figure 7.12b.



(a) Part 2a and part 2b

(b) Part 2a and part 2a with constant $\psi$-factor
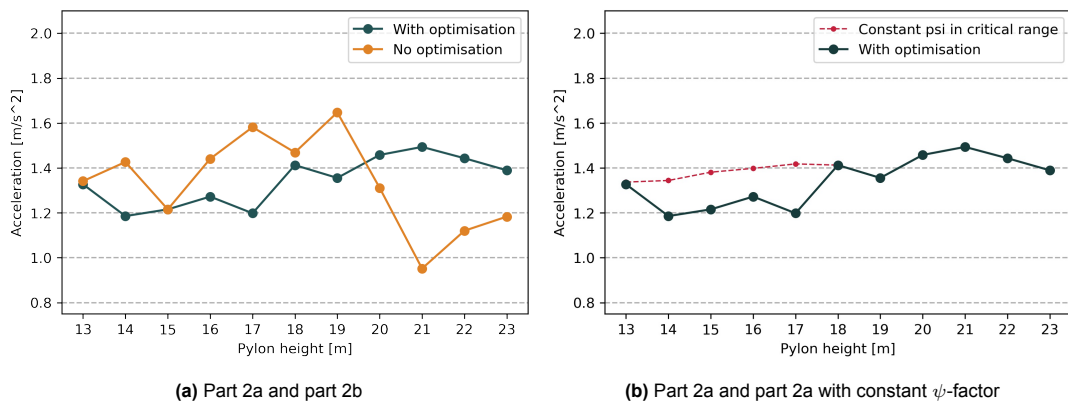
**Figure 7.12:** Vertical accelerations

46

| Pylon height | 13 | 14 | 15 | 16 | 17 | 18 | 19 | 20 | 21 | 22 | 23 |
|---|---|---|---|---|---|---|---|---|---|---|---|
| *With optimisation* | | | | | | | | | | | |
| Frequency | 1.89 | 1.88 | 2.12 | 2.12 | 2.13 | 2.10 | 1.76 | 1.74 | 1.72 | 1.70 | 2.06 |
| Type | vertical | torsion | vertical | vertical | vertical | vertical | torsion | torsion | torsion | torsion | vertical |
| *Without optimisation* | | | | | | | | | | | |
| Frequency | 1.63 | 1.71 | 2.12 | 1.94 | 2.01 | 2.07 | 2.07 | 1.80 | 1.91 | 1.83 | 1.87 |
| Type | torsion | torsion | vertical | torsion | torsion | torsion | pylon torsion | pylon vertical | pylon torsion | vertical | vertical |

**Table 7.13:** Mode shape types

Figure 7.13 shows the maximum lateral accelerations as a result of varying the height of the pylons. The accelerations in the models without optimisation slightly decrease with higher pylons. This leads to conclude that the height of the pylon has a very limited influence on the lateral accelerations and that the change in lateral accelerations of the results with optimisations is caused by the variation of the optimisation parameters rather than by the pylon height itself.

The results with optimisations show a clear trend of higher maximum accelerations with higher pylons. The reason for this is sought in the dimensions of the cable and the main beams that are larger for lower pylons and thus give more lateral stiffness.
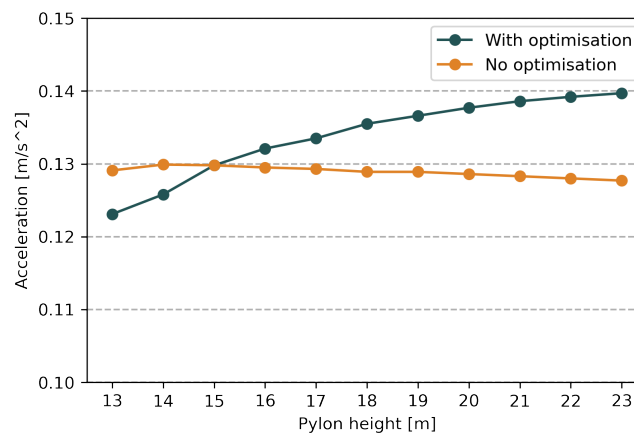


**Figure 7.13:** Lateral accelerations

| Pylon height | 13 | 14 | 15 | 16 | 17 | 18 | 19 | 20 | 21 | 22 | 23 |
|---|---|---|---|---|---|---|---|---|---|---|---|
| *With optimisation* | | | | | | | | | | | |
| Frequency | 0.71 | 0.72 | 0.72 | 0.73 | 0.73 | 0.74 | 0.74 | 0.74 | 0.74 | 0.74 | 0.75 |
| Type | lateral | lateral | lateral | lateral | lateral | lateral | lateral | lateral | lateral | lateral | lateral |
| *Without optimisation* | | | | | | | | | | | |
| Frequency | 0.72 | 0.72 | 0.72 | 0.72 | 0.72 | 0.72 | 0.72 | 0.72 | 0.72 | 0.72 | 0.72 |
| Type | lateral | lateral | lateral | lateral | lateral | lateral | lateral | lateral | lateral | lateral | laterall |

**Table 7.14:** Mode shape types

## Pylon shape

In table 7.15 the values of the studied parameters in the pylon shape runs are shown. Figure 7.14 shows a visualisation of the definition of negative and positive pylon shapes. The pylon shape is varied between -4 and 4 m, while the other two parameters have a constant value. The pylon height of 20 m was chosen because it was deemed a realistic height based on the dimensions of the Älvsbacka bridge. As was explained before, this applies to the selection of 4 cables as well. Pylon shape 0.5 was added since with that shape the cables are aligned with the z-axis. For the study without optimisation, the optimisation parameters of the optimised model with pylon shape 0 have been used as a basic model.

| Studied parameter | Value | Unit |
|---|---|---|
| Pylon height | 20 | m |
| Pylon shape | -4, -3, -2, -1, 0, 0.5, 1, 2, 3, 4 | m |
| Amount of cables | 4 | - |

**Table 7.15:** Studied parameters in shape study
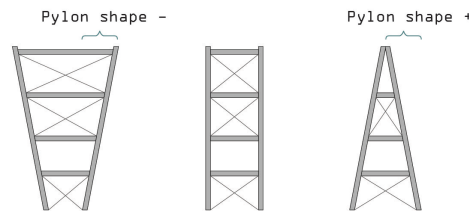


**Figure 7.14:** Negative and positive pylon shapes

**Result optimisation runs**

In figure 7.15 the total mass after the optimisation process is shown for each pylon shape. Table 7.16 shows the corresponding values of the optimisation parameters. Clearly, the influence of the shape of the pylons on the dimensions is small. The change in total mass is mainly caused by a decreasing pylon dimension and a decreasing length of the cross beams of the pylon. The diameter of the cables and the height of the main beams stay approximately constant. The height of the cross beams are constant too, except for the -3 and -4 variants. This is because in these models a very small tension force occurs in some of the cross beams, which becomes governing for the design (more information in appendix F).
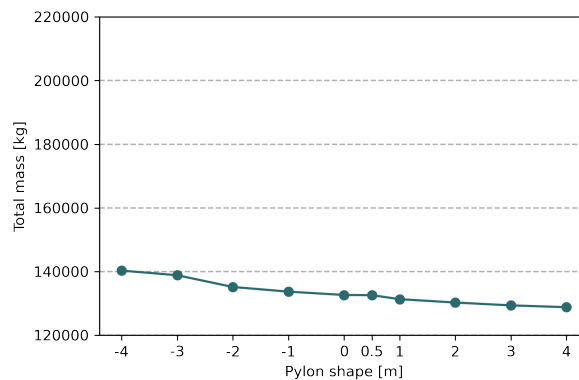


**Figure 7.15:** Total mass of models with different pylon shapes

| Pylon shape [m] | Total mass [kg] | Cable diameter [mm] | Pylon dimension [mm] | Main beam height [mm] | Cross beam height [mm] |
|---|---|---|---|---|---|
| -4 | 140307 | 55 | 773 | 715 | 433 |
| -3 | 138847 | 54 | 771 | 715 | 433 |
| -2 | 135157 | 54 | 766 | 714 | 399 |
| -1 | 133697 | 54 | 764 | 714 | 399 |
| 0 | 132646 | 54 | 763 | 715 | 400 |
| 0.5 | 132585 | 54 | 762 | 718 | 399 |
| 1 | 131328 | 54 | 761 | 715 | 400 |
| 2 | 130272 | 54 | 762 | 714 | 399 |
| 3 | 129382 | 54 | 762 | 714 | 400 |
| 4 | 128806 | 55 | 765 | 714 | 399 |

**Table 7.16:** Parameter results - shape runs

**Accelerations**

In figure 7.16 the maximum vertical accelerations as a result of varying the shape of the pylons is shown. The two lines are almost the same. This was to be expected since the variations in the dimensions shown in table 7.16 are small. This leads to conclude that the variation in acceleration is mainly caused by the shape of the pylon, rather than by changing dimensions.

For the V-shapes (negative shapes), the maximum vertical acceleration is approximately constant with a vertical governing mode. For the A-shapes (positive shapes), the acceleration increases till a maximum at pylon shape 1, after which it decreases again. Most of the governing modes for the A-shapes are torsion. These modes are present in the other models too, but result in lower accelerations than the vertical modes.

The notion that pylons do not add stiffness in vertical direction explains why the maximum accelerations remain constant in the models where vertical modes are governing. The maximum accelerations do change in models where the torsion modes are governing. This might be explained by the way the forces in the cables as a result of the rotating deck are transferred to the pylon. In models with V-shaped pylons the arm is large, as opposed to A-shaped pylons where the arm is small.
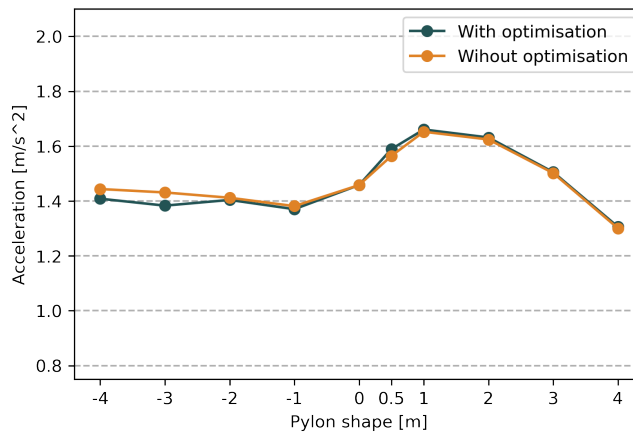


**Figure 7.16:** Vertical accelerations

| Shape | -4 | -3 | -2 | -1 | 0 | 0.5 | 1 | 2 | 3 | 4 |
|---|---|---|---|---|---|---|---|---|---|---|
| *With optimisation* | | | | | | | | | | |
| Frequency | 2.08 | 2.08 | 2.08 | 2.08 | 1.74 | 1.74 | 1.75 | 1.75 | 1.74 | 2.09 |
| Type | vertical | vertical | vertical | vertical | torsion | torsion | torsion | torsion | torsion | vertical |
| *Without optimisation* | | | | | | | | | | |
| Frequency | 2.08 | 2.08 | 2.09 | 2.09 | 1.74 | 1.75 | 1.76 | 1.76 | 1.75 | 2.08 |
| Type | vertical | vertical | vertical | vertical | torsion | torsion | torsion | torsion | torsion | vertical |

**Table 7.17:** Mode shape types

In figure 7.17 the maximum lateral accelerations as a result of changes in the shape of the pylon is shown. As was the case with the vertical accelerations, the two lines are almost the same. Based on this, the conclusion can be drawn that the variation in lateral accelerations is mainly caused by the shape of the pylon, rather than by changing dimensions.

The figure shows a clear trend of higher accelerations when the pylon changes from V-shape to A-shape. This is explained by the way the deck rotates in the lateral mode. In models with V-shaped pylons, the top of the deck is rotated towards the outside, see figure 7.18a. In models with A-shaped pylons, the top of the deck is facing inside. This difference can be understood by looking at figure 7.19, which shows the top view models with the two types of pylons and the way the cables connect to the deck.

The accelerations of pylon shape -3 and -4 do not follow the trend of the rest of the shapes. In the model with pylon shape -3 this is explained by the fact that the frequencies is below 0.7, causing the $\psi$-factor to be lower than 1. In the model with pylon shape -4, a pylon lateral mode is governing.
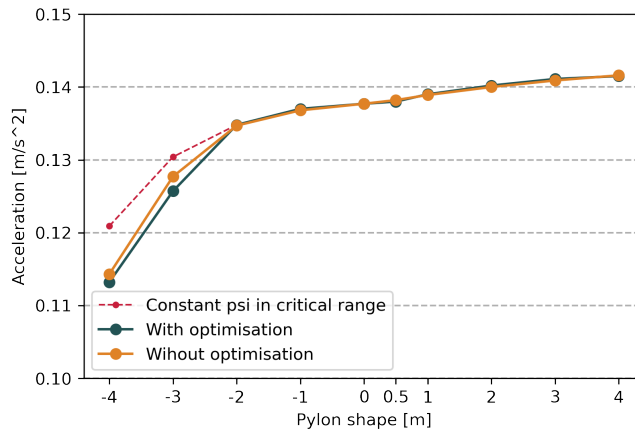
**Figure 7.17:** Lateral accelerations

| Shape | -4 | -3 | -2 | -1 | 0 | 0.5 | 1 | 2 | 3 | 4 |
|---|---|---|---|---|---|---|---|---|---|---|
| *With optimisation* | | | | | | | | | | |
| Frequency | 0.92 | 0.69 | 0.72 | 0.73 | 0.74 | 0.75 | 0.75 | 0.75 | 0.75 | 0.75 |
| Type | Pylon lateral | lateral | lateral | lateral | lateral | lateral | lateral | lateral | lateral | lateral |
| *Without optimisation* | | | | | | | | | | |
| Frequency | 0.93 | 0.70 | 0.72 | 0.73 | 0.74 | 0.75 | 0.75 | 0.75 | 0.75 | 0.75 |
| Type | Pylon lateral | lateral | lateral | lateral | lateral | lateral | lateral | lateral | lateral | lateral |

**Table 7.18:** Mode shape types



**(a)** V-shaped pylons
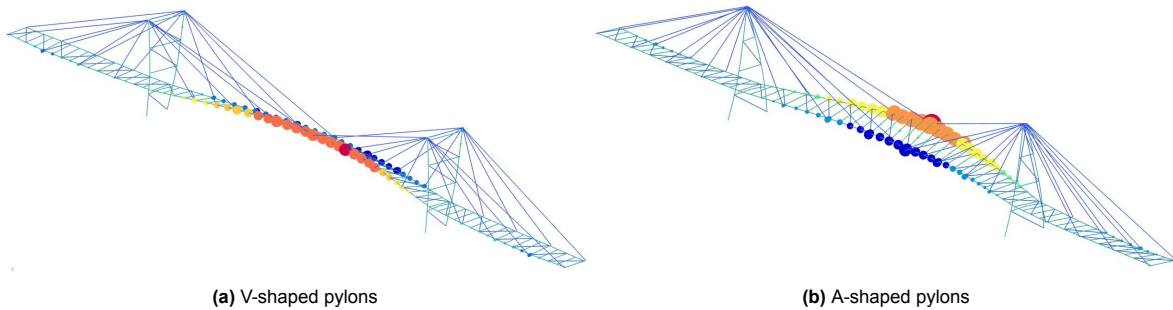


**(b)** A-shaped pylons

**Figure 7.18:** Rotation of the deck in lateral modes
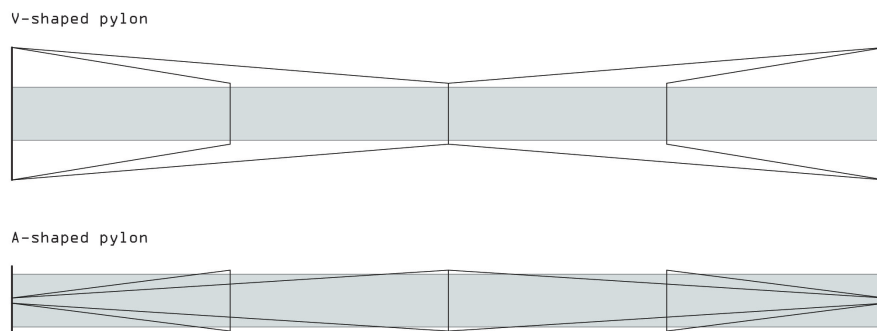


**Figure 7.19:** Top view of main span with a V-shaped and A-shaped pylon

## Amount of cables

In table 7.19 the values of the studied parameters in the height runs are shown. The amount of cables is varied between 2 and 6, while the other two studied parameters have a constant value, the explanation of which has been given before. For the study without optimisation, the optimisation parameters of the optimised model with 4 cables have been used as a basic model.

Figure 7.20 shows how the distribution of cross beams and bracing in the deck changes with the amount of cables.

| Studied parameter | Value | Unit |
|---|---|---|
| Pylon height | 20 | m |
| Pylon shape | 0 | m |
| Amount of cables | 2, 3, 4, 5, 6 | - |

**Table 7.19:** Studied parameters in cable study
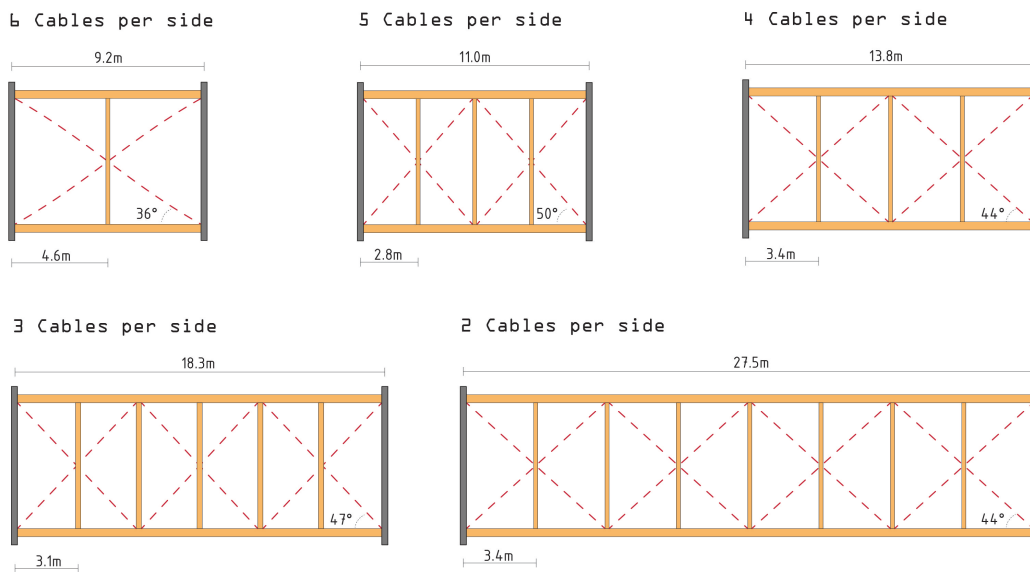


**Figure 7.20:** Crossbeams and bracing in the deck depending on the amount of cables

### Results optimisation runs

In figure 7.21 the total mass after the optimisation process is shown for each amount of cables. Table 7.20 shows the corresponding values of the optimisation parameters. It can be seen that the total mass decreases when the amount of cables is increased, which is mainly caused by a decreasing height of the main beam. The exception is the model with 6 cables. This can be explained by the fact that in this model the combined bending and tension becomes the governing UC for the main beam, as opposed to combined bending and compression in the other models. Therefore the dimensions increase.

51
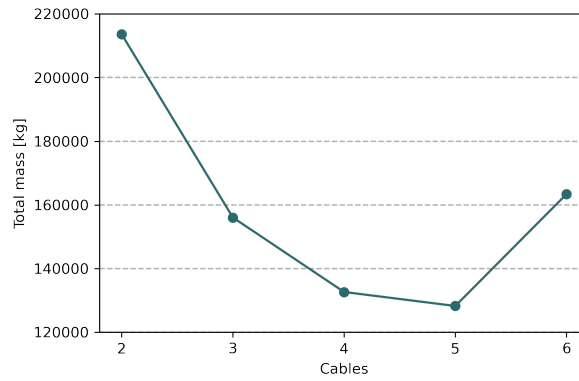
**Figure 7.21:** Total mass of models with different amount of cables

| Amount of cables | Total mass [kg] | Cable diameter [mm] | Pylon dimension [mm] | Main beam height [mm] | Cross beam height [mm] |
|---|---|---|---|---|---|
| 2 | 213610 | 64 | 780 | 1119 | 404 |
| 3 | 156039 | 57 | 767 | 851 | 387 |
| 4 | 132646 | 54 | 763 | 715 | 400 |
| 5 | 128249 | 53 | 763 | 653 | 375 |
| 6 | 163397 | 50 | 770 | 834 | 428 |

**Table 7.20:** Parameter results - cable runs

**Accelerations**

Figure 7.22 shows the maximum vertical accelerations as a result of varying the amount of cables. Looking at the green line of part 2a, it can be observed that going from 2 to 5 cables, the maximum vertical accelerations increase. This can be explained by the dimensions of the main beam and the cross beam, that decrease when more cables are added and thus give the bridge less mass and stiffness. The drop in the model with 6 cables is explained by the increase the optimisation parameters that was described before.

The line that represents the variation of the amount of cables without optimising the model (part 2b), is somewhat harder to interpret. The difference in maximum acceleration can not be explained by variation of the optimisation parameters and should be sought in the varying amount of cables and the resulting variance in the amount of cross beams, the amount of deck bracing and the angle of these bracings. With some imagination, and disregarding the model with 2 cables, a trend of decreasing maximum acceleration can be observed when increasing the amount of cables. The obvious explanation is that the extra cables increase the stiffness of the bridge. The low value in the model with 2 cables can be explained by the fact that there are no regular vertical modes in the critical frequency range and in the optimised model by the high main beam dimensions.

In both the trends, the value at 4 cables is lower than expected and/or the value at 5 cables is higher than expected. An explanation might be found in the angle of the bracing, knowing that a 45° angle is the most optimal for torsional stiffness, which is the governing mode in these models. As can be seen in figure 7.20, the angle with 5 cables is 50°, while the angle with 4 cables is 44°, giving a higher stiffness and lower acceleration.
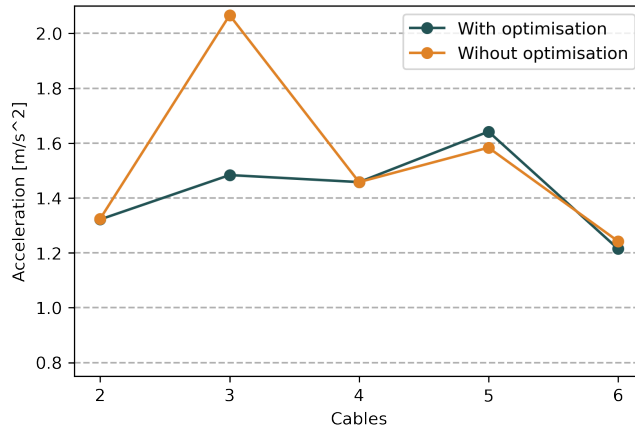
**Figure 7.22:** Vertical accelerations

| Cables | 2 | 3 | 4 | 5 | 6 |
|---|---|---|---|---|---|
| *With optimisation* | | | | | |
| Frequency | 1.93 | 2.01 | 1.74 | 1.68 | 2.08 |
| Type | vertical | pylon vertical | torsion | torsion | vertical |
| *Without optimisation* | | | | | |
| Frequency | 2.14 | 2.11 | 1.74 | 1.70 | 1.68 |
| Type | pylon vertical | vertical | torsion | torsion | torsion |

**Table 7.21:** Mode shape types

Figure 7.23 shows the change in maximum lateral accelerations when varying the amount of cables. The results without optimisation show a clear downward trend when increasing the amount of cables. This leads to conclude that the cables give stiffness in lateral direction, and that the lateral stiffness is not significantly influenced by the angle of the bracing in the deck or the amount of deck segments. The accelerations in the models with optimisation increase with the amount of cables, except for the model with 6 cables. The increase most likely caused by a decrease in the optimisation parameters. As with the vertical accelerations, the low maximum lateral acceleration in the model with 6 cables can partially be explained by the high optimisation parameters. The other part can be explained by the frequency of this mode, which is just below 0.7, decreasing the $\psi$-factor.
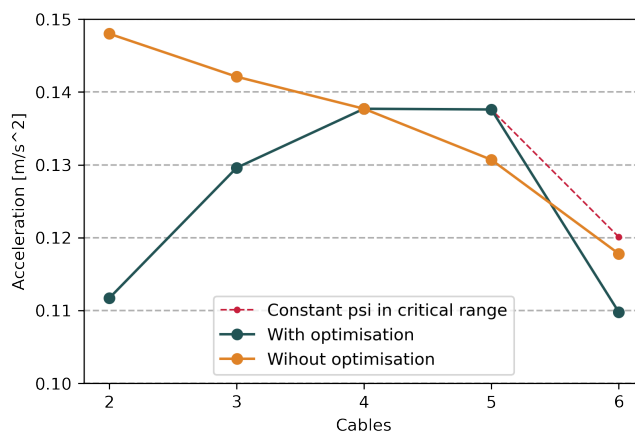


**Figure 7.23:** Lateral accelerations

| Cables | 2 | 3 | 4 | 5 | 6 |
|---|---|---|---|---|---|
| *With optimisation* | | | | | |
| Frequency | 0.74 | 0.76 | 0.74 | 0.73 | 0.68 |
| Type | lateral | lateral | lateral | lateral | lateral |
| *Without optimisation* | | | | | |
| Frequency | 0.77 | 0.76 | 0.74 | 0.74 | 0.68 |
| Type | lateral | lateral | lateral | lateral | lateral |

**Table 7.22:** Mode shape types

## 7.3. Part 3 - Additional studies

In part 3 of the parameter study, some additional studies are presented that investigate the influence of certain aspects on the results. First, the question what happens when other studied parameters are also a variable in the optimisation process is discussed, followed by the influence of the damping value and the traffic class. Finally, the influence of the connection stiffness is investigated. Appendix E contains the complete results of these studies. In this section only the noteworthy results are discussed.

### Part 3a - More optimisation parameters

This verification study was done to investigate to what extent the results are influenced by other parameters. This can be interesting, since for example the optimum amount of cables might change for different pylon heights. Therefore the two other studied parameters were treated as a optimisation parameter in the optimisation too, instead of having a set value as was the case in part 2a. For example, when investigating the pylon height, the pylon shape and the amount of cables become a optimisation parameter. This is schematically shown in figure 7.24.
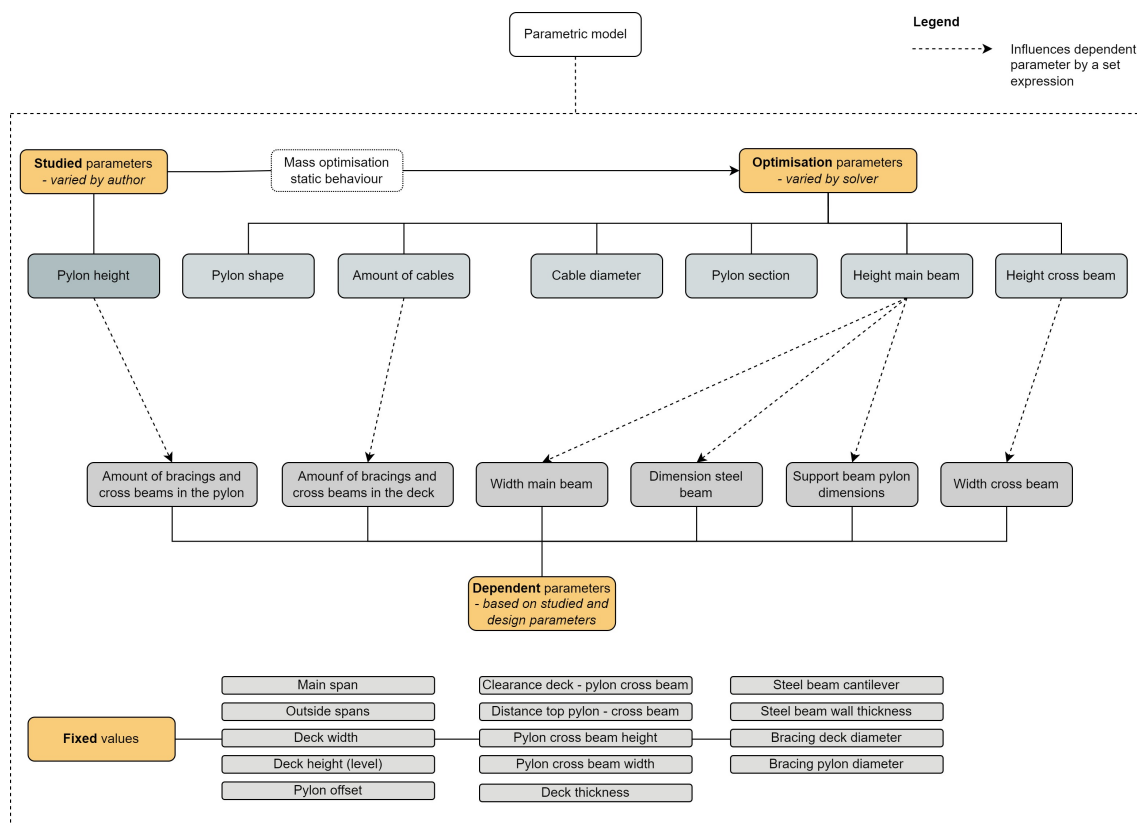


**Figure 7.24:** Parameters in the parameter study - part 3a

The results show that most of the trends found in part 2a are influenced by the values of the other two parameters. In some cases, the trend becomes less clear, in other cases the trend can not be found anymore.

54

In the runs of the pylon height and in the runs of the amount of cables, the main contribution of the variation is caused by the shape of the pylon. As in the optimisations, the pylon shape affected both the static behaviour and the total mass to a very limited extent, the found pylon shapes should be seen as partially random. The pylon shape does influence the maximum accelerations, therefore making the trends less clear. An exception is the lateral accelerations a a result of the pylon height, shown in figure 7.25. Here some deviations of the trend were found, but it is still clearly visible that the pylon height has an increasing effect on the lateral accelerations and that this effect is stronger than variations in the shape of the pylon.
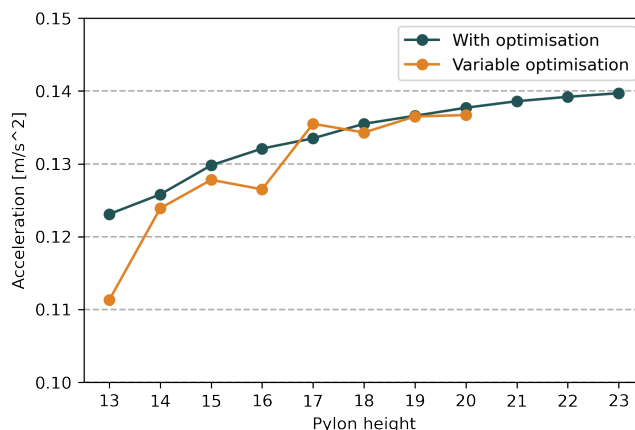


**Figure 7.25:** Lateral accelerations

An other part of the variation might be due to the fact that the models are not well optimised. This has two reasons. The first reason is that when the amount of cables is a design variable, the model becomes discontinuous. I.e. when the amount of cables switches from 4 to 5, the optimal main beam height has a jump. This makes it harder to find a sufficiently optimised solution. The second reason is that the maximum amount of evaluations was potentially too low to deal with the amount of parameters.

## Part 3b - Damping value and traffic class
In this study the influence of the damping value and the traffic class is investigated. Since both have a linear impact on the results, the effect is the same for all studied parameters. Therefore only the results for one parameter, the pylon shape, are shown.

### Damping value
As explained before, the damping value is an important, but unsure characteristic of the structure. Depending on many factors, like construction material, the type of structure, the type of connections and the amount of connections, it can vary significantly. Chapter 6 motivated why a damping value of 1.2% is the most realistic value for the design of this thesis. However, since the design is parametric and since there is uncertainty in the estimation, it is important to consider the effect of other values. Therefore results with damping values ranging from 0.5% to 3% are presented below. The lower limit corresponds to the lowest value found in literature and the upper limit corresponds to the highest value recommended in codes and guidelines. In literature, one value of 3.5% was found, but this was deemed unrealistic for the bridge of this thesis and the type of bridge with this damping value was unknown. It is expected that the true damping value of the design lies between 0.9% and 1.5%.

Figure 7.26 shows the effect of the damping value on the vertical and lateral accelerations on the results of part 2a for the pylon shapes. It shows a significant effect, that can be greater than the effect of changing the pylon shape.

**(a)** Vertical accelerations

**(b)** Lateral accelerations
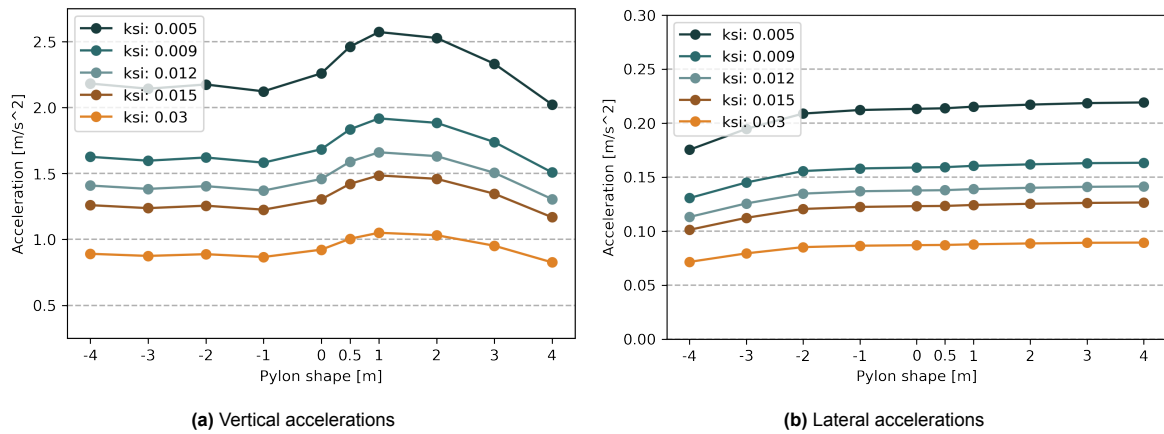
**Figure 7.26:** Effect of different damping values

**Traffic class**

The traffic class is a measure for the amount of people that are expected to be present on the bridge simultaneously (see appendix D). For which traffic class the bridge is designed, is a decision made by the project team, so it does not have the same type of uncertainty as the damping value has. However, is does have an impact on the accelerations, which is shown in figure 7.27. The traffic class used in the other results is TC2, which corresponds to 0.2 people per square metre. It can be observed that the effect of a varying TC is bigger than the effect of different pylon shapes.



**(a)** Vertical accelerations

**(b)** Lateral accelerations
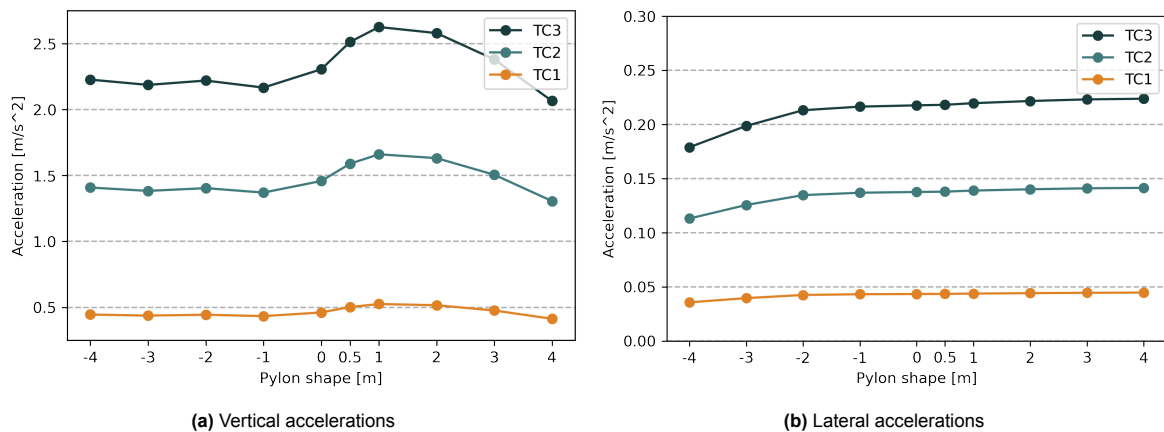
**Figure 7.27:** Effect of different traffic classes

# Part 3c - Connection stiffness

In this verification study the effect of the connection stiffness between the main beam and the steel beam is investigated. In the optimisation runs, these were modelled as hinged connections. It is interesting to know to what extent the results change when adding rotational stiffness around the y- and z-axes, since this effects the stiffness of the deck. Note that stiff connections would also change the distribution of forces and the requirements for the connection, which was not taken into account because the models obtained in part 2a were used. Therefore the dimensions of the bridge change based on the studied parameters, but are not tailored to stiff connections.

An interesting result is that the lateral accelerations do not change when the stiffness is changed, leading to conclude that the stiffness of the connection does not affect that lateral stiffness of the deck. The vertical accelerations are affected by the connection stiffness. The effect on the results of the pylon height is unclear, which was to be expected since the results in all parts of the parameter study were unclear. The effect on the results of the pylon shape and the amount of cables is shown in figure 7.28.

56

Interestingly, in the results for the pylon shape, it can be observed that the graph shows a clearer trend than when the connection between the main beam and the steel beam is stiff. This leads to conclude that with stiff connections, it is better for the accelerations to design the pylon in a V-shape. It goes together with a change in governing mode from vertical and torsion to pylon torsion.

The results of the cables show a reversed effect; the accelerations become lower with more cables, instead of higher. This leads to conclude that the stiffness overrules the effect of changing optimisation parameters and that with stiff connections, more cables add vertical stiffness.



(a) Pylon shape - Vertical accelerations



(b) Amount of cables - Vertical accelerations
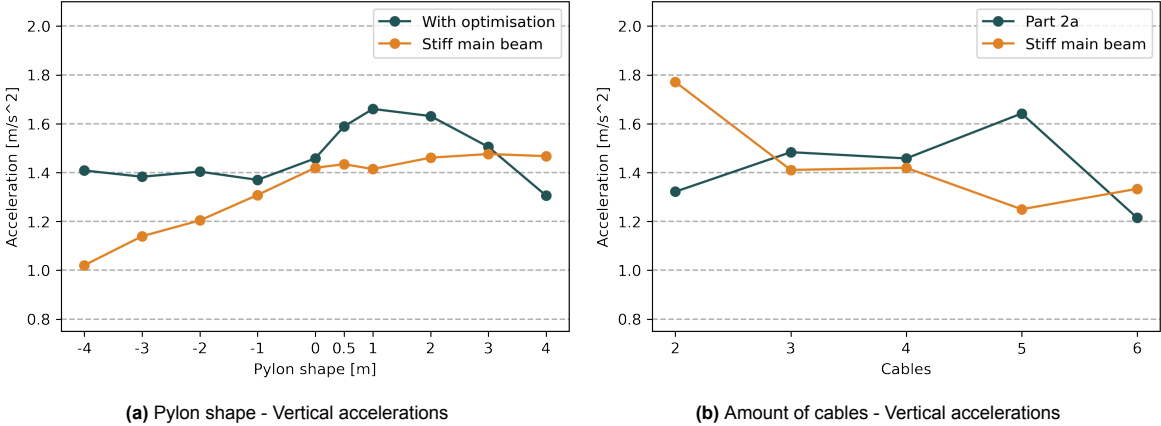
**Figure 7.28:** Effect of the connection stiffness on the accelerations
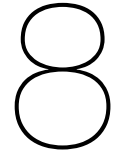
# Optimisation study investigating the influence of taking into account dynamic behaviour in the design of the case study

In this chapter the setup and the results of the optimisation study to avoid the need of dampers are described. This study researches to what extent it is possible to obtain a design variant that does not need dampers to control excessive vibrations. The design solution is compared to a solution in which dynamic behaviour is not taken into account, in order to understand the influence on the design.

## 8.1. Description of the study

To achieve this, an optimisation problem was set up that is comparable to the set up of the optimisations in the parameter study. There are differences in a few aspects. The first is that all studied parameters are treated as optimisation parameters, as shown in figure 8.1.
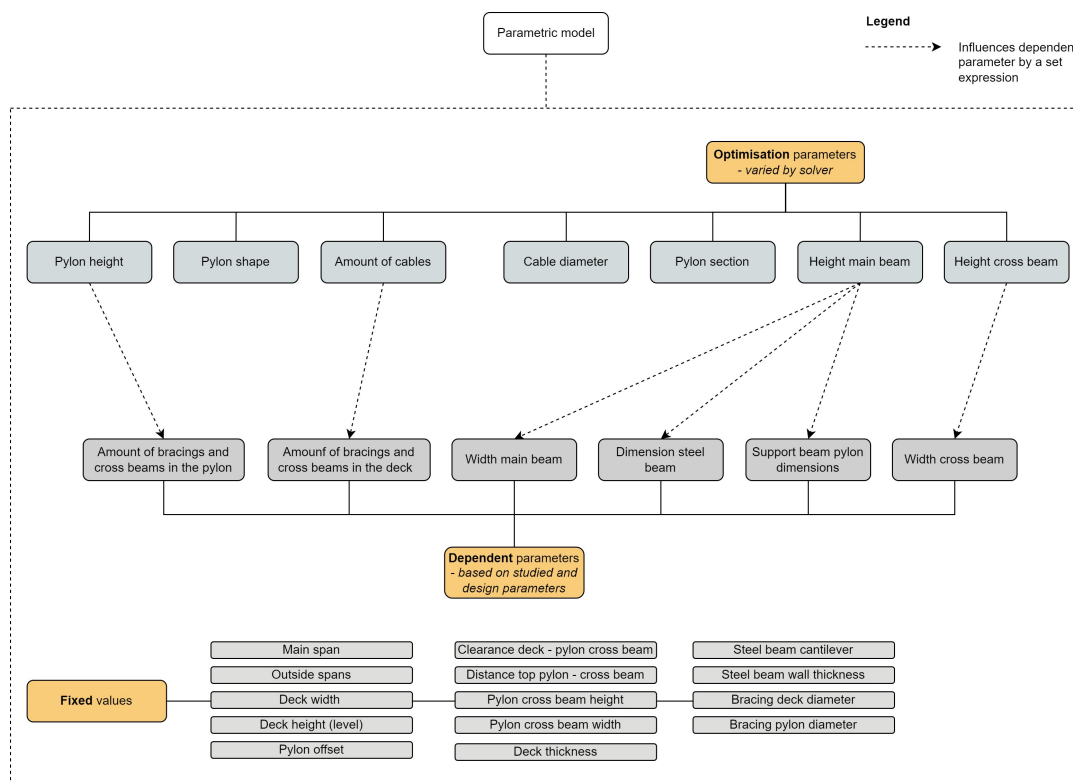


**Figure 8.1:** Parameters in final optimisations

The second is that the dynamic behaviour is now included in the optimisation process as a behavioural constraint, see figure 8.2. This means that next to a static analysis, a modal analysis is performed

after which the maximum accelerations are calculated. The maximum accelerations are evaluated in unity checks (UCs), which influence the value of the penalty function. The UCs for the vertical and lateral accelerations are calculated by dividing the maximum accelerations by the maximum allowed accelerations in the respective directions. The UC for the lateral lock-in effect is obtained by dividing the lateral acceleration by the threshold from which the effect can occur, namely 0.1 m/s². The resulting objective function is shown in equation 8.1. The mass and the penalty function are calculated with equation 8.2 and 8.3. Note that these equations are the same as in the parameter study. The only difference is the amount of UCs in the penalty function.

$$f_{\text{obj}}(x) = m_{\text{total}}(x) + f_{\text{pen}}(x) \qquad (8.1)$$

$$m_{\text{total}}(x) = V_{timber}(x) * \rho_{\text{timber}} + V_{steel}(x) * \rho_{\text{steel}} \qquad (8.2)$$

$$f_{\text{penalty}} = \sum_{i=1}^{n}(10000000000 + (UC_i - 1) * 10000000000)_{\text{if UC}>1} \qquad (8.3)$$
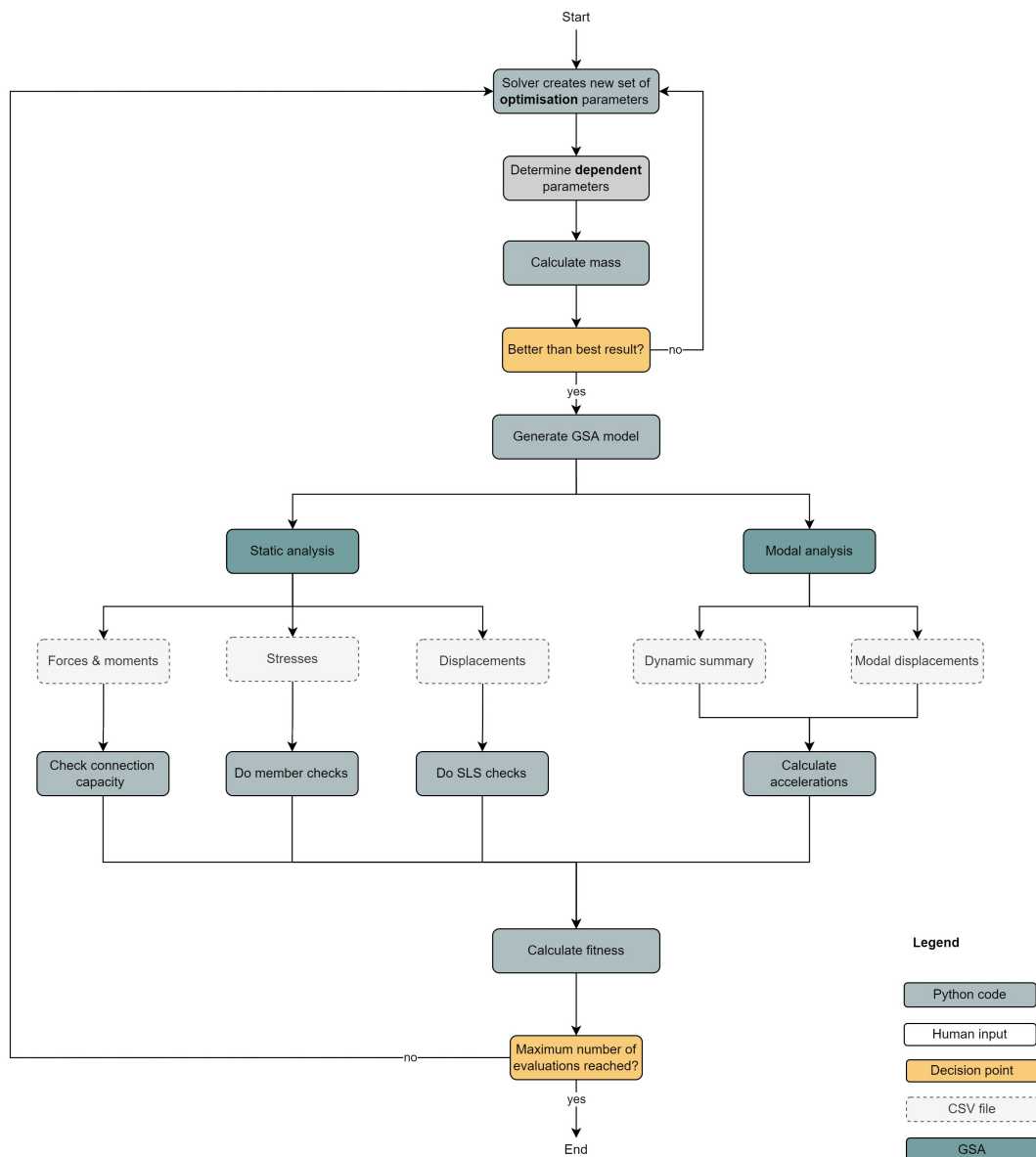


**Figure 8.2:** Overview final optimisations

59

## 8.2. Results

A set of initial runs was done that helped understanding the problem and gave insight in what settings to use for the optimisation. These runs are described in appendix G.4. For the optimisation study of this chapter, two optimisation runs were done in order to understand the influence on the design when dynamic behaviour is included. The first did not include dynamic behaviour and is referred to as the *basic model*. The second, the *final model*, was optimised taking into account dynamic behaviour. Based on the resulting parameters and unity checks, it is deemed likely that sufficiently optimised models were found. The two models are shown in figure 8.3. The corresponding parameters are shown in table 8.1 and the governing unity checks (UCs) in figure 8.4.



| **(a)** Basic model | **(b)** Final model |
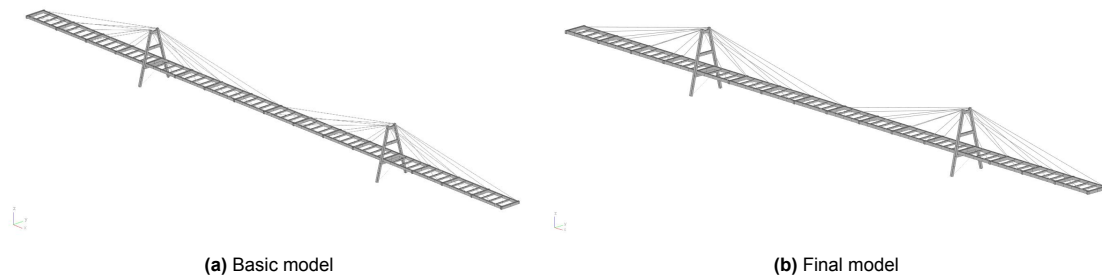
**Figure 8.3:** Results optimisations

Table 8.1 shows that compared to the basic model, the mass increases by 14% in the final model. This increase is comprised of a 17% increase in timber mass and a 10% increase in steel mass.

Part of this is caused by the difference in pylon height and pylon section. Based on the results of the parameter study, it is hard to explain why the pylon height increases. The pylon section increases slightly. Since stability is the governing UC for the pylon dimension, this increase is due to the bigger pylon height.

The cable diameter goes up by 5%. This can be explained by the decreasing effect on the accelerations found in part 1 of the parameter study.

The main beam height increases too. This is likely to be due to the dynamic requirements since its decreasing effect on accelerations found in part 1 of the parameter study and because in part 2a a lower main beam height was found for higher pylons. This is reflected in the rather low UC for the main beam. The cross beam height is the same in both models, supporting the conclusion of part 1 of the parameter study that it has a very limited effect on the accelerations.

The amount of cables is 4 in both models. Part 2a of the parameter study provides little help in explaining this outcome since the mass nor the accelerations were lowest in the models with 4 cables. Part 3a might help since it found the lowest result in a model with 4 cables, though these results are not entirely reliable. The final model has a pylon shape of 3m, which was the highest possible value. While based on part 2 of the parameter study, a negative shape was expected, it does correspond with the optimisation results of part 3a, which found lower results for positive pylon shapes. The pylon shape of the basic model is 3m too. This was to be expected since the parameter study showed that the pylon shape has a limited effect on the static behaviour and because an A-shaped pylon has a lower mass than a V-shaped pylon.

|  | Result [kg] | Cable diameter [mm] | Pylon section [mm] | Main beam height [mm] | Cross beam height [mm] | Cable number | Pylon height [m] | Pylon shape [m] |
|---|---|---|---|---|---|---|---|---|
| Basic | 145634 | 114 | 631 | 803 | 399 | 4 | 11.0 | 3.0 |
| Final | 166676 | 119 | 663 | 875 | 399 | 4 | 12.6 | 3.0 |
| Increase | 14% | 5% | 5% | 9% | 0% | n.a. | 14% | n.a. |

**Table 8.1:** Parameter results

| Model | Main beam | | | | Cross beam | | | | Cables | Other | | Dynamic | | |
|---|---|---|---|---|---|---|---|---|---|---|---|---|---|---|
| | My & - Fx | My & + Fx | Mz & - Fx | Mz & + Fx | My & - Fx | My & + Fx | Mz & - Fx | Mz & + Fx | Fx | Stabitlity | Deflection | Vertical | Lateral | Lock-in |
| Basic | 0.88 | nan | 0.70 | nan | 1.00 | nan | 0.71 | nan | 0.26 | 0.96 | 0.99 | - | - | - |
| Final | 0.64 | nan | 0.49 | nan | 1.00 | nan | 0.71 | nan | 0.21 | 0.96 | 0.69 | 0.95 | 0.33 | 0.99 |

**Figure 8.4:** Unity checks - the colours indicate how close the UC is to 1

Tables 8.2 and 8.3 show the modes of the two models and their corresponding natural frequencies, modal mass, type, maximum acceleration and comfort class. The modes are visualised in figure 8.5 and 8.6. With regards to dynamic behaviour, the requirements for the final model were a comfort class 2 and a maximum acceleration of 0.1 m/s² in lateral direction to prevent the lock-in effect.

For vertical accelerations, the basic model would be categorised in comfort class 3, with a torsion governing mode. The comfort class for the lateral accelerations is 2, but with 0.11 m/s² it does not fully fulfill the requirement of the lock-in effect.

In the final model, the vertical accelerations are almost 1 m/s², which is the maximum value for comfort class 2. In lateral direction, the lock-in effect is governing. As with the basic model, a torsion mode is governing the vertical accelerations.

| Mode | Frequency [Hz] | Modal Mass | Type | Max acceleration [m/s²] | Comfort class |
|---|---|---|---|---|---|
| 1 | 0.6922 | 79080 | lateral | 0.11 | 2 |
| 2 | 0.83 | 70670 | out of range (v) | - | - |
| 3 | 1.18 | 56290 | out of range (v) | - | - |
| 4 | 1.42 | 104700 | vertical | 0.39 | 1 |
| 5 | 1.53 | 110000 | out of range (l) | - | - |
| 6 | 1.63 | 94970 | out of range (l) | - | - |
| 7 | 1.70 | 93630 | out of range (l) | - | - |
| 8 | 1.85 | 51420 | vertical | 1.08 | 3 |
| 9 | 1.91 | 67300 | torsion | 1.21 | 3 |
| 10 | 2.13 | 58770 | vertical | 0.99 | 2 |
| 11 | 2.33 | 128100 | out of range total | - | - |

**Table 8.2:** Dynamic summary - basic model

| Mode | Frequency [Hz] | Modal Mass | Type | Max acceleration [m/s²] | Comfort class |
|---|---|---|---|---|---|
| 1 | 0.69 | 89450 | lateral | 0.10 | 1 |
| 2 | 0.96 | 78970 | out of range (v) | - | - |
| 3 | 1.34 | 62000 | torsion | 0.25 | 1 |
| 4 | 1.51 | 133100 | out of range (l) | - | - |
| 5 | 1.60 | 101900 | out of range (l) | - | - |
| 6 | 1.64 | 112200 | vertical | 0.84 | 2 |
| 7 | 1.70 | 102400 | out of range (l) | - | - |
| 8 | 2.09 | 69540 | vertical | 0.85 | 2 |
| 9 | 2.14 | 74280 | torsion | 0.95 | 2 |
| 10 | 2.15 | 86660 | pylon_vertical | 0.34 | 1 |
| 11 | 2.20 | 64440 | out of range (pl) | - | - |
| 12 | 2.45 | 58120 | out of range total | - | - |

**Table 8.3:** Dynamic summary - final model

1 - Lateral  2 - Vertical (out of range)  3 - Torsion (out of range)

4 - Vertical  5 - Lateral (out of range)  6 - Lateral (out of range)

7 - Lateral (out of range)  8 - Vertical  9 - Torsion

10 - Vertical  11 - Out of range total  12 - Out of range total
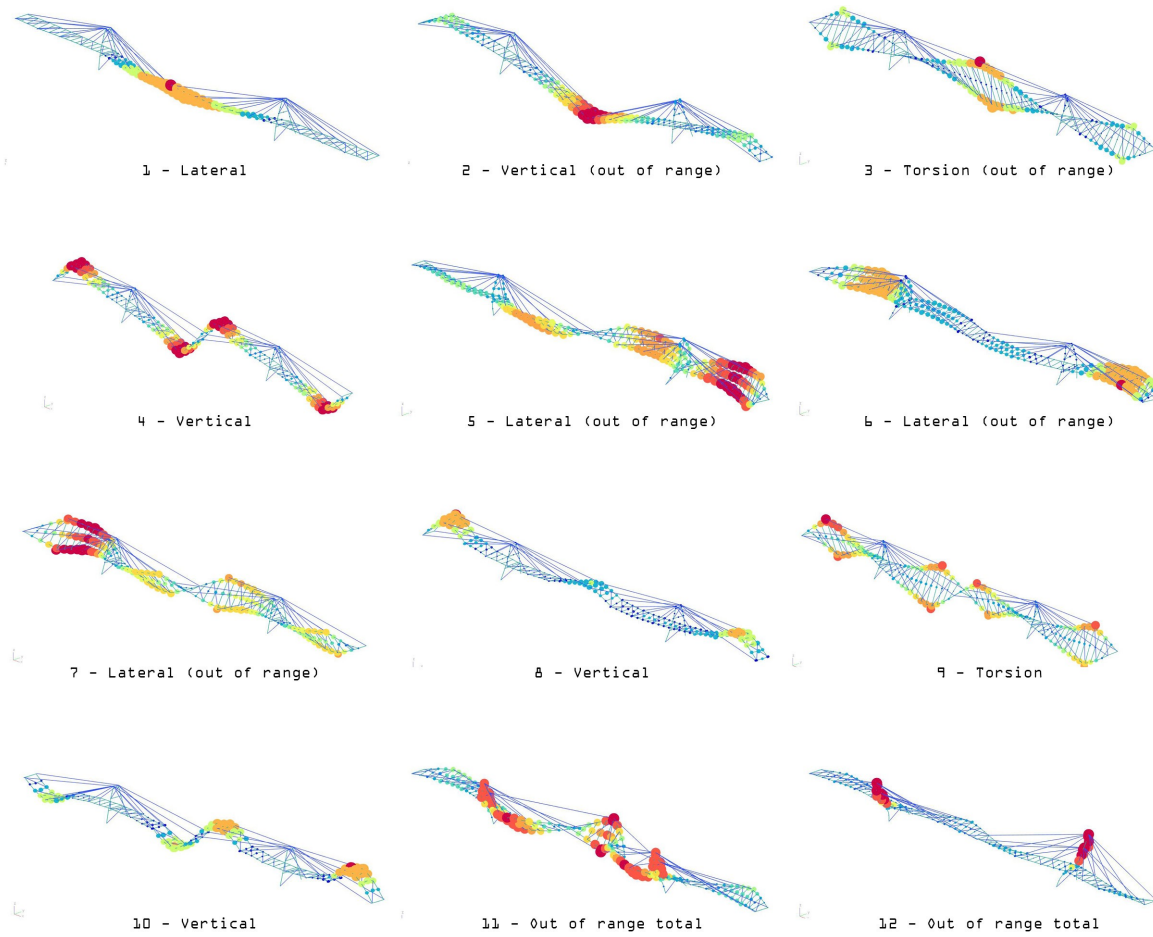
**Figure 8.5:** Modes basic optimisation - the colours show the absolute modal displacement
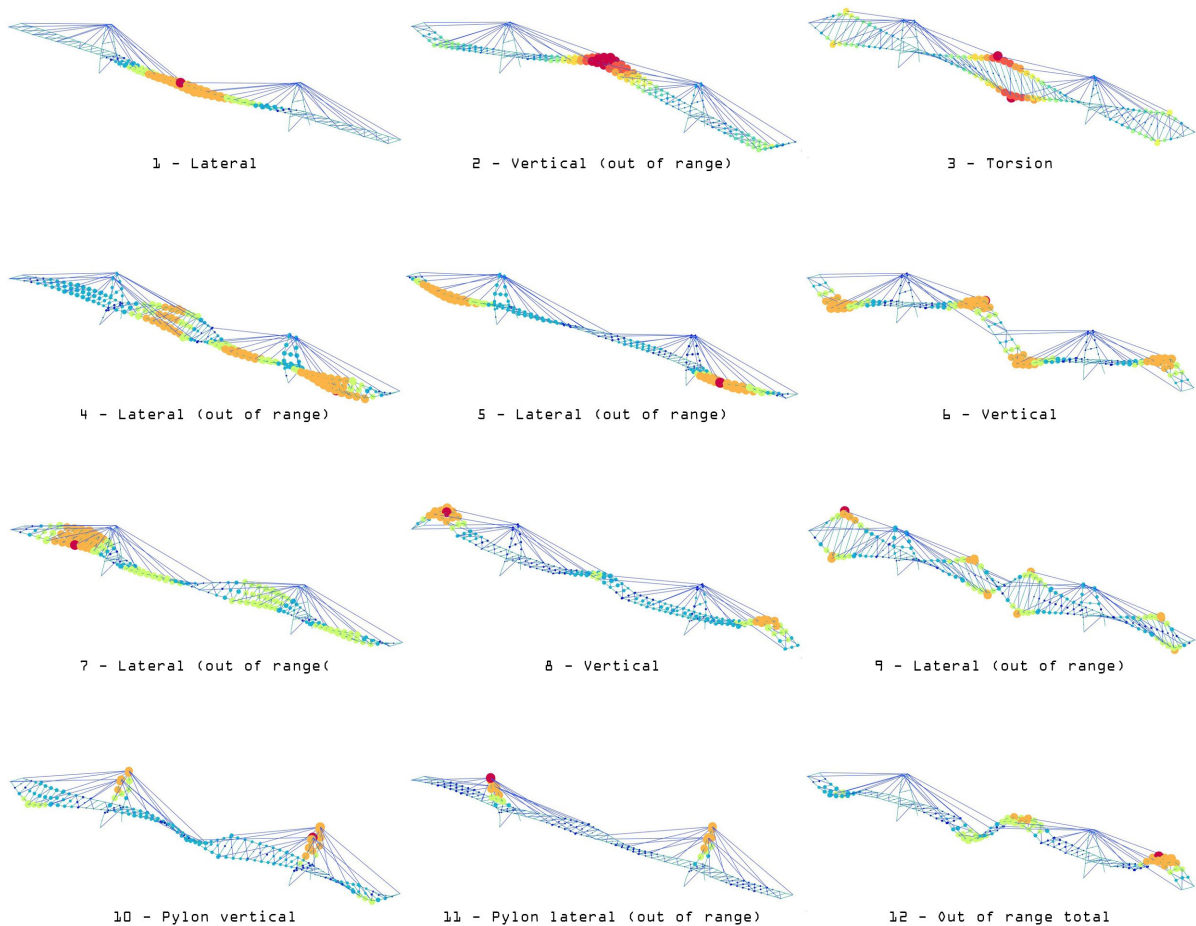
**Figure 8.6:** Modes final optimisation - the colours show the absolute modal displacement

## 8.3. Influence of damping values, traffic class and comfort requirements

The effect on the design when considering dynamic behaviour, depends on three factors. The parameter study showed that the influence of the damping and the traffic class is considerable. The third factor is the comfort requirements, which limit the maximum allowable accelerations. To estimate the impact of these factors, the obtained models were analysed with different values of the damping and the traffic class.

In the figures the maximum acceleration of the comfort classes are given on the right y-axis. In the figures with lateral accelerations the red area indicates the lateral accelerations that can trigger the lock-in effect. As explained in section 3.5, this effect starts from 0.1 to 0.15 m/s², marked light red. The values of the accelerations are given in the figure too.

Figure 8.7a shows the vertical accelerations when the models are analysed with different damping values. From the figure it can be observed that when the damping value is 0.9%, it is likely that a slight extra increase in mass is needed to comply with the comfort class 2 requirements for vertical accelerations. When the damping value is higher than expected, the increase in mass can be less. It also shows that to comply with comfort class 1 requirements, a more significant increase in mass would be required.

Figure 8.7b shows the results for the lateral accelerations. To comply with the most strict lock-in criterion of 0.1 m/s², the final model would need some more mass when the damping value is lower than expected, and less when the damping value is higher than expected. Accepting a less strict

requirement of maximum 0.15 m/s² for the lock-in effect, the basic model would comply with the comfort class 2 requirements, without additional mass.



(a) Vertical accelerations



(b) Lateral accelerations
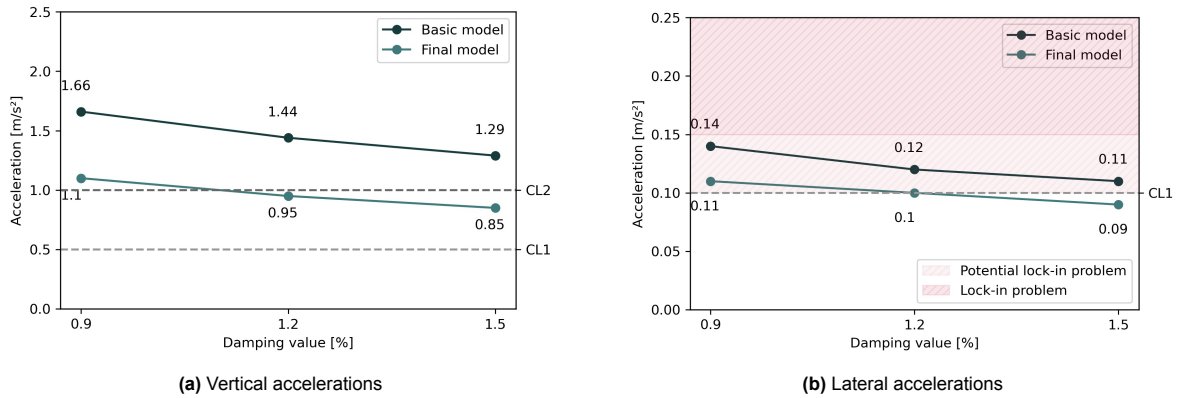
**Figure 8.7:** Several damping values

Figure 8.8a shows the vertical accelerations when the models are analysed with different traffic classes. It shows that for traffic class 1, even the basic model complies with the requirements for comfort class 1. With traffic class 3, a significant increase in mass is likely to be needed for the vertical accelerations to be categorised in comfort class 2.

Lastly, figure 8.8b shows the lateral accelerations for different traffic classes. As with the vertical accelerations, no extra mass is needed with regards to the basic model to comply with the requirements of comfort class 1. Using traffic class 3, a slight increase in mass would be required for the final model to comply with the least strict requirement of the lateral lock-in effect of 0.15 m/s². A more significant increase would be needed to comply with the strict requirement and seems unrealistic.



(a) Vertical accelerations



(b) Lateral accelerations
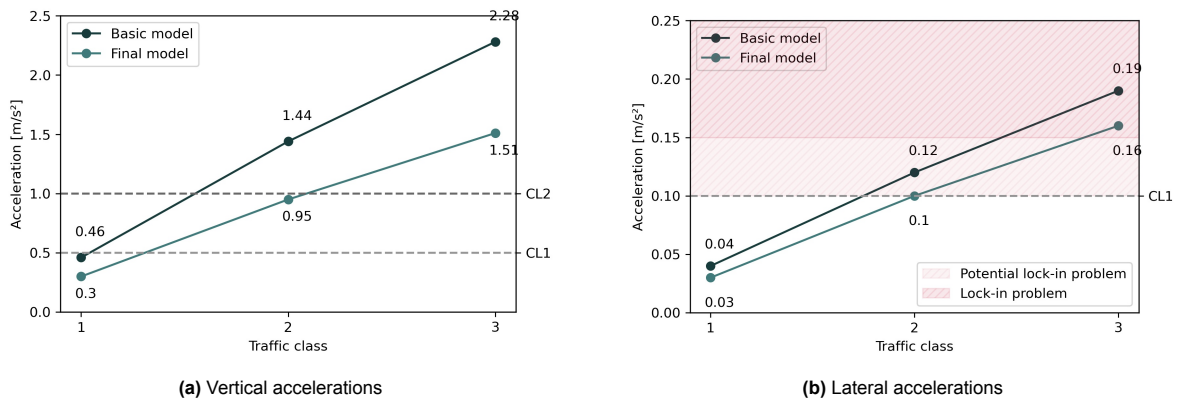
**Figure 8.8:** Several damping values

# 9

# Conclusion

This research served two main goals. One was to increase knowledge about the influence of three preliminary design parameters on the dynamic behaviour of a long-span timber footbridge, namely the height of the pylons, the shape of the pylons and the amount of cables. The second was to investigate to what extent it is possible to design a long-span timber footbridge that does not need dampers to control excessive vibrations. With this, advice might be given to bridge designers on how to deal with dynamic behaviour in the early stage of a design process. To achieve these goals, the following research question was formulated:

*What is the influence of preliminary design parameters on the human-induced dynamic behaviour of a long-span timber footbridge and to what extent is it possible to design a long-span timber footbridge that does not need dampers to control excessive vibrations?*

To answer the first part of the research question, a parameter study was carried out. Two optimisation studies were done to answer the second part. With due regard of the limitations of this research, discussed in the next chapter, the conclusions of the studies are described below.

## 9.1. Parameter study

**Part 1 - Optimisation parameters**
The parameter study gave insight in the dynamic behaviour of the bridge at different levels. The first level, what happens when only the dimensions of some of the members are varied, was investigated in part 1 of the parameter study. Here it was found that an increased cable diameter in general has a decreasing effect on the vertical accelerations, although accelerations increase around certain values, that differ per design variant. The cable diameter has an unambiguous diminishing effect on the lateral vibrations, explained by the added stiffness. The pylon section has a slight increasing effect on the vertical accelerations. This can be explained by the increased difference in stiffness between the deck and the pylon. It hardly affects the lateral accelerations. The height of the main beam has a decreasing effect on both the vertical and lateral accelerations, which is explained by the increased stiffness in the respective directions. The dimensions of the crossbeam have a very modest diminishing effect on both the vertical and the lateral accelerations.

The changing dimensions result in a different stiffness to mass ratio, which results in different natural frequencies. This is an important notion since only the modes in the critical range of frequencies (frequencies that can be excited by pedestrian loading) are considered in the verification, which is reflected in the $\psi$-factor. When the frequencies change, other modes can become governing, which often yields results that do not follow a linear trend. An example is the vertical accelerations as a result of changing the main beam height. They first decrease rapidly, followed by a more gradual decrease. This is explained by the fact that the natural frequency of a mode changes to the range where the $\psi$-factor becomes lower than 1, causing an other mode to become governing.

An overview of the results of part 1 is given in table 9.1. Note that an *increasing* influence means a positive correlation between the value of the optimisation parameter and the maximum acceleration.

| | Direction | Influence | Impact | Trend | Comments |
|---|---|---|---|---|---|
| **Cable diameter** | Vertical | Decreasing | High | Unclear | - |
| | Lateral | Decreasing | High | Clear | Kink because psi-factor |
| **Pylon section** | Vertical | Increasing | Low | Clear | Kink because psi-factor |
| | Lateral | Decreasing | Very low | Clear | - |
| **Main beam height** | Vertical | Decreasing | High | Clear | Kink because psi-factor |
| | Lateral | Decreasing | High | Clear | Kink because psi-factor |
| **Cross beam height** | Vertical | Decreasing | Very low | Clear | - |
| | Lateral | Decreasing | Very low | Clear | - |

**Table 9.1:** Overview results part 1 - optimisation parameters

**Part 2 - Studied parameters**

In part 2 of the parameter study, the influence of the studied parameters was investigated, which were height of the pylons, the shape of the pylons and the amount of cables. In part 2a the models were optimised in each step. The results were compared to results without optimisations in each step, referred to as part 2b.

The height of the pylons seems to have an increasing effect on the vertical accelerations, although the results are ambiguous. This can be explained by a large change in natural frequencies and the corresponding $\psi$-factors. Regarding the lateral accelerations, merely increasing the height of the pylons (part 2b) has a very minimal effect, whereas the results of part 2a show a clear upward trend. This led to conclude that the change in accelerations is mainly caused by the changing optimisation parameters such as the diameter of the cables.

Varying the shape of the pylons yields the same results with and without optimisations, because the optimisation parameters are influenced only to a very small extent by running optimisations. This led to conclude that the shape itself influences the vertical and lateral accelerations. The vertical accelerations remain approximately constant for negative pylon shapes, while it increases for positive pylon shapes, up till a maximum around 1 m, caused by different types of governing modes. The lateral accelerations are lowest with negative pylon shapes, and they increase when the shape becomes more positive. This is explained by the way the deck rotates in the lateral vibration.

Merely adding cables without optimising the optimisation parameters has a decreasing effect on the vertical accelerations, although the model with 2 cables does not follow this trend. This can be because the frequencies of the modes that are governing in other models yield a low $\psi$-factor. Adding cables has a decreasing effect on the lateral accelerations as well. These decreasing trends lead to conclude that adding cables adds both vertical and lateral stiffness to the structure. When optimisations are run when adding cables, as done in part 2a of the parameter study, this trend is reversed, explained by the decreasing optimisation parameters.

An overview of the results of part 2a (with optimisation) and part 2b (without optimisation) are given in table 9.2 and 9.3 respectively.

| | Direction | Influence | Impact | Trend | Comments |
|---|---|---|---|---|---|
| **Pylon height** | Vertical | Increasing | Medium | Unclear | - |
| | Lateral | Increasing | Medium | Clear | Changing optimisation parameters |
| **Pylon shape** | Vertical | Unclear | Medium | Unclear | Kinks because psi-factor |
| | Lateral | Increasing | High | Clear | Kink because psi-factor |
| **Cable number** | Vertical | Increasing | High | Medium | Model with 6 cables has high dimensions |
| | Lateral | Increasing | High | Medium | Model with 6 cables has high dimensions |
| **Cross beam height** | Vertical | Decreasing | Very low | Clear | - |
| | Lateral | Decreasing | Very low | Clear | - |

**Table 9.2:** Overview results part 2a - studied parameters with optimisation

| | Direction | Influence | Impact | Trend | Comments |
|---|---|---|---|---|---|
| **Pylon height** | Vertical | Unclear | High | Unclear | - |
| | Lateral | Decreasing | Very low | Clear | - |
| **Pylon shape** | Vertical | Unclear | Medium | Unclear | Kinks because psi-factor |
| | Lateral | Increasing | High | Clear | Kink because psi-factor |
| **Cable number** | Vertical | Decreasing | High | Unclear | - |
| | Lateral | Decreasing | High | Clear | - |
| **Cross beam height** | Vertical | Decreasing | Very low | Clear | - |
| | Lateral | Decreasing | Very low | Clear | - |

**Table 9.3:** Overview results part 2b - studied parameters without optimisation

**Part 3 - Verification studies**
In part 3 of the parameter study, a set of verification studies was done to investigate the way the other studied parameters, the damping, the traffic class and the connection stiffness affect the results. It showed that the effect of other parameters often overruled the effect of the studies performed in part 2, although part of this was explained by not sufficiently optimised models. In the case of the influence of the pylon height on the lateral accelerations, the trend was still clearly visible.

It also showed that the damping value and the traffic class has a significant impact on the accelerations. Since this effect is linear, it does not effect the trends found in part 1 and part 2.

Lastly it showed that the connection stiffness only affects the vertical accelerations; the lateral accelerations are hardly affected. The most noteworthy result is that with stiff connections, the results of the pylon shape becomes a clear trend that shows lower accelerations for negative pylon shapes.

## 9.2. Optimisation study to avoid the need of dampers

This study was led by the question to what extent it is possible to obtain a design variant that does not need dampers to control excessive vibrations. In the model where dynamic behaviour was taken into account, a damping value of 1.2% was used, which was deemed the most realistic value based on literature, together traffic class 2 and comfort class 2, which were also deemed most realistic.

Compared to a standard model, where dynamic behaviour was not taken into account in the optimisation process, a 14% increase in mass was found. This additional mass is comprised of a 17% increase in timber and a 10 % increase in steel. Depending on the chosen damping value, traffic class and comfort class, these numbers are expected to vary.

With respect to the basic model, the dynamic requirements were met by increasing the pylon height, the main beam height and the dimension of the cables. The cross beam height and the amount of cables were not affected.

**Concluding remarks**
Since the influence of changing a parameter depends on many factors, advice that is valid in all situations (e.g. always aim for higher pylons) can not be given for the early stage of a design process. When aiming to avoid the need of dampers, the design can be adjusted in a later stage in a way that the $\psi$-factors of the governing modes become lower than 1. Depending on the mode and frequency, this could imply trying to increase or decrease the frequency of the mode. As found in the optimisation study, the new design is likely to have a higher mass. However, the result will heavily depend on the damping value, the traffic class and the required comfort class and for some combinations (e.g. traffic class 3 and a comfort class 2), it might not be possible. The exact damping value will remain uncertain until the bridge has been built, which is why a conservative damping value would need to be assumed in the design. To be able to judge whether adding material to obtain a design without the need of dampers is a sensible option, a life cycle assessment and an investigation of the costs is advised.

# 10

# Discussion and recommendations

This chapter presents a discussion of the the model, the results and the conclusions as well as recommendations for further research.

## 10.1. Discussion

Interpreting the conclusions, the assumptions and simplifications discussed in this section should be considered. First some notes about the mechanical model of the design are discussed, followed by comments about the finite element model representing the mechanical model. Lastly, some considerations about the parametric model and the optimisation process are discussed.

**Mechanical model**
The mechanical model is a simplified version of the design and is used to determine the distribution of forces. Therefore it should be assessed to what extent it represents reality. Although the influence on the results is deemed small, there is a few assumptions and simplifications that might have affected the results. These are the way the connections are modelled, the loads that are taken into account and the way in which the geometry is simplified.

The connections between the main beam and the steel beams are modelled to be fully stiff around the x-axis and free around the y- and z-axes as well as in translational directions. However, in a real connection, there would be some flexibility around the x-axis and some stiffness in the other directions, having an impact on the stiffness of the entire system.

Regarding the loads, not all possible loads and load combinations are taken into account and not all possible checks are performed. For example, the wind in positive z-direction is not taken into account, as well as the weight of the cables, the temperature load and stresses due to changing moisture content. Unloading of the cables is only checked in a very simplistic way and stresses due to torsion are neglected. This is acceptable since in this phase of a design process it is common to not take into account all possible loads and load combinations, but it might be unconservative. In the modal analysis, the pedestrian mass is not taken into account and in the calculation of the accelerations, jogger loading is neglected. As discussed in chapter 5, this last simplification might imply a loss of accuracy of the results.

The geometry is slightly simplified. The opening for the bracing in the cross beams of the deck and the eccentricity of the cross beam with respect to the main beam are not modeled. This is slightly unconservative.

**Finite element model**
As discussed in chapter 5, the cables and bracing are modelled with bar elements, whereas cable elements would be a better representation of the mechanical model. Although the solution to avoid compression in these elements is deemed suitable, in some models still some minor tension forces were found, resulting in increased cross beam sections. Since the cross beam dimensions only have a very small impact on the maximum accelerations, this error is acceptable.

The second point of attention is the way the connection between the pylon and the deck was modelled. In the optimisation runs of the parameter studies, spring elements with different stiffnesses in different directions were used. Later it was found that moment equilibrium around the x-axis was not satisfied this way, caused by the high difference in stiffness. Therefore link elements were used to evaluate the maximum accelerations in the parameter studies. Since the effect on the force distribution was small, it is expected that the influence was minor, though it is possible that some dimensions and

therefore the dynamic behaviour would have been slightly different had link elements been used during the optimisation.

**Parametric model and optimisation**
A parametric model made with the intention to optimise, needs the dependent parameters and/or fixed values used in this thesis, provided computation time is a limiting factor. Even though care was taken to select the most influential parameters as variables in the optimisation process, introducing the dependent parameters and fixed values might have influenced the results. In the parameter study, some studied and/or optimisation parameters had a fixed value. Since nearly all parameters were found to influence the accelerations, the selection of these values is likely to have influenced the results. Based on the trends, it is expected that with different values, the accelerations will change but that the effect as shown in the conclusion chapter (increasing or decreasing) will remain the same. In some cases, the trends might become more or less clear since some of the results showed that a minor variation of a parameter can cause an abrupt change in accelerations.

The settings of the optimisation algorithm might have influenced the results too. Although the results of both the parameter study and the final optimisation seemed reliable, there is an inherent possibility to the use of heuristic algorithms that it finds a local optimum or that it has approached the global optimum but did not find the best result.

## 10.2. Recommendations for further research

To better understand the influence of preliminary design parameters on the dynamic behaviour of pedestrian bridges, some recommendations for further research are given below. First suggestions are given on how to increase the reliability of the results of this thesis, followed by suggestions on how to broaden the scope.

**Obtaining more reliable results**
To obtain more reliable results it is advised to evaluate the fitness of the optimisation algorithm and to investigate whether the way the parametric model is built can improve the results. Although in the parameter studies most optimised models followed an explainable pattern, the runs took a considerable amount of time. In the initial runs of the optimisation study, non-optimal solutions were found, which improved after the settings were changed, though this resulted in long run times. Trying out different optimisation workflows might help in improving this process. Running optimisations with a more narrow range of parameter values after an initial run and using the more accurate mass calculation might improve the outcome too, though the former also increases the total time of an optimisation.

The parametric model could be made more refined in order to find a better optimised design. As discussed before, dependent parameters were used to decrease computation time, because it reduced the design space. The same logic goes for the fixed parameters. It would be interesting to investigate to what extent using other values or making them optimisation parameters affects the results.

**Parameters**
To widen the scope, it might be interesting to look at more (combinations of) studied parameters. One example is the structural system of the deck. In this thesis the steel beams were integrated in the deck (i.e. the main beams were between the steel beams). When the steel beams are placed under the main beam, the main beam is continuous over a longer length, which results in other dimensions and, more importantly, a higher stiffness around the y-axis, affecting the vertical vibrations.

A second example is the type of deck finish, affecting the lateral vibrations. In the models of this thesis, a deck with planks was chosen that does not contribute to the lateral stiffness of the deck, together with a fixed-diameter bracing. It might be interesting to investigate to what extent this decision has influenced the results and whether or not a solid top deck layer can contribute to the dynamic behaviour.

Other examples of interesting parameters are the railing stiffness, the amount of cross beams and the configuration of the cables. It might also be interesting to investigate to what extent asymmetry in the pylon height and shape affects the dynamic behaviour.

With regards to the material properties, a different glulam grade would be worth investigating. For instance, a higher glulam grade will lead to smaller dimensions and a different mass to stiffness ratio

because the strength, the density and the Young's modulus will increase. This will have an effect on the dynamic behaviour.

Zooming out, it is suggested to investigate whether the same patterns found in this thesis are applicable to other type of bridges, for example with different spans, structural system and main construction material. Since the damping value has an big effect on the results, it would be very beneficial to research the influence of design characteristics on the damping of a bridge by performing tests on existing structures.

# References

[1]   M. Aenlle, Martin Juul, and R. Brincker. "Modal Mass and Length of Mode Shapes in Structural Dynamics". In: *Shock and Vibration* 2020 (2020). ISSN: 10709622. DOI: `10.1155/2020/8648769`.

[2]   Hiram Arellano, Dante Tolentino, and Roberto Gómez. "Optimum Criss Crossing Cables in Multi-span Cable-stayed Bridges using Genetic Algorithms". In: *KSCE Journal of Civil Engineering* 23.2 (Feb. 2019), pp. 719–728. ISSN: 19763808. DOI: `10.1007/s12205-018-5736-2`.

[3]   Ali Awaludin. *Static and Dynamic Behavior of Bolted Timber Joints with Steel Splice Plates*. Tech. rep.

[4]   Jan Bencat and Daniel Papan. *Dynamic Modeling and Testing of Cable–Stayed Pedestrian Bridge*. Tech. rep. 2011.

[5]   Dominicus Johannes Bergsma. *Krúsrak, brug over A7 (Sneek)*. URL: `https://commons.wikimedia.org/wiki/File:Kr%C3%BAsrak,_brug_over_A7_(Sneek)_(d.j.b.)_03.jpg`.

[6]   Niclas Björngrim. *Monitoring of a timber footbridge*. Tech. rep. 2015.

[7]   H J Blaß and C Sandhaas. *PRINCIPLES FOR DESIGN*. Tech. rep. 2017.

[8]   Jean-François Bocquet, Romain Lemaître, and Thomas K Bader. *Design recommendations and example calculations for dowel-type connections with multiple shear planes*. Tech. rep. 2018. URL: `https://www.researchgate.net/publication/332153269`.

[9]   Bridon. *Product Selection*. Tech. rep.

[10]  Elsa Caetano et al. "Studies for controlling human-induced vibration of the Pedro e Inês footbridge, Portugal. Part 1: Assessment of dynamic behaviour". In: *Engineering Structures* 32.4 (Apr. 2010), pp. 1069–1081. ISSN: 01410296. DOI: `10.1016/j.engstruct.2009.12.034`.

[11]  Reto Cantieni. *Cable-Stayed Footbridge: Investigation Into Superstructure and Cable Dynamics*. Tech. rep. URL: `www.rcidynamics.ch`.

[12]  James Chen and Roger Wohlner. *Heuristics*. 2021. URL: `https://www.investopedia.com/terms/h/heuristics.asp#:~:text=A%20heuristic%2C%20or%20heuristic%20technique,a%20limited%20timeframe%20or%20deadline.`.

[13]  Peter Christensen and Anders Klarbring. *An Introduction to Structural Optimization*. 2009. URL: `www.springer.com/series/6557`.

[14]  P Clemente et al. *Vibration characteristics of a cable-stayed footbridge via modal testing*. Tech. rep. 2008.

[15]  Conzett Bronzini. *Viamala truss*. URL: `https://cbp.ch/taetigkeiten/traversiner-steg-viamala/`.

[16]  Conzett Bronzini. "Zweiter Traversinersteg Viamala". In: (). URL: `https://cbp.ch/taetigkeiten/zweiter-traversiner-steg/`.

[17]  Rouven Erhardt, Matthias Gerord, and Thorsten Helbig. *Brücken aus Holz*. Tech. rep. Feb. 2019.

[18]  Angela Feldmann et al. *Dynamic properties of tall Timber Structures under wind-induced Vibration*. Tech. rep. 2016. URL: `https://www.researchgate.net/publication/307139428`.

[19]  karl Gotsch. *Neckarsteg in Wernau*.

[20]  Warren Hare, Julie Nutini, and Solomon Tesfamariam. "A survey of non-gradient optimization methods in structural engineering". In: *Advances in Engineering Software* 59 (2013), pp. 19–28. ISSN: 09659978. DOI: `10.1016/j.advengsoft.2013.03.001`.

[21]  Sander Hegger. *Vergelijkende LCA studie bruggen*. Tech. rep. 2013.

[22]  Christoph Heinemeyer and Markus Feldmann. *European design guide for footbridge vibration*. Tech. rep. 2008.

[23]  Christoph Heinemeyer et al. *Design of Lightweight Footbridges for Human Induced Vibrations*. Tech. rep. 2009.

[24] Holzbrückenbau. *Roermond bridge*. URL: `https://holzbrueckenbau.com/wp-content/uploads/Balkentragwerk_Trogbruecke_Roermond.pdf`.

[25] R. Kliger et al. *Vibration response of long cable-stayed timber footbridge-case study*. Tech. rep. 2013.

[26] Nathalie Labonnote. *Damping in Timber Structures*. Tech. rep. 2012.

[27] Andrew Lawrence. *Modern timber bridges - an international perspective*. Tech. rep. 2010.

[28] F Magalhães et al. *Output-only Modal Identification of Lively Footbridges*. Tech. rep. June 2017. DOI: `10.1201/b18175-93`.

[29] Álvaro Magdaleno et al. "Dynamic Assessment of the Longest Single-Span Timber Footbridge in Spain". In: Structurae, Oct. 2021. DOI: `10.24904/footbridge2022.150`.

[30] John Marshall. *Fiets- en voetgangersbrug, Harderwijk*. 2014. URL: `https://www.zja.nl/nl/Botterbrug-Harderwijk`.

[31] Maurer. *Tuned Mass and Viscous Dampers Technical Information and Products*. Tech. rep. 2011.

[32] Eugenio Mergagora. *Ponte dello Scout*. 2015. URL: `https://structurae.net/en/structures/scout-bridge`.

[33] Miebach. *Gutenstein bridge*. URL: `https://www.ib-miebach.de/de/projekte/holzbruecken/holz-bogenbruecke/holz-bogenbruecke-gutenstein-bei-sigmaringen.html`.

[34] Miebach. *Wolfratshausen*. URL: `https://www.ib-miebach.de/de/projekte/holzbruecken/holz-pylonbruecke/holz-pylonbruecke-wolfratshausen.html`.

[35] C. Moutinho, A. Cunha, and E. Caetano. "Analysis and control of vibrations in a stress-ribbon footbridge". In: *Structural Control and Health Monitoring* 18.6 (Oct. 2011), pp. 619–634. ISSN: 15452255. DOI: `10.1002/stc.390`.

[36] Reyn O'Born. "Life cycle assessment of large scale timber bridges: A case study from the world's longest timber bridge design in Norway". In: *Transportation Research Part D: Transport and Environment* 59 (Mar. 2018), pp. 301–312. ISSN: 13619209. DOI: `10.1016/j.trd.2018.01.018`.

[37] Marco Prandina. "Spatial Damping Identification". PhD thesis. 2010.

[38] Redactie Het Houtblad. *Botterbrug Harderwijk*. URL: `https://www.hethoutblad.nl/projectnieuws/botterbrug-harderwijk/7300/`.

[39] *Restauro conservativo Ponte di Morca*. 2003. URL: `https://www.maffeiarchitetto.com/architetto_borgosesia_dett/it/it-restauro-conservativo-ponte-di-morca-anno-2003.html`.

[40] Schaffitzel. *Nackartenzlingen*. URL: `https://www.schaffitzel.de/holzbrueckenbau/referenzen/neckartenzlingen`.

[41] Mike Schlaich et al. *Guidelines for the design of footbridges*. International Federation for Structural Concrete, 2005. ISBN: 288394072X.

[42] Sétra. *Footbridges Assessment of vibrational behaviour of footbridges under pedestrian loading*. Tech. rep. 2006. URL: `http://www.afgc.asso.fr`.

[43] Nicholas Simpson and Andrew Glover. *Recommendations for the assessment of footbridge response under footfall loading*. Tech. rep. 2016. URL: `www.arup.com`.

[44] Michelle Sonneveld. *Sensitivities and prerequisites of the application of the Energy Flux Analysis to high-rise structures excited by wind using in situ measurements*. Tech. rep. 2020. URL: `http://repository.tudelft.nl/..`.

[45] Structurae. *Momosuke Bridge*. URL: `https://structurae.net/en/structures/momosuke-bridge`.

[46] Structural Timber Association. *Glued laminated timber structures*. Tech. rep. 2014.

[47] StructureCraft. *Bow River Pedestrian Bridge*. URL: `https://structurecraft.com/projects/bow-river-pedestrian-bridge`.

[48] Yukio Tamura. *Damping in Buildings*. 2008.

[49] Tedder. *Dafne Schippersbrug*. 2017. URL: `https://nl.wikipedia.org/wiki/Dafne_Schipper sbrug#/media/Bestand:Dafne_Schippersbrug_wide_shot_looking_north.jpg`.

[50] H W Van Der Laan. *Structural Optimization of Stiffened Plates Application on an Orthotropic Steel Bridge Deck*. Tech. rep. 2021. URL: `http://repository.tudelft.nl/..`

[51] Pablo Van der Lugt. *Tomorrow's Timber: Towards the next building revolution*. Naarden: MaterialDistrict, 2020.

[52] Veronika Vašková, Lenka Poništová, and Roman Fojtík. *Dynamics effects on a wooden footbridge*. Tech. rep.

[53] Šána Vladimír, Polák Michal, and Plachý Tomáš. "A Dynamic Analysis of the Cable-Stayed Footbridge in Čelákovice Town". In: *Procedia Engineering*. Vol. 199. Elsevier Ltd, 2017, pp. 2877–2882. DOI: `10.1016/j.proeng.2017.09.582`.

[54] Peng Wang et al. "Fractional Critical Damping Theory and Its Application in Active Suspension Control". In: *Shock and Vibration* 2017 (2017). ISSN: 10709622. DOI: `10.1155/2017/2738976`.

[55] West8. "Oirschot bridge". In: (). URL: `https://www.west8.com/projects/oirschot_bridge/`.

[56] Wijma Kampen. *Arch bridge, Frederikssund*. URL: `https://www.lesserknowntimberspecies.com/cases/arch-bridge-frederikssund`.

[57] M. R. (Michael R.) Willford and P. (Peter) Young. *A design guide for footfall induced vibration of structures : [a tool for designers to engineer the footfall vibration characteristics of buildings or bridges]*. Concrete Society for the Concrete Centre, 2006, p. 83. ISBN: 1904482295.

[58] Nigel Young. *Millennium Bridge, London*. 2000. URL: `https://arquitecturaviva.com/works/puente-del-milenio-1`.

[59] Heidi Zengerling. *Dunajec River Bridge*. URL: `https://structurae.net/en/media/91321-dunajec-river-bridge`.

# A

# Overview bridges

## A.1. Timber bridges

In this appendix a selection of timber bridges is presented, selected with the criteria discussed in chapter 2.

| Bridge | Type | Use | Span | Year |
|---|---|---|---|---|
| Truss Bridge Sneek | Truss | Highway | 32 | 2010 |
| Girder bridge Roermond | Girder trough | Cyclist/pedestrian | 38 | 2014 |
| Arch bridge Frederikssund | Arch | Cyclist/pedestrian | 40 | 2013 |
| Vakwerkbrug Oirschot | Truss | Pedestrian | 40 | 2020 |
| Traversiner Steg, Viamala | Truss | Pedestrian | 42 | 1996 |
| Arch bridge, Gutenstein | Arch | Cars | 42 | 2011 |
| Cable-stayed bridge Příbor | Cable stayed | Pedestrian | 43 | 2013 |
| Girder bridge Neckartenzlingen | Girder | Cyclist/pedestrian | 45 | 2017 |
| Pylonbrücke, Wolfratshausen | Cable stayed | Cyclist | 47 | 2013 |
| Cable-stayed bridge Harderwijk | Cable stayed | Cyclist/pedestrian | 49 | 2014 |
| Suspension bridge Viamala | Suspension | Pedestrian | 56 | 2005 |
| Cable-stayed bridge Wernau | Cable-stayed | Cyclist/pedestrian | 62 | 1990 |
| Arch bridge Tynset | Arch | Highway | 70 | 2001 |
| Girder bridge Banff | Girder | Cyclist/pedestrian | 80 | 2013 |
| Dunajec River Bridge, Czorstyn | Cable stayed | Cyclist/ Pedestrian | 90 | 2006 |
| Arch bridge scout | Tied arch | Cyclist/pedestrian | 93 | Unknown |
| Ponte di Morca | Suspension | Cyclist/pedestrian | 94 | 1928 |
| Momosuke Bridge Japan | Suspension | Pedestrian | 105 | 1993 |
| Älvsbacka Timber Bridge, Skelleftea | Cable stayed | Cyclist/ Pedestrian | 130 | 2011 |

**Table A.1:** Overview timber bridges [5, 24, 56, 55, 15, 33, 52, 40, 34, 30, 16, 19]

Truss bridge Sneek



Girder bridge Roermond



Arch bridge Frederikssund



Truss bridge Oirschot



Truss bridge Viamala



Arch bridge Gutenstein



Cable-stayed bridge Pribor



Girder bridge Neckartenzlingen



Cable-stayed bridge Wolfratshausen



Cable-stayed bridge Harderwijk


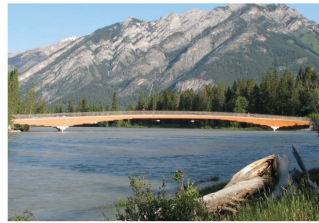
Suspension bridge Viamala



Cable-stayed bridge Neckarsteg

**Figure A.1:** Overview timber bridges [5, 24, 56, 55, 15, 33, 52, 40, 34, 30, 16, 19]

Arch brirdge Tynset


Girder bridge Bow


Cable-stayed bridge Dunajec


Arch bridge Scout


Suspension bridge Morca


Suspension bridge Momosuke


Cable-stayed bridge Alvsbacka

**Figure A.2:** Overview timber bridges [27, 47, 59, 32, 39, 45, 25]

## A.2. Damping ratios footbridges

In this appendix an overview of pedestrian bridges with their damping values is presented. The characteristics of the bridges are given in table A.2, a collection of pictures is shown in figure A.3.

| Name/location | Material | Type | Span [m] | Damping |
|---|---|---|---|---|
| Alvsbacka brirde | Timber | Cable-stayed | 130 | 1.2% (walking group) |
| Armentia bridge | Timber | Arch/girder | 61 | 2.91% (lateral, 1.64Hz), 2.85% (vertical, 2.38Hz) |
| Forchheim | Steel, timber deck | Cable-stayed | 88, 29 | 1% |
| Zürich - Winterthur | Concrete | Cable-stayed | 32, 32 | 1.89% |
| Hron river bridge | Steel | Cable-stayed | 50, 50 | 0.72-0.9% (vertical bending), 1.55-1.85% (torsion) |
| Celakovice | Concrete & steel | Cable-stayed | 43, 156, 43 | 2.2% (lateral), 1.9% and 1.5% (vertical) |
| Kochenhofsteg, Stuttgart | Concrete & steel | Suspension | 42 | 0.53% |
| Enzsteg II, Pforzheim | Concrete & steel | Suspension | 82 | 0.25% |
| Glacis Bridge, Minden | Concrete & steel | Suspension | 33, 105, 33 | 0.99%-1.77 |
| Stress ribbon, Porto | Concrete & steel | Stress-ribbon | 28 and 30 | 1.7% (first mode), 2.6% (second mode) |
| Glacis-Bridge, Ingolstadt | Concrete | Stress-ribbon | 42, 76, 46 | 0.11% before handrail and surfacing, 0.30% after handrail and surfacing |
| Solférino bridge, Paris | Steel | Arch | 106 | 0.4% (lateral), 0.5% (vertical) |
| Pedro and Ines, Coimbra | Steel | Arch/girder | 111 | 0.58 (lateral), 0.53, 1.04 (vertical) |

**Table A.2:** Examples of footbridges with damping ratios [25, 29, 14, 11, 4, 53, 28, 41, 35, 23, 10]

Cable-stayed bridge Alvsbacka

Forchheim bridge

Zürich - Winterthur

Hron river bridge

Celakovice bridge

Kochenhofsteg, Stuttgart

Enzsteg II

Glacis bridge, Minden

Stress ribbon bridge, Porto

Glacis bridge, Ingolstadt

Solférino bridge, Paris

Pedro and Ines, Coimbra

**Figure A.3:** Overview footbridges [25, 29, 14, 11, 4, 53, 28, 41, 35, 23, 10]

# B

# Wood modification

In this appendix some extra information about three wood modification techniques is presented to give a better view about what is possible.

**Acelytation**
Acelytation is the only way to obtain timber that is fit for structural use because the structural properties are largely unaffected [51]. By means of a vacuum pressure autoclave, acetic andryhide is pressed into the wood, replacing the OH-groups. Therefore, deep penetration of the wood is needed which is why only the sapwood of permeable species are fit for this use. Maple, beech and pine wood are fit for acelytation, particularly radiata pine is used most often. By acelytation durability class 1 can be reached.

**Furfurylation**
Since with furfurylation the timber looses some of its structural quality, the resulting timber is usually not used in structural parts but rather in decking or cladding [51]. Under high pressure the timber is impregnated with furfuryl alchohol, which cross-links OH-groups. Since with this technique deep penetration is required too, the same species as for acelytation are used. By furfurylation durability class 2 to 1 can be reached.

**Thermal modification**
The last method described here is thermal modification. As the name suggests, timber is heated to around 200 °C which destroys part of the OH-groups. Since this makes the timber more brittle and reduces the strength, the result is only used for non-structural purposes such as cladding. By thermal modification durability class 3 to 1 can be reached.

# C
# Static assessment

In this appendix the static assessment of the model is described. It starts with the material properties, followed by the considered loads and the performed checks.

## C.1. Material properties

The material properties for GL32h as given in NEN-EN 14080 Table 5 are shown in table C.1. The material properties for S355 are shown in the table C.2. The material properties for the cables are shown in figure C.3, which are obtained from the Bridon Structures Brochure and the eurocode [9]. Cables with different diameters have slightly different properties, but for the sake of simplicity the values of one type of cable (LC100) are taken.

| Symbol | Description | Value | Unit |
|--------|-------------|-------|------|
| $f_{t0k}$ | Characteristic tensile strength along the grain | 25.6 | N/mm² |
| $f_{c0k}$ | Characteristic compressive strength along the grain | 32 | N/mm² |
| $f_{vk}$ | Characteristic shear strength | 3.5 | N/mm² |
| $f_{mk}$ | Characterisctic bending strength | 32 | N/mm² |
| $E_{0.05}$ | Characteristic modulus of elasticity | 11800 | N/mm² |
| $\rho_{mean}$ | Mean density | 490 | kg/m³ |
| $\rho_k$ | Characteristic density | 440 | kg/m³ |

**Table C.1:** Material properties GL32h

| Symbol | Description | Value | Unit |
|--------|-------------|-------|------|
| $f_y$ | Strength | 355 | N/mm² |
| $E$ | Modulus of elasticity | 205000 | N/mm² |
| $G$ | Shear modulus | 76923.1 | N/mm² |
| $\rho$ | Density | 7850 | kg/m³ |
| $\nu$ | Poisson's ration | 0.3 | - |

**Table C.2:** Material properties S355

| Symbol | Description | Value | Unit | Comments |
|--------|-------------|-------|------|----------|
| $f_y$ | Strength | 1860 | $N/mm^2$ | Given in eurocode |
| $\rho$ | Density | 8040 | $kg/m^3$ | for LC100 [9] |
| $E$ | Modulus of elasticity | 160000 | $N/mm^2$ | Given in eurocode |

**Table C.3:** Material properties cables

## C.2. Loads

For the static assessment, the self-weight, the permanent load, pedestrian load and wind load are taken into account. Since according to Arup experience temperature load has a very limited influence on the results, it was decided to exclude it from the analysis in order to save computational costs. Stress due to changing moisture content was neglected too since the structural parts are clad and since the support conditions of the deck allow for expansion. The values of each load are explained below.

**Self-weight**

The self weight of the members of the bridge is included as a gravity load applied on all beam elements, see figure C.1. Bar elements were left out because they would take unrealistic deformations and non-existing moments. To account for parts of the structure that are not modelled (such as dowels, connection plates, cladding and cables) and for tolerances of the beam sections, the gravity load is multiplied by a factor 1.1, which is common practice in bridge design.
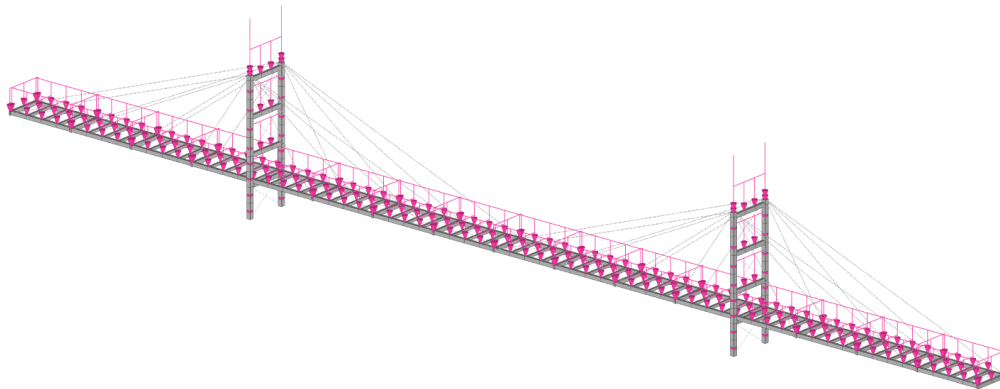


**Figure C.1:** Application of self-weight in the model

**Permanent load**

The permanent load represents the non-constructive elements of the bridge, which are not in the model. These include the deck, the wear layer, the railing and the lights. It is applied as a combination of grid loads and line loads, as can be seen in figure C.3. The values are displayed in table C.4. The weight of the deck is based on the structure of the Älvsbacka bridge, an schematic drawing of which is shown in figure C.2. The dimensions of the deck planks are scaled to their maximum span.

| What | Value | Applied as | Comments |
| --- | --- | --- | --- |
| Deck | $0.57kN/m^2$ | Grid load on deck | - |
| Wear layer | $0.2kN/m^2$ | Grid load on deck | Standard value, 10 mm wear layer |
| Railing | $1kN/m$ | Beam load on main beams | Standard value |

**Table C.4:** Permanent load



**Figure C.2:** Bridge deck with main girders, cross beams, decking planks and finish layer

**Figure C.3:** Application of permanent load in the model

## Pedestrian load

According to EN1991-2, section 5.3.2.1, the recommended value for pedestrian load is $5\ kN/m^2$. The pedestrian load should be applied in the most unfavourable positions. The two patterns that are exp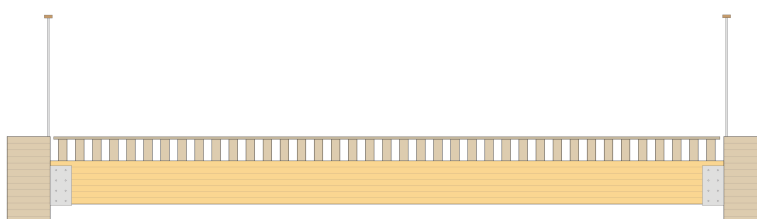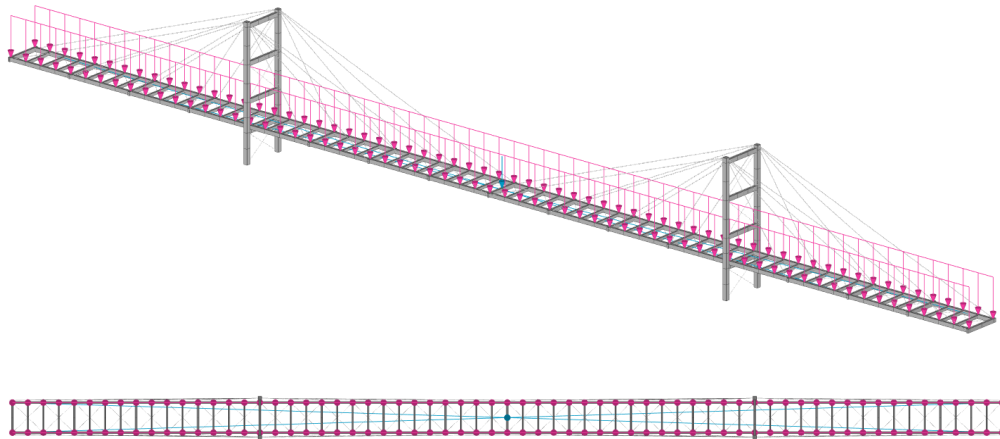ected to be governing for the stability of the pylons, the bending moments in the main beams and the global deflection, are applied in the model. They are shown in figure C.4 and C.5.

Depending on the influence length, the pedestrian load can be reduced with formula C.1, in which $L$ is the influence length (EN1991-2, section 5.3.2.1). These influence lengths differ per load combination, which are discussed at the end of this section. In the ULS load combinations, the shortest (and therefore governing) relevant influence length for the main beam is the distance between two cables. The longest influence length is the entire deck, governing the design of the pylons. For the sake of simplicity, it was chosen to use the distance between two cables in a bridge with 4 cables as the influence length for the ULS combinations. This results in a distributed load of $4.74\ kN/m^2$. In the SLS load combination, the influence length is the main span, resulting in a distributed load of $2.86\ kN/m^2$.

$$q_{\text{fk}} = 2,0 + \frac{120}{L+30} kN/m^2$$
$$q_{\text{fk}} \geq 2,5 kN/m^2; q_{\text{fk}} \leq 5,0 kN/m^2$$

(C.1)



Pedestrian load on entire deck

Pedestrian load on main span
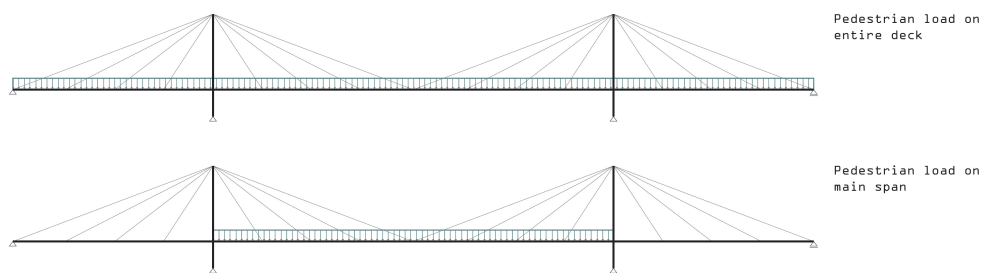
**Figure C.4:** Load patterns pedestrian traffic

(a) Pedestrian load on entire deck                    (b) Pedestrian load on main span
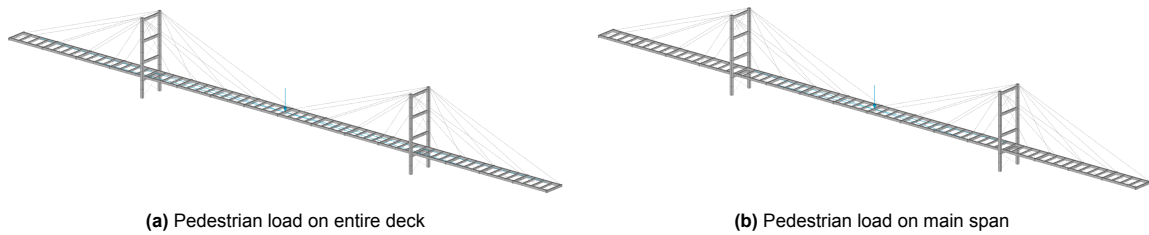
**Figure C.5:** Application of static pedestrian load in the model

## Wind load

The wind load is applied in accordance with EN1991-1-4 to the deck and the pylons. The formulas used to determine the values of the wind load are shown in table C.5. The values used in the expressions are given in table C.6.

| Section | Title | Formula |
|---------|-------|---------|
| 4.2 | Basic values | 4.1, 4.2 |
| 4.3 | Mean wind | 4.3 |
| 4.4 | Wind turbulence | 4.6, 4.7 |
| 4.5 | Peak velocity pressure | 4.8, 4.9, 4.10 |
| 5.3 | Wind forces | 5.3 |

**Table C.5:** EN1991-1-4 sections to determine wind loading

| Symbol | Description | Value | Unit | Comments |
|--------|-------------|-------|------|----------|
| $c_{dir}$ | Directional factor | 1 | - | Recommended value |
| $c_{season}$ | Season factor | 1 | - | Recommended value |
| $v_{b0}$ | Fundamental value of basic wind velocity | 24.5 | m/s | Zone III in figure NB.1 |
| $K$ | Shape parameter | 0.281 | - | Zone III in figure NB.1 |
| $n$ | Exponent | 0.5 | - | Zone III in figure NB.1 |
| $p$ | 1 over design life | 0.01 | - | 100 year design life |
| $z_0$ | Roughness length | 0.2 | m | Undeveloped area table NB.3 |
| $z_{min}$ | Minimum height | 4 | m | Undeveloped area table NB.3 |
| $z_{max}$ | Maximum height | 200 | m | Given value NB 4.3.2 |
| $z$ | Deck height at NAP level | 9 | m | |
| $z_p$ | Pylon top height at NAP level | 32 | m | Top maximum pylon height, conservative |
| $c_o$ | Orography factor | 1 | - | Given value |
| $k_l$ | Turbulence factor | 1 | - | Recommended value |
| $\rho$ | Air density | 1.25 | kg/m³ | |
| $c_{scd}$ | Structural factor | 1 | - | Given value |
| $c_{fx0}$ | Force coefficient deck lateral direction | 1.28 | - | Figure 8.3 |
| $c_{fz}$ | Force coefficient deck z direction | 0.9 | - | Recommended value 8.3.3 |
| $\Psi_r$ | Reduction factor for square sections with rounded corners | 1 | - | Figure 7.24, sharp edges, no reduction |
| $\Psi_{lambda}$ | End-effect factor for elements with free-end flow | 0.9 | - | From section 7.13 |
| $c_{f0y}$ | Force coefficient pylon lateral direction | 2.1 | | Figure 7.23, square section |
| $c_{f0x}$ | Force coefficient pylon longitudinal direction | 2.1 | | Figure 7.23, square section |

**Table C.6:** Values used to determine wind load

The forces in x-direction are calculted as 40% of the forces in y-direction, as directed by NB8.3.4. The resulting loads are shown in table C.7.

| What | Value | Applied as |
|---|---|---|
| q-load y deck | Depends on dimensions | Beam load on right main beam |
| q-load y deck 2 | $\frac{2}{3}$ of q-load y deck | Beam load on left main beam |
| q-load x deck | 40% of total q-load y | Grid load on deck |
| q-load z deck | 0.66 $kN/m^2$ | Grid load on deck |
| q-load x pylon | Depends on dimensions | Beam load on columns and cross beams |
| q-load y pylon | Depends on dimensions | Beam load on columns |

**Table C.7:** Wind load

With these loads, different load combinations can be made, shown in equation C.2, in which $F_z$ can be both directed upwards and downwards. The wind in positive z-direction is disregarded because it has a relieving effect for all checks, except unloading of the cables which is outside the scope of this thesis. Therefore, two wind combinations (Wind-1 and Wind-2) are left, which are shown in figure C.6.

$$F_{\text{y deck \& pylon}} + F_z$$
$$F_{\text{x pylon}} + 40\% F_{\text{y deck \& pylon}} + F_z$$

(C.2)



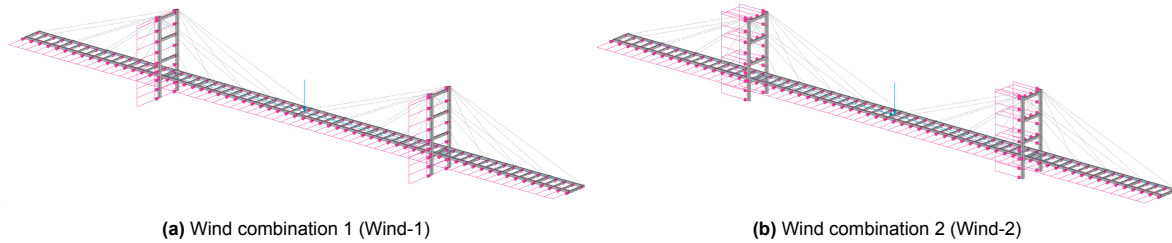**(a)** Wind combination 1 (Wind-1)    **(b)** Wind combination 2 (Wind-2)

**Figure C.6:** Application of wind load in the model

**Load combinations**

The load combination were determined as per EN1990. This resulted in the load combinations shown in table C.8. In the initial runs, all load combinations were used. Later a study was done to find out what load combinations were governing the design, after which it was decided to only include the governing ones in order to save computation time. These load combinations are C2, C5, C6, C8 and C9.

| C | Name | gamma | load | | psi | gamma | load | | psi | gamma | load |
|---|---|---|---|---|---|---|---|---|---|---|---|
| 1 | Selfweight 1 | 1.4 | SW + PL | + | 0.4 | 1.5 | Traffic_all | + | 0.3 | 1.65 | Wind_1 |
| 2 | Traffic 1 | 1.25 | SW + PL | + | 1 | 1.5 | Traffic_all | + | 0.3 | 1.65 | Wind_1 |
| 3 | Wind 1 | 1.25 | SW + PL | + | 0.4 | 1.5 | Traffic_all | + | 1 | 1.65 | Wind_1 |
| 4 | Selfweight 2 | 1.4 | SW + PL | + | 0.4 | 1.5 | Traffic_main | + | 0.3 | 1.65 | Wind_1 |
| 5 | Traffic 2 | 1.25 | SW + PL | + | 1 | 1.5 | Traffic_main | + | 0.3 | 1.65 | Wind_1 |
| 6 | Wind 2 | 1.25 | SW + PL | + | 0.4 | 1.5 | Traffic_main | + | 1 | 1.65 | Wind_1 |
| 7 | Selfweight 3 | 1.4 | SW + PL | + | 0.4 | 1.5 | Traffic_all | + | 0.3 | 1.65 | Wind_2 |
| 8 | Traffic 3 | 1.25 | SW + PL | + | 1 | 1.5 | Traffic_all | + | 0.3 | 1.65 | Wind_2 |
| 9 | Wind 3 | 1.25 | SW + PL | + | 0.4 | 1.5 | Traffic_all | + | 1 | 1.65 | Wind_2 |
| 10 | Selfweight 4 | 1.4 | SW + PL | + | 0.4 | 1.5 | Traffic_main | + | 0.3 | 1.65 | Wind_2 |
| 11 | Traffic 4 | 1.25 | SW + PL | + | 1 | 1.5 | Traffic_main | + | 0.3 | 1.65 | Wind_2 |
| 12 | Wind 4 | 1.25 | SW + PL | + | 0.4 | 1.5 | Traffic_main | + | 1 | 1.65 | Wind_2 |
| 31 | SLS_deflection | 1 | SW + PL | + | 0.8 | 1 | Traffic_main | + | 0 | 1 | Wind |

**Table C.8:** Load combinations

## C.3. Checks

### Member checks

To obtain the design values of the material properties, the formula in table C.9 is used, with the values shown in table C.10. The checks for timber cross sections are listed in table C.11. The values used in these checks are shown in table C.12. A buckling length of $1 * L$ is assumed for the pylons, see

figure C.7. This is slightly unconservative since the cables do not fully restrain the top of the pylon from moving in x-direction.

| Section | Title | Formula |
|---------|-------|---------|
| 2.4.1 | Design value of material property | 2.14 |

**Table C.9:** EN1995-1-1 section to obtain design values

| Symbol | Description | Value | Unit | Comments |
|--------|-------------|-------|------|----------|
| $k_{mod}$ | Modiciation factor taking into account effect of load duration and moisture content | 1.1 | - | Service class 2 and permanent action |
| $\gamma_m$ | Partial factor | 1.25 | - | Glulam members |

**Table C.10:** Values used to obtain design values for the material properties

| Section | Title | Formula |
|---------|-------|---------|
| 6.1.7 | Shear | 6.13 |
| 6.2.3 | Combined bending and axial tension | 6.17, 6.18 |
| 6.2.4 | Combined bending and axial compression | 6.19, 6.20 |
| 6.3.2 | Columns subjected to either compression or combined compression and bending | 6.23, 6.24 |

**Table C.11:** Member checks from EN1995-1-1 Ultimate limit states

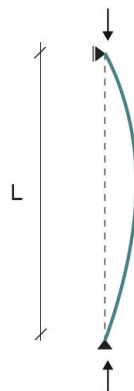| Symbol | Description | Value | Unit | Comments |
|--------|-------------|-------|------|----------|
| $k_m$ | Factor to account for the effects of imperfections for lateral torsional buckling | 0.7 | - | Rectangular cross-sections |
| $\beta$ | Factor for members within straightness limits | 0.1 | - | Glulam members |

**Table C.12:** Values used in member checks



**Figure C.7:** Buckling length

The cables are checked with a simple formula, shown in equation C.3. As a residue of an earlier model, the stresses in the cables are multiplied by a factor 1.33 in the python script. This was a mistake, however, inspecting the results it was found that the global deflection rather than the axial tension was governing the design. Besides, it might compensate the unconservative approach to not take into account the chainline effect and other verifications that are not performed. This effect was not taken into account because a nonlinear analysis would be needed since the stiffness of the cables depend

on the stress in the cables. The steel beam members are not checked since their dimensions are not a variable in the model. In a separate verification it was found that the chosen section is able to carry the loads.

$$UC = \sigma/f_y \qquad (C.3)$$

## Connection checks

In section 2.5, four connections in cable-stayed timber footbridges were given. Two connections that are expected to be important for the design are checked during the optimisation process; the connection between the cross beam and the main beam (figure C.8a), and the connection between the main beam and the steel beam (figure C.8b). In the connection between the pylon and the cables, the load is spread over the full cross-sectional area of the pylon. Therefore this connection is expected not to be critical in the design and is not checked. The connection between the pylon and its crossbeams is also expected not to be critical in the design, which is why it is left out of the checks as well. In addition, the loads on these connections will only vary slightly with different design variants.
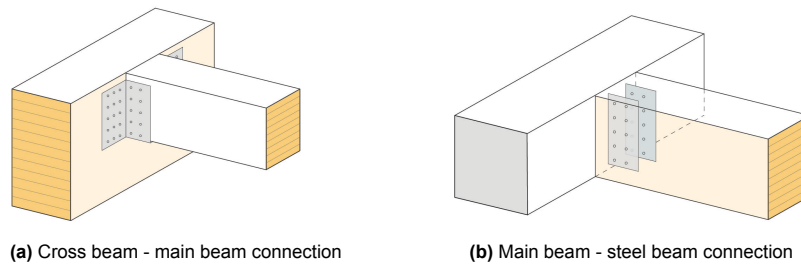


**(a)** Cross beam - main beam connection       **(b)** Main beam - steel beam connection

**Figure C.8:** Checked details

The connection capacity is checked with the intention to determine if it is possible to make a connection of reasonable size within the dimensions of the members. This method was chosen because the dimensions vary with each design variant in the optimisation process, which makes it hard to actually design a connection for each variants. The UC is simply the maximum possible capacity divided by the needed capacity. The maximum dimensions of the connections is shown in figure C.9. In connection a) the maximum width of the joist hanger on one side is the width of the cross beam. The maximum height is the height of the cross beam. Similarly, the size of the shear plate in connection b) is constraint by the height of the main beam. The amount of fasteners is constraint by the minimum edge- and end-distances. Table C.13 shows where they can be found in the eurocode. The capacity of the fasteners of the two connections will be set out in the following paragraphs.



**(a)** Maximum dimensions cross beam - main beam connection       **(b)** Maximum dimensions main beam - steel beam connection
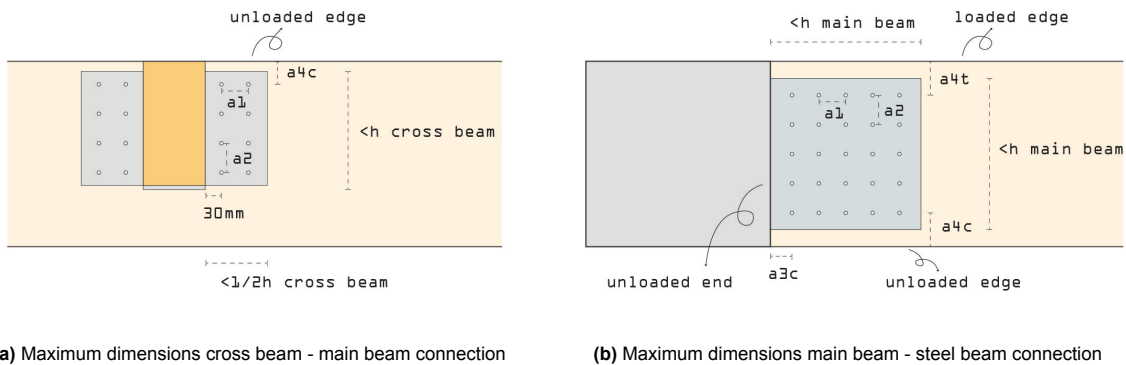
**Figure C.9:** Checked details

### Connection cross beam - main beam

The fasteners of this connection are screws. Since the diameter is more than 6mm, according to EN1995-1-1 section 8.7.1, the rules of section 8.5.1 apply. The formulas needed to calculate the

| Section | Title | Table | Name |
|---------|-------|-------|------|
| 8.5 | Bolted connections | 8.4 | Minimum values of spacing and edge and end distances for bolts |
| 8.6 | Dowelled connections | 8.5 | Minimum spacings and edge and end distances for dowels |

**Table C.13:** EN1995-1-1 Edge and end distances

connection are given in table C.14. The input of these checks is given in table C.15. In the formulas, the rope effect is not taken into account. Since the connections were not governing the design, this assumption has no influence on the result. For the same reason, the connection checks were left out of the optimisation runs in order to save computation time.

| Section | Title | Formula |
|---------|-------|---------|
| 8.2.3 | Steel-to-timber connections | 8.9, 8.10 |
| 8.5.1 | Laterally loaded bolts | 8.30, 8.31, 8.21, 8.33 |

**Table C.14:** Connection checks from EC5-1 - Section 8: Connections with metal fasteners

| Symbol | Description | Value | Unit | Comments |
|--------|-------------|-------|------|----------|
| $f_{uk}$ | Characteristic tensile strength | 800 | N/mm² | Strength class 8.8 |
| $d$ | Diameter of the fastener | 8 | mm | |
| $\gamma_m$ | Partial factor | 1.3 | - | Value for connections |
| $k_{90}$ | Factor | 1.35 + 0.015d | - | Softwoods |
| $\alpha$ | Angle of the load to the grain | 90 | deg | |

**Table C.15:** Values used in connection checks cross beam - main beam

**Connection main beam - cross beam**

For connections with more than two shear planes, which is the case for the connection between the main beam and the steel beam, EN1995 gives no guidance. Instead the failure mechanisms as proposed by Bocquet [8] are used, shown in the equations below. Formulas (f), (g) and (h) represent failure mechanisms on the outside, while (l) and (m) represent failure mechanisms on the inside. Together, six combinations can be made, of which 5 possible failure modes are composed. These modes are shown in table C.16 and figure C.10.

$$(f): F_{v,Rk} = 0.5 \cdot f_{h,1,k} \cdot t_1 \cdot d \tag{C.4}$$

$$(g): F_{v,Rk} = f_{h,1,k} \cdot t_1 \cdot d \cdot \left[ \sqrt{2 + \frac{4 \cdot M_{y,Rk}}{f_{h,1,k} \cdot d \cdot t_1^2}} - 1 \right] + \frac{F_{ax,Rk}}{4} \tag{C.5}$$

$$(h): F_{v,Rk} = 2.3 \cdot \sqrt{M_{y,Rk} \cdot f_{h,1,k} \cdot d} + \frac{F_{ax,Rk}}{4} \tag{C.6}$$

$$(l): F_{v,Rk} = 0.5 \cdot f_{h,2,k} \cdot t_2 \cdot d \tag{C.7}$$

$$(m): F_{v,Rk} = 2.3 \cdot \sqrt{M_{y,Rk} \cdot f_{h,2,k} \cdot d} + \frac{F_{ax,Rk}}{4} \tag{C.8}$$

| Mode | | | | | | |
|---|---|---|---|---|---|---|
| 1 | f | + | 2 * | l | + | f |
| 2 | g | + | 2 * | l | + | g |
| 3 | h | + | 2 * | l | + | h |
| 5 | g | + | 2 * | m | + | g |
| 6 | h | + | 2 * | m | + | h |

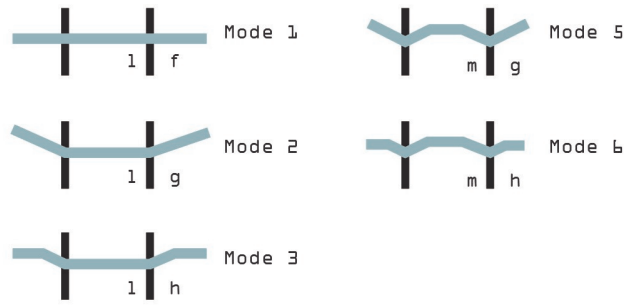**Table C.16:** Failure modes in a connection with 2 shear planes



**Figure C.10:** Failure modes

# D

# Dynamic assessment

In this appendix an outline of the steps in the JRC guideline for the assessment of human-induced vibrations to calculate maximum accelerations is presented as well as how these steps are applied in the model.

**Critical range of natural frequencies**
The calculations of the maximum accelerations are based on the accelerations in resonance. Therefore the range of natural frequencies where resonance can occur under pedestrian loading has to be determined. The critical ranges of natural frequencies for vertical and lateral modes are shown in table D.1. These are dependent on the step frequencies of pedestrians, as discussed in chapter 3.

|          | Lower limit [Hz] | Upper limit [Hz] |
|----------|------------------|------------------|
| Vertical | 1.25             | 2.3              |
| Lateral  | 0.5              | 1.2              |

**Table D.1:** Critical range natural frequencies [23]

**Modal analysis**
The second step when calculating the maximum accelerations in a structure, is determining the natural frequencies and mode shapes. In this research this is done by a modal analysis in GSA. The amount of modes analysed differs. In the optimisation study 15 modes were sufficient to cover the range of frequencies that need to be checked. In the parameter study 30 modes were needed to ensure the entire range was covered because in that study some more extreme variants were considered. To include the mass of the deck and the railing, the load case of the permanent load is included in the analysis.

**Determine type of mode**
To calculate the accelerations, the type of mode needs to be known. The corresponding procedure was explained in section 5.3. In the end of this appendix some examples are shown.

**Traffic classes**
Naturally, during its lifetime a bridge is subjective to different loading intensities. These are divided in traffic classes, based on the amount of people per square meter. The traffic classes used in the JRC document are shown in table D.2.

| Traffic class | Description                 | Density $[people/m^2]$ |
|---------------|-----------------------------|------------------------|
| TC1           | Very weak traffic           | $d = 0.02$             |
| TC2           | Weak traffic                | $d = 0.2$              |
| TC3           | Dense traffic               | $d = 0.5$              |
| TC4           | Very dense traffic          | $d = 1.0$              |
| TC5           | Exceptionally dense traffic | $d = 1.5$              |

**Table D.2:** Pedestrian traffic classes and densities from JRC document [23]

In the dynamic analyses of both the parameter studies and the final optimisations, mostly TC2 has been used. However, to show the influence of different traffic classes on the results, TC1 and TC3 have been used as well.

## Load per person P

Based on table 4-8 from JRC document, the amplitude of the load per person $P$ can be obtained, shown in table D.3. The effect of torsion is not included in the JRC document, nor in any of the consulted guidelines [22, 41, 42, 57]. Based on advice from Arup, torsional modes are regarded as vertical modes, which is a conservative approach since the highest modal displacements are only at the edge of the deck.

| Direction | Load P [N] |
|-----------|------------|
| Vertical  | 280        |
| Lateral   | 35         |

**Table D.3:** Amplitude of the load for a single pedestrian [23]

## Equivalent number of pedestrians

With the pedestrian density and the surface of the deck, the total number of pedestrians can be determined with $n = d * span * width$. This number represents a stream of $n$ random pedestrians. To calculate the idealised stream of perfectly synchronised pedestrians, $n$ is reduced to $n'$. The formula for TC1-TC3 is shown in equation D.1.

$$n' = \frac{10.8\sqrt{\xi * n}}{S} \left[ m^{-2} \right] \tag{D.1}$$

## Reduction coefficient

In figure D.1, the reduction coefficient $\psi$ that reflects the critical ranges for natural frequencies of footbridges with pedestrian excitation is shown. Outside the critical range the factor is zero. Since in vertical direction footbridges might also be excited by the second harmonic of pedestrian loading, there are $\psi$-factors for the second harmonic too. However, since according to Arup experience this is hardly ever governing, the second harmonic of footfall loading is not taken into account in this thesis. Since torsional modes are treated as vertical modes, the $\psi$ factors for vertical vibrations are used for torsional vibrations.
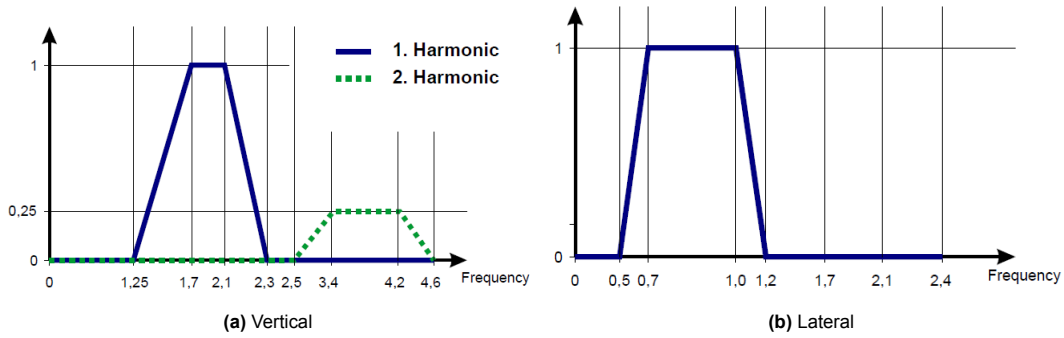


**(a)** Vertical          **(b)** Lateral

**Figure D.1:** Reduction coefficient $\psi$ [23]

## Uniformly distributed load and modal load

With this information, the uniformly distributed load $p$ in $N/m$ can be calculated using formula D.2.

$$p = P * n_{eq} * \psi * width \tag{D.2}$$

The modal load $P_{eq.m}$ can be calculated as the integral of the load per linear meter times the absolute values of the mode shape, as shown in equation D.3. To compute the integral numerically, the approximation of equation D.4 can be used.

$$P_{eq.m} = \int_0^L p \cdot Modeshape_{abs}(x)dx \tag{D.3}$$

90

$$P_{eq.m} = p * \sum_{i=1}^{segment_{number}} [(Modeshape_{abs})_i * (Segment_{length})_i] \tag{D.4}$$

**Damping**
To calculate the maximum acceleration, a damping value is needed. Given the large uncertainty, the analyses were done with different damping values. The exact values and motivation of these were given in section 6.4.

**Maximum acceleration**
When $P_{eq.m}$, $\xi$ and $M_m$ are known, the maximum acceleration at resonance can be calculated with equation D.5

$$a_{max} = \frac{P_{eq.m}}{2 * \xi * M_m} m/s^2 \tag{D.5}$$

**Comfort classes**
As explained in chapter 3, the JRC document uses comfort classes to assess the maximum accelerations. For completeness, they are given in table D.4 again. There are four comfort classes, ranging from 'maximum comfort' to 'unacceptable discomfort', each coupled to vertical and lateral acceleration limits. The comfort classes used for a specific bridge project can be determined in the project specifications.

| Comfort class | Degree of comfort | Vertical $a_{\text{limit}}[m/s^2]$ | Lateral $a_{\text{limit}}[m/s^2]$ |
|---|---|---|---|
| CL1 | Maximum | $< 0.50$ | $< 0.10$ |
| CL2 | Medium | $0.50 - 1.00$ | $0.10 - 0.30$ |
| CL3 | Minimum | $1.00 - 2.50$ | $0.30 - 0.80$ |
| CL4 | Unacceptable discomfort | $> 2.50$ | $> 0.80$ |

**Table D.4:** Comfort classes according to the JRC document [23]

**Lateral lock-in effect**
The lock-in effect was explained in section 3.5. Two methods for determining whether or not this effect occurs were described, one that calculates a maximum amount of people and a second one that links the maximum lateral accelerations to the lock-in effect. Since the span of the bridge of this thesis is rather long, the amount of people on the bridge in a traffic class 2 situation would always be more than the allowed amount based on the first method, which was deemed an unrealistic approach. Therefore the decision was made to use the second method for checking the lateral lock-in effect, namely to expect that the effect can occur from a lateral acceleration of 0.1 $m/s^2$.

**Effect of joggers**
As explained in chapter 5, loading by joggers is not taken into account. With the type of assessment used for groups of people, this often gives a conservative result, which would make the results less realistic. To realistically assess the influence of jogger loading, an analysis with a moving load would be needed, which was outside the scope of this thesis.

**Examples of mode types**
In figure D.2, the modes of one model are shown with their categorisation. The colours in the plots indicate the absolute displacement. 'Out of range' means that the mode is outside the critical range of frequencies and will therefore not be considered in the calculation.
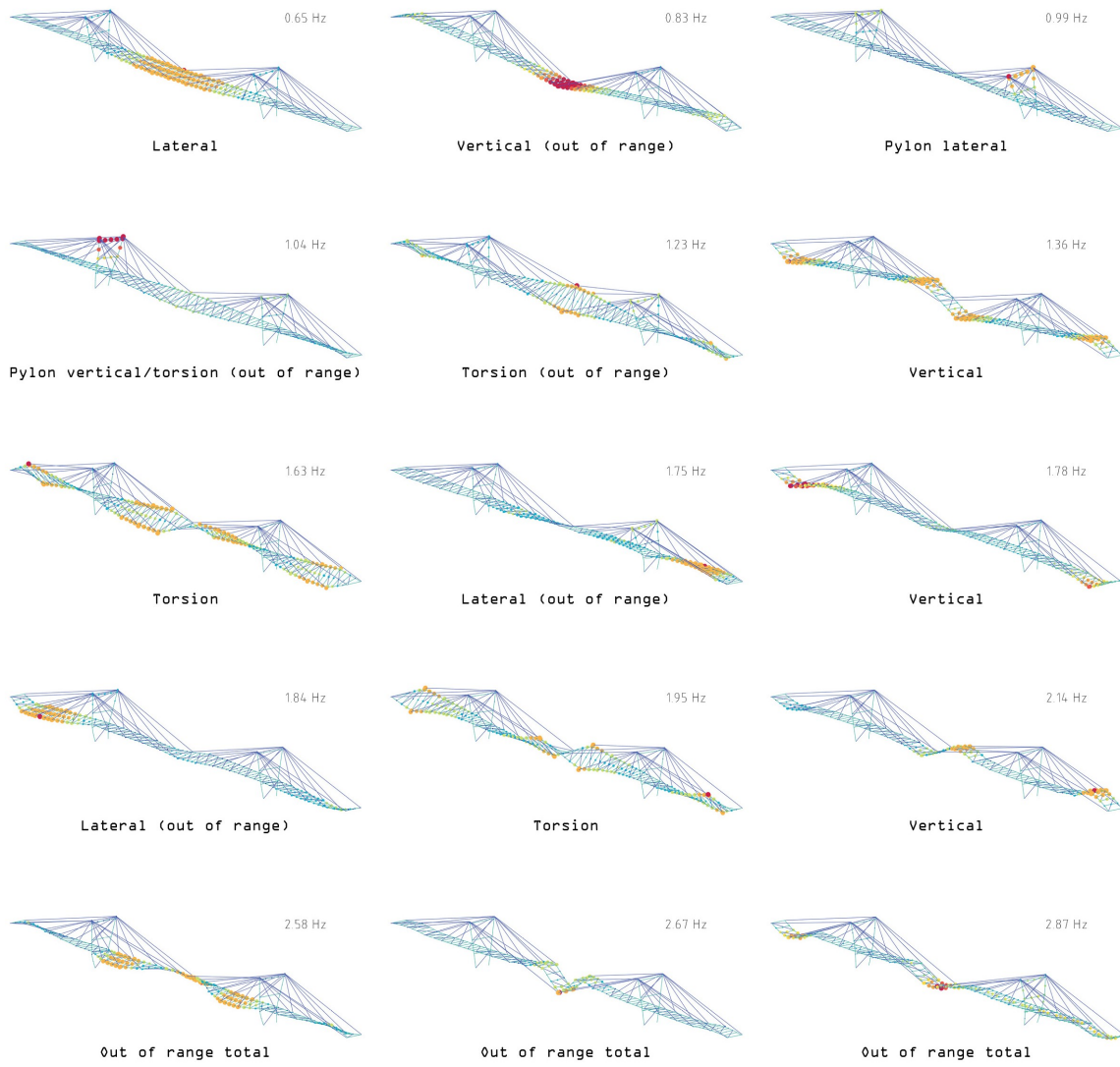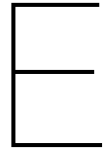
**Figure D.2:** Mode type examples

# Verification studies parameter study

This appendix presents the extended version of the results discussed in section 7.3, which contained three verification studies. First, the question what happens when other studied parameters are also a variable in the optimisation process is discussed, followed by the influence of the damping value and the traffic class. Finally, the influence of the connection stiffness is investigated. Additionally, the influence of excluding torsion modes from the analysis is investigated.

## E.1. Part 3a - More optimisation parameters

As was explained in section 7.3, this verification study was done to investigate to what extent the results are influenced by other parameters. This can be interesting, since for example the optimum amount of cables might change for different pylon heights. Therefore the two other studied parameters were treated as a optimisation parameter in the optimisation too, instead of having a set value as was the case in part 2a. More information about the optimisation can be found in appendix F.3. Inspecting the results, it was deemed possible that the optimisation runs did not find a sufficiently optimised model in all runs. Therefore the results presented in this section might not be entirely reliable. However, it is still interesting to investigate to what extent the trends found in part 2 of the parameter study survive the variation of the other parameters.

### Pylon height

Runs are done for pylon heights varying from 13 till 20 m.

**Result optimisation runs**

In figure E.1 the total mass after the optimisation process is shown. Table E.1 shows the corresponding values of the optimisation parameters. The total mass stays in the same range as in part 2a when the pylon height is increased, but does not follow a clear trend. The shape of the pylon is seemingly random. This is explained by the notion that the pylon shape has a limited influence on the distribution of forces (as was seen in section 7.2) and that the mass of the pylons was not accurately calculated in these runs. That is, the angle of the pylons and the length of the pylon cross beams was not taken into account.
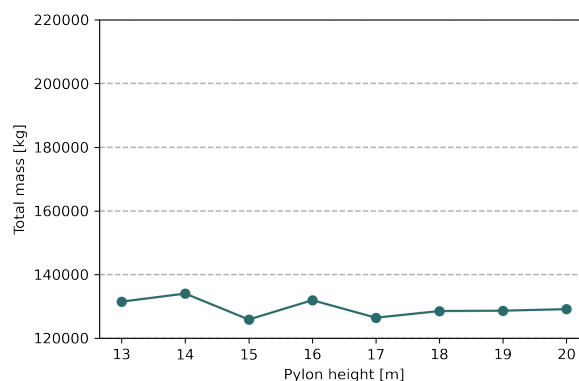


**Figure E.1:** Total mass of models with different pylon heights

| Pylon height [m] | Total mass [kg] | Cable diameter [mm] | Pylon dimension [mm] | Main beam height [mm] | Cross beam height [mm] | Pylon shape [m] | Amount of cables |
|---|---|---|---|---|---|---|---|
| 13 | 131496 | 93 | 662 | 683 | 406 | 0.0 | 5 |
| 14 | 134035 | 80 | 681 | 726 | 383 | 1.3 | 5 |
| 15 | 125877 | 76 | 686 | 679 | 389 | 0.7 | 5 |
| 16 | 131947 | 69 | 705 | 701 | 408 | -0.7 | 5 |
| 17 | 126453 | 64 | 717 | 726 | 400 | 1.2 | 4 |
| 18 | 128545 | 59 | 737 | 690 | 386 | 1.8 | 5 |
| 19 | 128658 | 56 | 748 | 672 | 377 | 1.1 | 5 |
| 20 | 129140 | 54 | 763 | 646 | 406 | -0.2 | 5 |

**Table E.1:** Parameter results - height part 3

**Accelerations**

The vertical accelerations follow approximately the same trend as in part 2a of the parameter study. The variations can be explained by variations in the optimisation parameters. The lower value at pylon height 13 for example, is explained by a relatively high cable diameter. The higher values at pylon height 14, 17, 18 and 19 are explained by positive pylon shapes. The higher value at pylon height 20 is explained by a relatively low main beam.
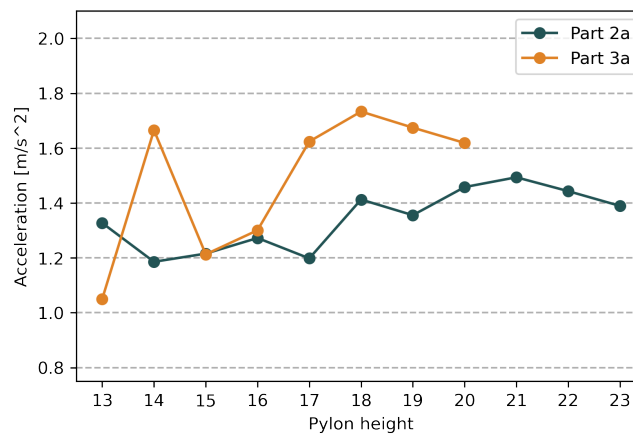


**Figure E.2:** Vertical accelerations

| Pylon height | 13 | 14 | 15 | 16 | 17 | 18 | 19 | 20 | 21 | 22 | 23 |
|---|---|---|---|---|---|---|---|---|---|---|---|
| Part 2a | vertical | vertical | vertical | vertical | vertical | vertical | torsion | torsion | torsion | torsion | vertical |
| Part 3a | vertical | torsion | torsion | torsion | torsion | torsion | torsion | torsion | - | - | - |

**Table E.2:** Mode shape types

The lateral accelerations follow the same trend in part 2a of the parameter study. The explanation is the same too: as the cable diameter decreases, the maximum acceleration increases. Though from the results this was unsure, it might also be that a higher pylon brings less lateral stiffness to the structure. The deviations from the trend can be explained by the varying pylon shapes.
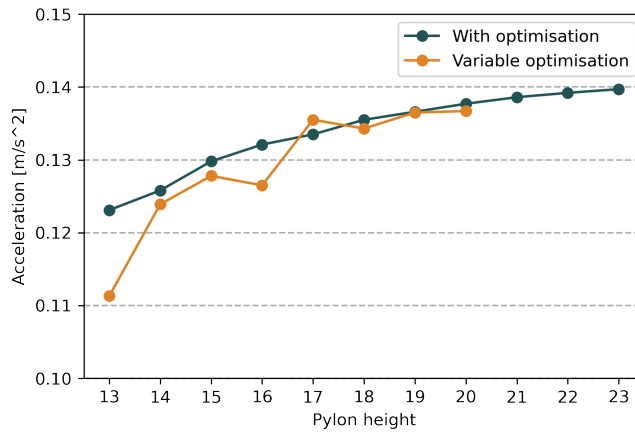
**Figure E.3:** Lateral accelerations

| Pylon height | 13 | 14 | 15 | 16 | 17 | 18 | 19 | 20 | 21 | 22 | 23 |
|---|---|---|---|---|---|---|---|---|---|---|---|
| Part 2a | lateral | lateral | lateral | lateral | lateral | lateral | lateral | lateral | lateral | lateral | lateral |
| Part 3a | lateral | lateral | lateral | lateral | lateral | lateral | lateral | lateral | - | - | - |

**Table E.3:** Mode shape types

## Pylon shape

Runs are done for pylon shapes varying from -4 till 4 m.

**Result optimisation runs**

In figure E.1 the total mass after the optimisation process is shown when varying the shape of the pylons. The mass does not follow a clear trend. Table E.4 shows the corresponding values of the optimisation parameters.
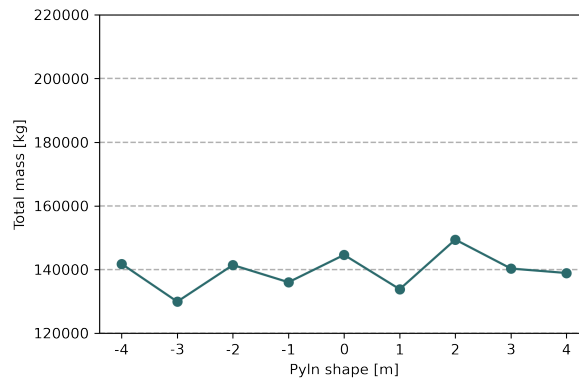


**Figure E.4:** Total mass of models with different pylon shapes

95

| Pylon shape [m] | Total mass [kg] | Cable diameter [mm] | Pylon dimension [mm] | Main beam height [mm] | Cross beam height [mm] | Amount of cables | Pylon height [m] |
|---|---|---|---|---|---|---|---|
| -4 | 141777 | 68 | 790 | 707 | 406 | 5 | 15.8 |
| -3 | 129924 | 74 | 732 | 655 | 416 | 5 | 15.8 |
| -2 | 141429 | 92 | 761 | 692 | 423 | 5 | 13.2 |
| -1 | 136022 | 74 | 693 | 721 | 410 | 5 | 14.8 |
| 0 | 144609 | 96 | 668 | 757 | 384 | 5 | 12.2 |
| 1 | 133831 | 98 | 650 | 696 | 406 | 5 | 12.3 |
| 2 | 149412 | 110 | 637 | 760 | 408 | 5 | 11.3 |
| 3 | 140322 | 91 | 659 | 802 | 406 | 4 | 12.6 |
| 4 | 138917 | 101 | 654 | 786 | 403 | 4 | 11.8 |

**Table E.4:** Parameter results - shape part 3

**Accelerations**

In figure E.5 the vertical accelerations are shown. Except from the models with pylon shape -3, -4, and 3, the accelerations are more or less constant. This might be explained by the fact that they are governed by vertical modes, which are not effected by the shape of the pylon. The high value at pylon shape 3 might be explained by the fact that there are only 4 cables in that model (shape 4 has 4 cables too, but a higher cable diameter). The lower values of shape -3 and -2 are hard to explain.
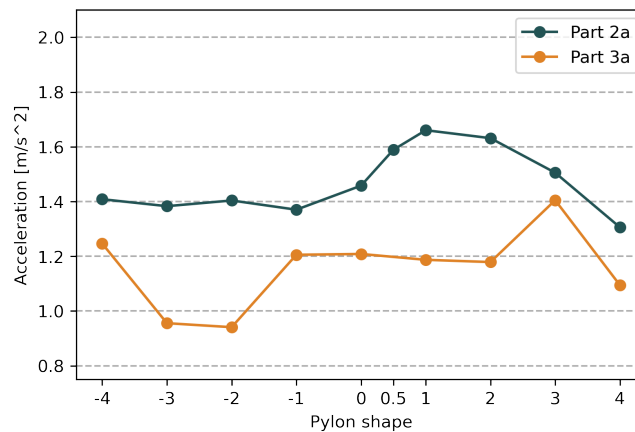


**Figure E.5:** Vertical accelerations

| Shape | -4 | -3 | -2 | -1 | 0 | 0.5 | 1 | 2 | 3 | 4 |
|---|---|---|---|---|---|---|---|---|---|---|
| Part 2a | vertical | vertical | vertical | vertical | torsion | torsion | torsion | torsion | torsion | vertical |
| Part 3a | vertical | vertical | vertical | vertical | vertical | - | | vertical | vertical | vertical | vertical |

**Table E.5:** Mode shape types

In figure E.6 the lateral accelerations are shown. In the runs of part 3a, the maximum accelerations are lower than in the runs of part 2a. This can be explained by higher cable dimensions. The diameters differ and this might explain the deviations from the expected upward trend. The higher the cable diameter, the higher the deviation from the trend. The higher accelerations at shape 3 and 4 despite the high cable diameters can be explained because in these models there are 4 cables, while the other models have 5 cables.
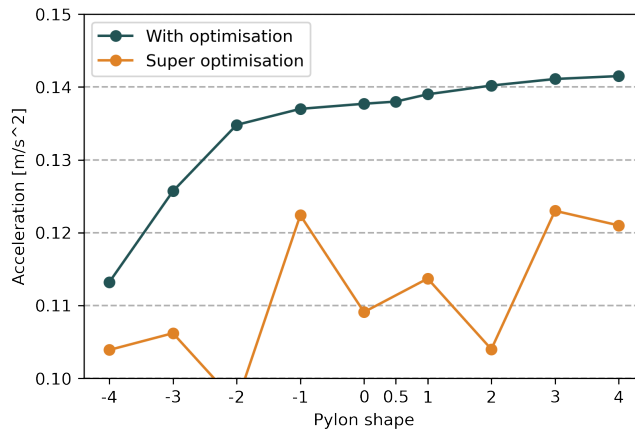
**Figure E.6:** Lateral accelerations

| Shape | -4 | -3 | -2 | -1 | 0 | 0.5 | 1 | 2 | 3 | 4 |
|---|---|---|---|---|---|---|---|---|---|---|
| Part 2a | Pylon lateral | lateral | lateral | lateral | lateral | lateral | lateral | lateral | lateral | lateral |
| Part 3a | pylon lateral | pylon lateral | pylon lateral | lateral | lateral | | lateral | lateral | lateral | lateral |

**Table E.6:** Mode shape types

## Amount of cables

Runs are done 2, 3, 4, 5 and 6 cables.

**Result optimisation runs**

Figure E.7 shows the total mass after the optimisations. In table E.7 the corresponding optimisation parameters are shown. The mass decreases with more cables, though it rises again with 6 cables. The decrease is mainly caused by different main beam heights. The higher mass with 6 cables is caused by the same mechanism as in the normal optimisation, namely that combined bending around the z-axis and tension becomes governing for the dimensions of the main beam.
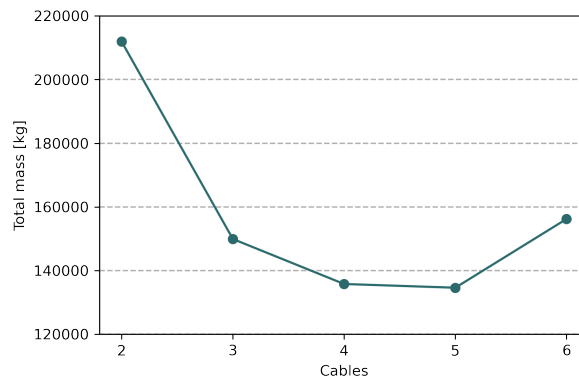


**Figure E.7:** Total mass of models with different amount of cables

| Pylon height [m] | Total mass [kg] | Cable diameter [mm] | Pylon dimension [mm] | Main beam height [mm] | Cross beam height [mm] | Pylon shape [m] | Pylon height [m] |
|---|---|---|---|---|---|---|---|
| 2 | 211910 | 98 | 678 | 1143 | 445 | -0.8 | 13.4 |
| 3 | 149910 | 81 | 687 | 868 | 388 | -0.1 | 14.3 |
| 4 | 135783 | 94 | 662 | 765 | 401 | 0.9 | 13.2 |
| 5 | 134611 | 89 | 679 | 711 | 403 | 1.2 | 13.0 |
| 6 | 156205 | 69 | 694 | 843 | 428 | 1.2 | 14.9 |

**Table E.7:** Parameter results - cables part 3

**Accelerations**

Figure E.8 shows the vertical accelerations. They do not follow a clear trend. This corresponds with the variations in the optimisation parameters.
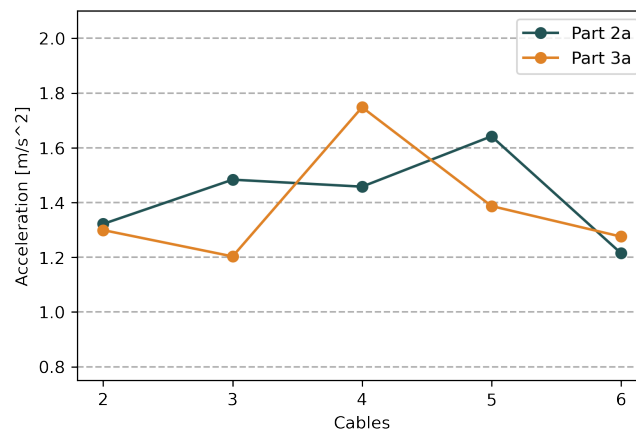


**Figure E.8:** Vertical accelerations

| Cables | 2 | 3 | 4 | 5 | 6 |
|---|---|---|---|---|---|
| Part 2a | vertical | pylon vertical | torsion | torsion | vertical |
| Part 3a | vertical | vertical | vertical | torsion | vertical |

**Table E.8:** Mode shape types

Figure E.9 displays the lateral accelerations. They approximately follow the same trend as in part 2a, except that the accelerations become lower after 3 cables. This can not be explained by the optimisation parameters, since in the models with 3, 4, and 5 cables they either do not follow a trend (e.g. cable diameters are 81, 94 and 89 mm). This leads to the hypothesis that in these runs the amount of cables overrule the effect of changing optimisation parameter, so that the accelerations are more like the trend found in part 2b. The fact that the downward trend is less strong can be explained by the influence of the optimisation parameters.
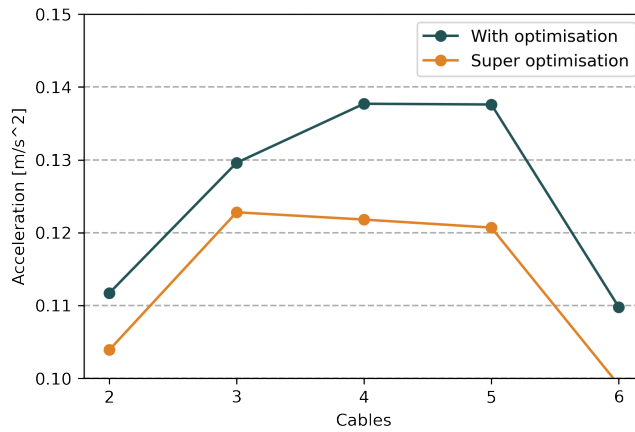
**Figure E.9:** Lateral accelerations

| Cables | 2 | 3 | 4 | 5 | 6 |
|---|---|---|---|---|---|
| Part 2a | lateral | lateral | lateral | lateral | lateral |
| Part 3a | lateral | lateral | lateral | lateral | lateral |

**Table E.9:** Mode shape types

## E.2. Part 3b - Damping value and traffic class

Per studied parameter, the influence of the damping value and the traffic class on the results of part 2a is shown in the graphs. As explained in section 7.3, the influence is linear. Therefore no further comments are given.
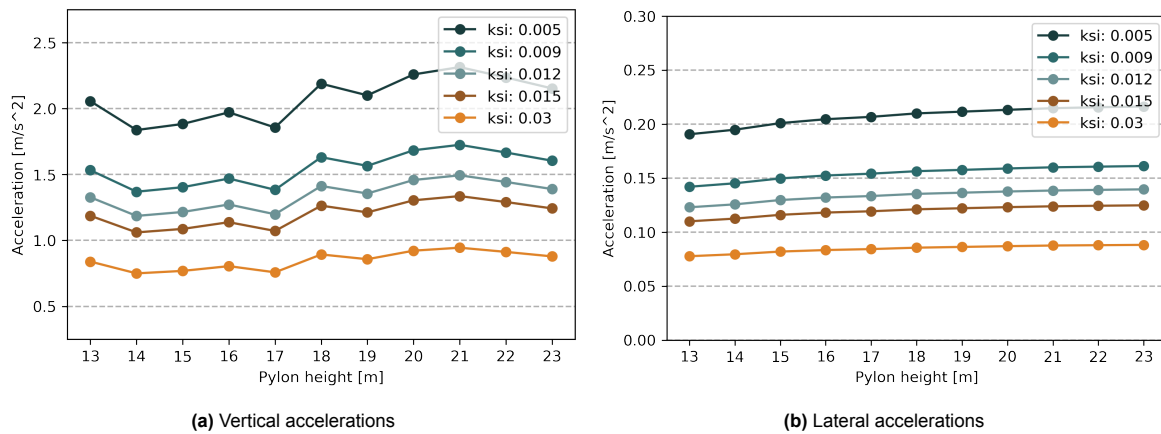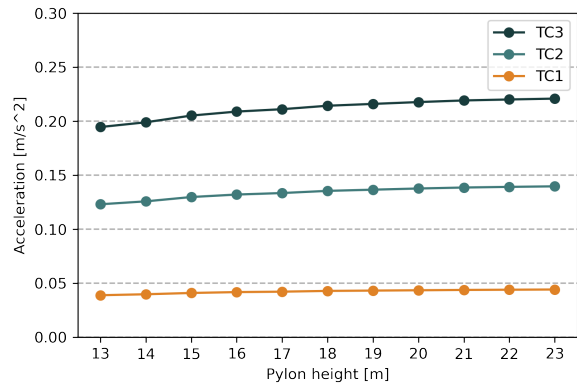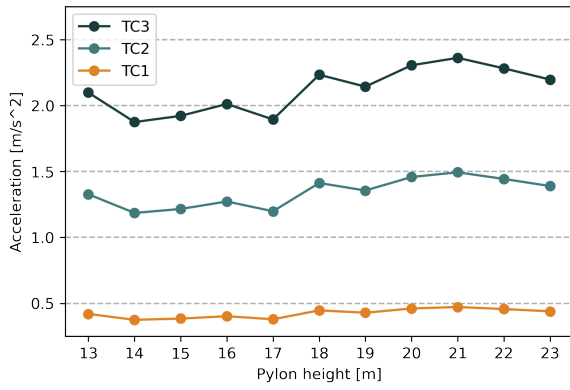
**Pylon height**



**(a)** Vertical accelerations



**(b)** Lateral accelerations

**Figure E.10:** Effect of different damping values

**(a)** Vertical accelerations

**(b)** Lateral accelerations

**Figure E.11:** Effect of different traffic classes

## Pylon shape



**(a)** Vertical accelerations

**(b)** Lateral accelerations

**Figure E.12:** Effect of different damping values
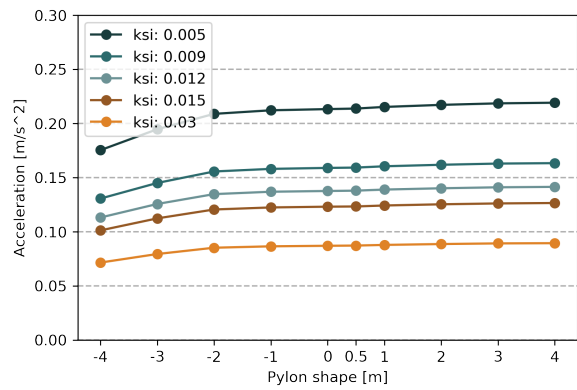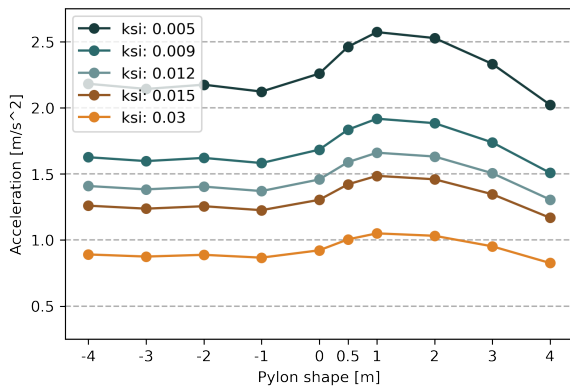


**(a)** Vertical accelerations

**(b)** Lateral accelerations

**Figure E.13:** Effect of different traffic classes

**Amount of cables**



**(a)** Vertical accelerations       **(b)** Lateral accelerations

**Figure E.14:** Effect of different damping values



**(a)** Vertical accelerations       **(b)** Lateral accelerations

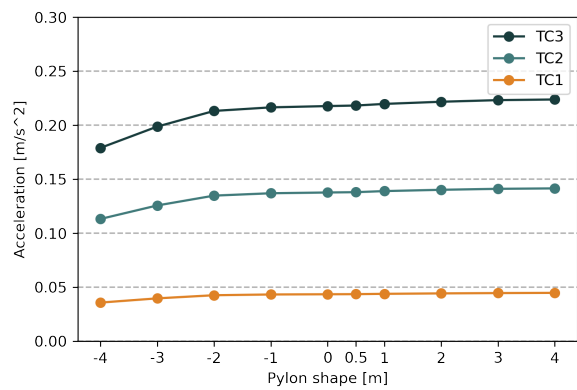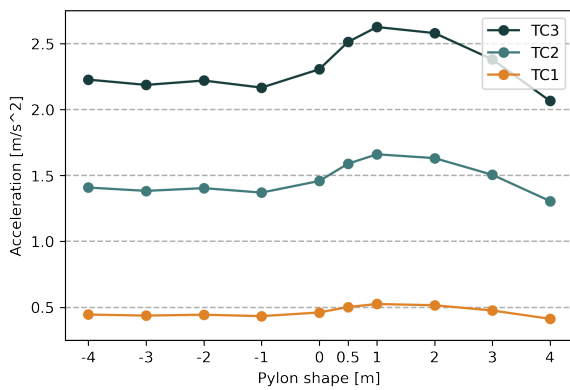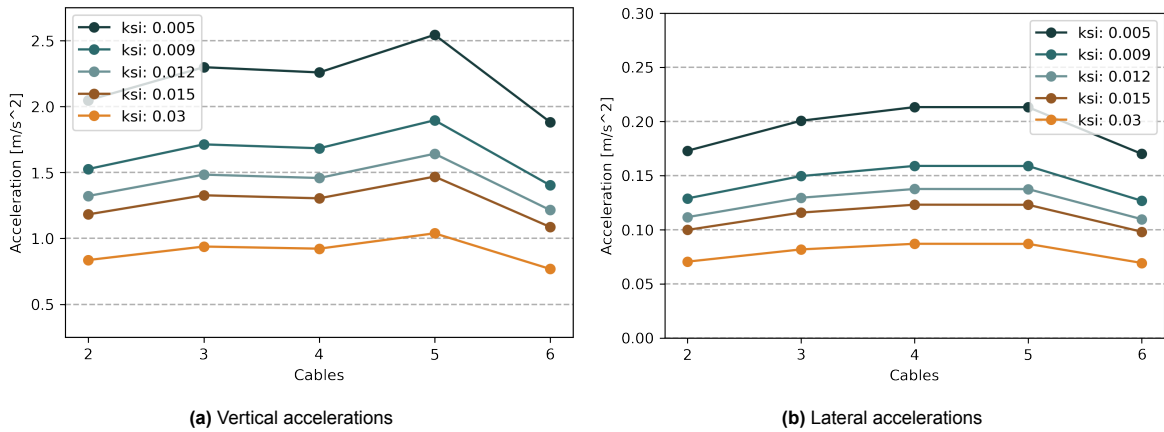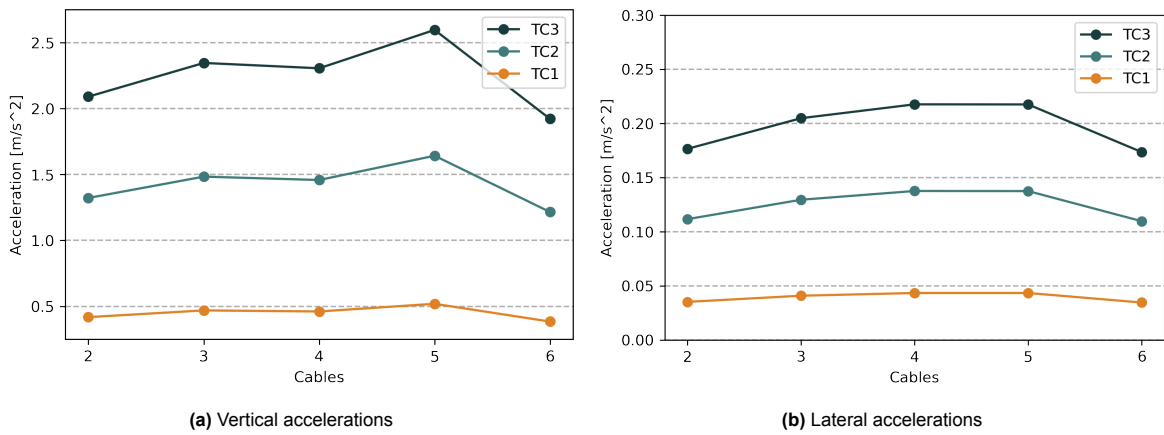**Figure E.15:** Effect of different traffic classes

# E.3. Part 3c - Stiffness main beam

In this verification study the effect of the connection stiffness between the main beam and the steel beam is investigated. In the optimisation runs, these were modelled as hinged connections. It is interesting to know to what extent the results change when adding rotational stiffness around the y- and z-axes, since this effects the stiffness of the deck. Note that stiff connections would also change the distribution of forces and the requirements for the connection, which was not taken into account because the models obtained in part 2a were used. Therefore the dimensions of the bridge change based on the studied parameters, but are not tailored to stiff connections.

**Pylon height**
In figure E.16 the effect of a different stiffness of the main beam connection on the results of the pylon height runs is shown. There is an effect on the vertical accelerations. However, as we have seen in other results, these are hard to interpret. There is no influence on the lateral accelerations. This leads to conclude that the connection stiffness does not play a role for lateral vibrations.
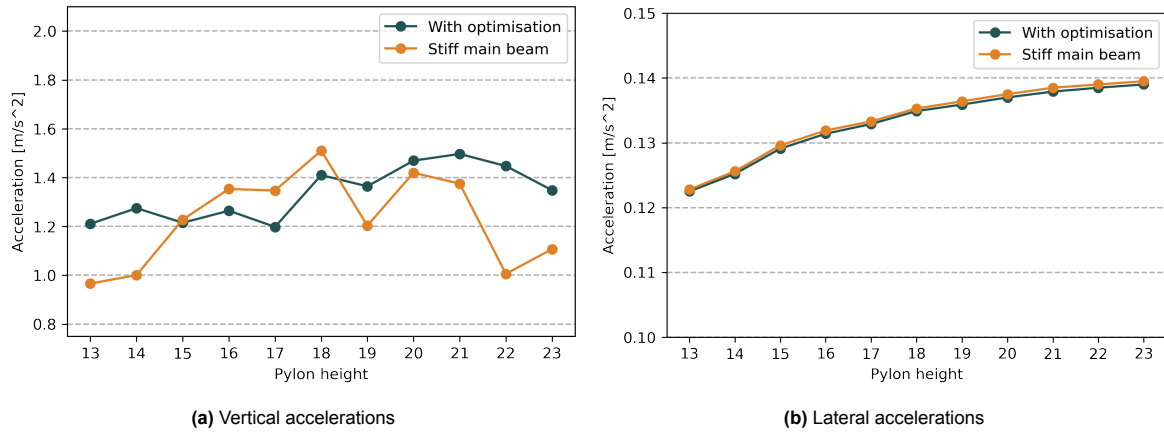
**(a)** Vertical accelerations      **(b)** Lateral accelerations

**Figure E.16:** Effect of omitting torsion modes out of the calculation of the maximum acceleration

**Pylon shape**

In figure E.17 the effect of a different stiffness of the main beam connection on the results of the pylon shape runs is shown. In the vertical accelerations it can be observed that the graph shows a clearer trend than when the connection between the main beam and the steel beam is stiff. This leads to conclude that with stiff connections, it is better for the accelerations to design the pylon in a V-shape. It goes together with a change in governing mode from vertical and torsion to pylon torsion. The stiffness does not effect the lateral vibrations.



**(a)** Vertical accelerations      **(b)** Lateral accelerations
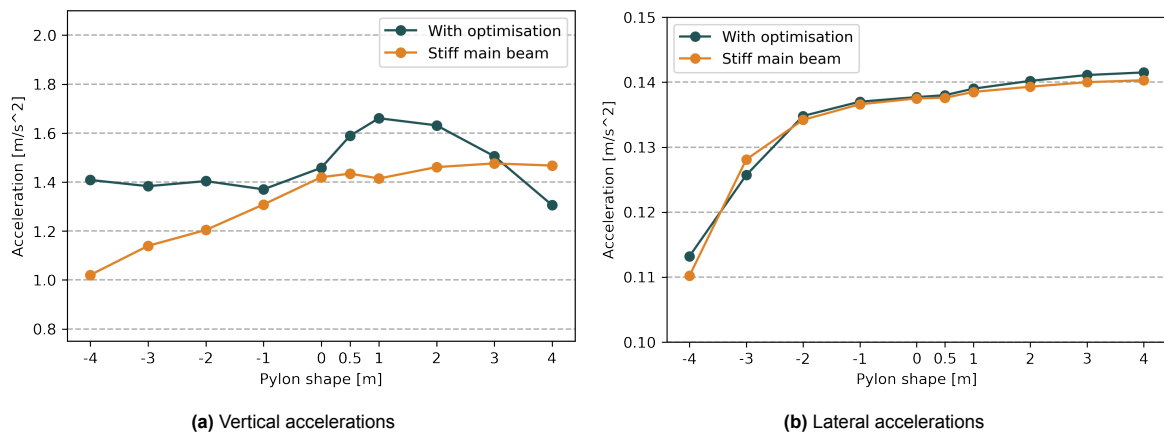
**Figure E.17:** Effect of omitting torsion modes out of the calculation of the maximum acceleration

**Amount of cables**

In figure E.18 the effect of a different stiffness of the main beam connection on the results of the cable runs is shown. As is the case with the other studied parameters, the stiffness of the connection between the main beam and the steel beam hardly effects the lateral accelerations. The maximum vertical accelerations are effected. Whereas with low stiffness, the accelerations increase when cables are added, with high stiffness this trend is opposite, although the results are somewhat ambiguous.

**(a)** Vertical accelerations    **(b)** Lateral accelerations

**Figure E.18:** Effect of omitting torsion modes out of the calculation of the maximum acceleration

# E.4. No torsion

Since treating torsion modes as vertical modes can be seen as conservative, in this sections the results of omitting the torsion modes out of the analysis of the parameter study is shown.

**Pylon height**
In figure E.19 the effect of excluding torsion modes in the pylon height runs from the analysis is shown. It straightens the line for the higher pylons, but it doesn't provide a clearer result in general.
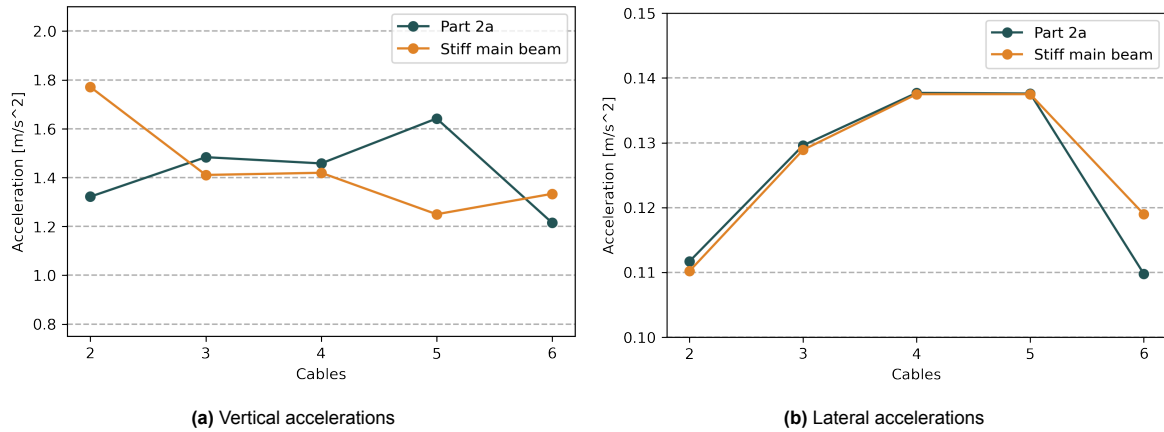


**Figure E.19:** Effect of omitting torsion modes out of the calculation of the maximum vertical acceleration

**Pylon shape**
In figure E.20 the effect of excluding torsion modes in the pylon shape runs from the analysis is shown. Whereas with torsion modes the graph shows the highest accelerations for positive pylon shapes, the results without torsion are lower for positive pylon shapes. Note the low value for pylon shape 0.5. This might be explained by the fact that this model mainly has torsion modes and no normal vertical modes in the critical range of frequencies because in this model the cables straight compared to the z-axis.
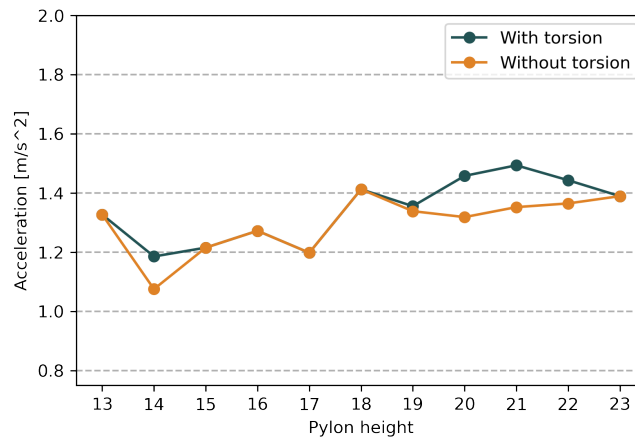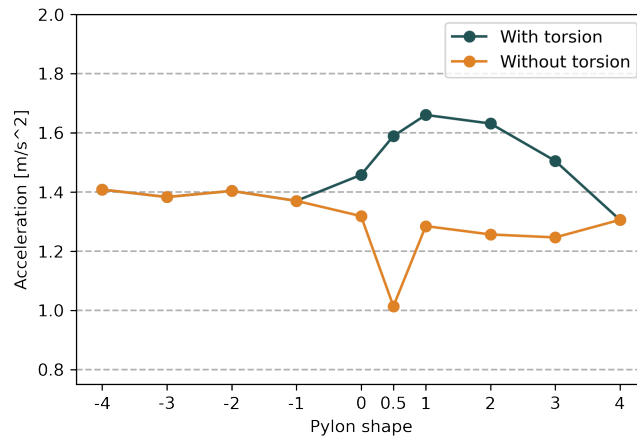
**Figure E.20:** Effect of omitting torsion modes out of the calculation of the maximum vertical acceleration

**Amount of cables**

In figure E.21 the effect of excluding torsion modes from the analysis in the cable runs is shown. Apart from the model with 2 cables, the accelerations decrease with more cables when torsion modes are excluded, whereas they increase with torsion modes. It might be that a lighter deck, which is the case in models with more cables, is more likely to have torsion modes in the range of critical frequencies.
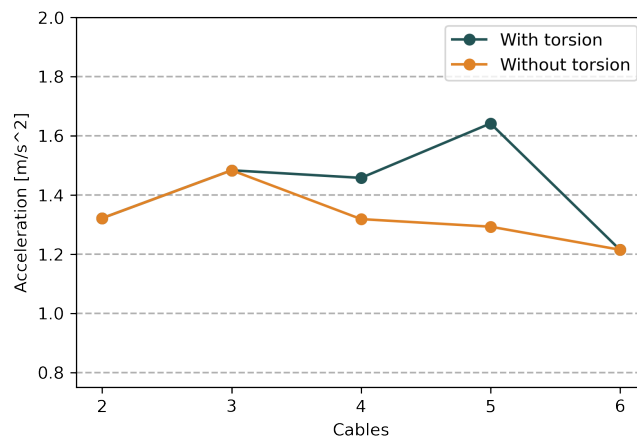


**Figure E.21:** Effect of omitting torsion modes out of the calculation of the maximum vertical acceleration

# Background optimisations

In this appendix additional information about the optimisations is given. It starts with a more detailed description of the dependent parameters and the fixed values. Afterwards the background information of the optimisations performed in part 2a and 3a of the parameter studies and in the optimisation study is given. These include for example optimisation settings, results per cycle and unity checks (UCs).

## F.1. Dependent parameters and fixed values

In table F.1, the way the dependent parameters depend on the other parameters is given. For example, the main beam width is always equal to the main beam height divided by 2. In table F.2, the fixed values are shown. For example, the main span is 110 m in all models.

| Dependent parameters | Depending on | How |
|---|---|---|
| Main beam width | Main beam height | Main beam width / 2 |
| Cross beam width | Cross beam height | Cross beam width / 2 |
| Steel beam dimension | Main beam height | Main beam height |
| Amount of bracings deck | Amount of cables | round (Span / 2 / cable number per side / deck width) * cable number per side * 4 |
| Amount of crossbeams deck | Amount of cables | round (Span / 2 / cable number per side / deck width - 1) * cable number per side * 4 |
| Amount of bracings pylon | Pylon height | (Pylon height - pylon topclear - pylon clearance) / pylon width + 1 |
| Amount of crossbeams pylon | Pylon height | (Pylon height - pylon topclear - pylon clearance) / pylon width + 1 |
| Pylon support beam height | Main beam height | Main beam height |
| Pylon support beam width | Main beam width | Main beam width |

**Table F.1:** Dependent parameters

| Fixed parameters | Value | Unit |
|---|---|---|
| Main span | 110 | m |
| Outside span | 55 | m |
| Deck width | 6.66 | m |
| Height of deck | 6.73 | m |
| Pylon offset | 1 | m |
| Opening deck - first pylon cross beam | 4 | m |
| Pylon topclear | 0.9 | m |
| Pylon cross beam height | 800 | mm |
| Pylon cross beam width | 400 | mm |
| Deck thickness | 195 | mm |
| Steel beam cantilever | 0.5 | m |
| Steel beam wall thickness | 15 | mm |
| Bracing deck diameter | 35 | mm |
| Bracing pylon diameter | 35 | mm |

**Table F.2:** Fixed values in the model

## F.2. Parameter study - Part 2a

This section section present results of the optimisation runs performed in part 2a of the parameter study that were thought to make the information presented in the main part of the report cluttered, but can provide useful insight in the results. Per studied parameter, the limits of the optimisation parameters, the results per cycle and the insightful UCs are given. The limits of the optimisation parameters show the minimum and maximum values the optimisation parameters can have in the optimisation. The results by cycle show the best objective function value found up till a certain point in the optimisation run. It gives insight in the way the solution is found. The UCs cast light on how well a model has been optimised and whether it behaves as expected.

The following UCs are expected to be governing and should therefore be very close to 1. Note that this is specific for the models and that these 'checks' are based on the outcome of the models itself. For the other UCs it goes that only the UCs that are deemed helpful in understanding the results are presented.

- Main beam: the combined bending around the y-axis and compression (My & -Fx)
- Cross beam: the combined bending around the y-axis and compression (My & -Fx)
- Pylon: stability (which includes axial compression and bending around the y-axis)
- Cables: global deflection

For part 2a of the parameter studies, the settings of the ABC algorithm have been used that are shown in table F.3. The motivation behind these number is presented in appendix G.

| Runs | Population number | Maximum evaluations | Limit |
|---|---|---|---|
| Pylon height | 35 | 1500 | 30 |
| Pylon shape | 35 | 1500 | 30 |
| Amount of cables | 35 | 1500 | 30 |

**Table F.3:** ABC settings

## Pylon height

**Optimisation settings**

The limits of the optimisation parameters were changed according to the expected outcome of the optimisation. The limits are shown in table F.4.

| | Pylon heights | Minimum | Maximum | Unit |
|---|---|---|---|---|
| Cable diameter | 13 - 17 | 60 | 100 | mm |
| | 18 - 20 | 50 | 80 | mm |
| | 21 - 23 | 40 | 70 | mm |
| Pylon dimension | all | 600 | 1150 | mm |
| Mainbeam height | all | 600 | 1000 | mm |
| Crossbeam height | all | 300 | 500 | mm |

**Table F.4:** Limits optimisation parameters

**Optimisation results**

Figure F.2 displays the objective function value after each cycle in the pylon height runs. At the first cycles, some results were higher than 4.5e7 kg. These have been adjusted to 4.5e7 to improve the readability of the graph. The graphs show that the objective functions were stable for a few cycles before the run stopped, indicating that it has found a good solution.

This is confirmed by the UCs, shown in figure F.2. In this figure, green stands for a value close to 1 and red for a value close to 0. The UCs that are expected to be governing are all almost 1. There is no tension in the cross beams, which is a good sign. In pylons of 17 meter and higher, there is some tension in the main beams. Inspecting the models, a small tension force of 27kN was found in the model of 17 m, while there was none in the model of 16 m. In models with higher pylons, the tension force the tension force increased slightly.
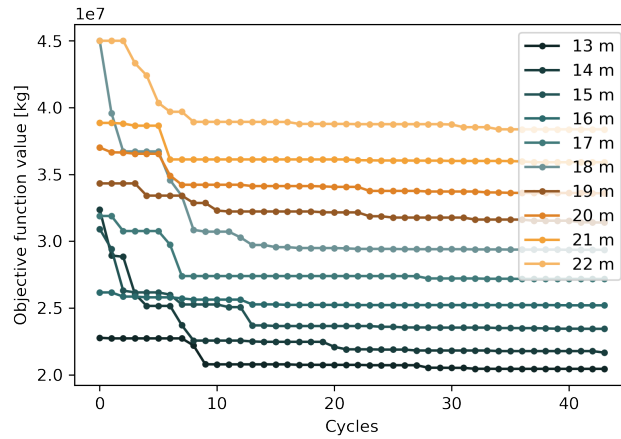
106

**Figure F.1:** Results by cycle - height runs

| Pylon height [m] | Main beam | | | | Cross beam | | | | Cables | Other | |
|---|---|---|---|---|---|---|---|---|---|---|---|
| | My & - Fx | My & + Fx | Mz & - Fx | Mz & + Fx | My & - Fx | My & + Fx | Mz & - Fx | Mz & + Fx | Fx | Stabitlity | Global deflection |
| 13 | 0.992 | nan | 0.770 | nan | 0.999 | nan | 0.706 | nan | 0.351 | 0.950 | 1.000 |
| 14 | 0.992 | nan | 0.763 | nan | 0.996 | nan | 0.704 | nan | 0.397 | 0.996 | 0.997 |
| 15 | 0.991 | nan | 0.756 | nan | 0.992 | nan | 0.701 | nan | 0.445 | 0.993 | 0.999 |
| 16 | 0.996 | nan | 0.755 | nan | 0.994 | nan | 0.703 | nan | 0.487 | 1.000 | 0.996 |
| 17 | 0.994 | 0.783 | 0.748 | 0.833 | 0.996 | nan | 0.705 | nan | 0.512 | 0.998 | 0.970 |
| 18 | 1.000 | 0.800 | 0.749 | 0.849 | 0.999 | nan | 0.706 | nan | 0.573 | 0.987 | 1.000 |
| 19 | 0.998 | 0.810 | 0.744 | 0.858 | 0.991 | nan | 0.701 | nan | 0.600 | 0.997 | 0.983 |
| 20 | 0.998 | 0.824 | 0.741 | 0.869 | 0.994 | nan | 0.703 | nan | 0.641 | 1.000 | 0.989 |
| 21 | 0.999 | 0.837 | 0.739 | 0.878 | 0.999 | nan | 0.707 | nan | 0.683 | 1.000 | 0.997 |
| 22 | 0.996 | 0.847 | 0.734 | 0.885 | 0.998 | nan | 0.706 | nan | 0.719 | 0.998 | 0.998 |
| 23 | 0.997 | 0.858 | 0.732 | 0.893 | 0.998 | nan | 0.706 | nan | 0.745 | 1.000 | 0.992 |

**Figure F.2:** Unity checks

## Pylon shape

### Optimisation settings

The limits of the optimisation parameters were changed according to the expected outcome of the optimisation. The limits are shown in table F.5.

| | Minimum | Maximum | Unit |
|---|---|---|---|
| Cable diameter | 50 | 80 | mm |
| Pylon dimension | 600 | 1150 | mm |
| Main beam height | 600 | 1000 | mm |
| Cross beam height | 300 | 500 | mm |

**Table F.5:** Limits optimisation parameters

### Optimisation results

In figure F.3 the objective function value after each cycle is shown. As in the results of the pylon heights, some of the results of the first cycles have been adjusted to improve the readability of the graph. The graphs show that the objective functions were stable for a few cycles before the run stopped, indicating that it has found a good solution.

This is backed up by the UCs, shown in figure F.4. The UCs that are expected to be governing are all almost 1. The exceptions are the models with pylon shape -3 and -4. In these models the combined bending and tension is governing for the cross beams. This is because in these models a very small tension force occurs in some of the cross beams, which becomes governing for the design. Since the dimensions of the cross beams have a very limited effect on the maximum accelerations, the error due to this error in the model is negligible.
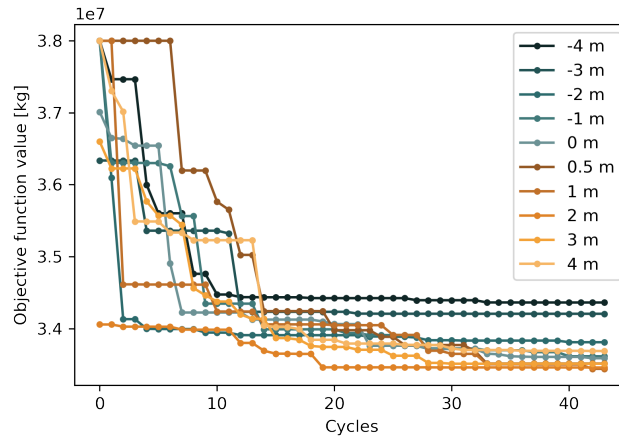
107

**Figure F.3:** Results by cycle - shape runs

| Pylon shape [m] | Main beam My & - Fx | My & + Fx | Mz & - Fx | Mz & + Fx | Cross beam My & - Fx | My & + Fx | Mz & - Fx | Mz & + Fx | Cables Fx | Other Stabitlity | Global deflection |
|---|---|---|---|---|---|---|---|---|---|---|---|
| -4 | 1.000 | 0.829 | 0.741 | 0.875 | 0.786 | 0.995 | 0.556 | 0.855 | 0.633 | 1.000 | 0.988 |
| -3 | 0.996 | 0.822 | 0.738 | 0.868 | 0.786 | 0.995 | 0.556 | 0.855 | 0.645 | 0.992 | 1.000 |
| -2 | 1.000 | 0.825 | 0.742 | 0.873 | 0.998 | nan | 0.706 | nan | 0.645 | 0.999 | 0.997 |
| -1 | 1.000 | 0.825 | 0.742 | 0.871 | 0.997 | nan | 0.705 | nan | 0.648 | 0.999 | 0.999 |
| 0 | 0.998 | 0.824 | 0.741 | 0.869 | 0.994 | nan | 0.703 | nan | 0.641 | 1.000 | 0.989 |
| 1 | 0.998 | 0.824 | 0.741 | 0.868 | 0.994 | nan | 0.703 | nan | 0.650 | 1.000 | 1.000 |
| 2 | 0.999 | 0.825 | 0.742 | 0.868 | 0.999 | nan | 0.707 | nan | 0.650 | 0.999 | 1.000 |
| 3 | 1.000 | 0.825 | 0.743 | 0.868 | 0.996 | nan | 0.704 | nan | 0.649 | 1.000 | 0.999 |
| 4 | 1.000 | 0.826 | 0.742 | 0.868 | 0.999 | nan | 0.707 | nan | 0.637 | 0.999 | 0.985 |

**Figure F.4:** Unity checks

# Amount of cables

## Optimisation settings
The limits of the optimisation parameters were changed according to the expected outcome of the optimisation. They are shown in table F.6.

| | Amount of cables | Minimum | Maximum | Unit |
|---|---|---|---|---|
| Cable diameter | all | 40 | 80 | mm |
| Pylon dimension | all | 600 | 1150 | mm |
| Main beam height | 2 | 600 | 2000 | mm |
| | 3 - 5 | 600 | 1000 | mm |
| | 6 | 500 | 1000 | mm |
| Cross beam height | all | 300 | 500 | mm |

**Table F.6:** Limits optimisation parameters

## Optimisation results
In figure F.5 the objective function value after each cycle is shown. At the first cycles, some results were higher than 5.0e7 kg. These have been adjusted to 5.0e7 to improve the readability of the graph. The graphs show that the objective functions were stable for a few cycles before the run stopped, indicating that it has found a good solution.

Most of the UCs that are expected to be governing are almost 1. The exception is in the models with 5 and 6 cables. In the model with 5 cables, the UC for the main beam is 0.9. This could indicate the model could be optimised more. In the model with 6 cables, the combined lateral bending and tension are governing the dimension of the main beam. This explains the higher dimensions in this model. Note that in the model with 2 cables, there is no tension force in the main beam. This is explained by the fact that also beams in the middle part of the main span have a substantial compression force. The crossbeams are all in compression which is a sign they behave as expected.
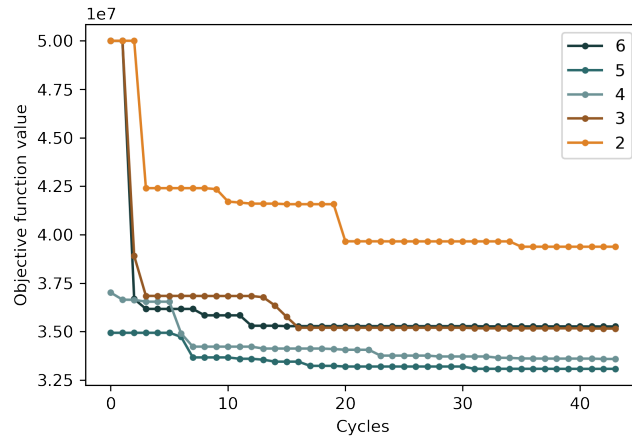
**Figure F.5:** Results by cycle - cable runs

| Cables | Main beam | | | | Cross beam | | | | Cables | Other | |
|---|---|---|---|---|---|---|---|---|---|---|---|
| | My & - Fx | My & + Fx | Mz & - Fx | Mz & + Fx | My & - Fx | My & + Fx | Mz & - Fx | Mz & + Fx | Fx | Stabitlity | Global deflection |
| 2 | 1.00 | nan | 0.71 | nan | 0.97 | nan | 0.69 | nan | 0.52 | 0.98 | 1.00 |
| 3 | 1.00 | 0.62 | 0.72 | 0.65 | 1.00 | nan | 0.71 | nan | 0.61 | 1.00 | 1.00 |
| 4 | 1.00 | 0.82 | 0.74 | 0.87 | 0.99 | nan | 0.70 | nan | 0.64 | 1.00 | 0.99 |
| 5 | 0.90 | 0.70 | 0.69 | 0.75 | 1.00 | nan | 0.70 | nan | 0.67 | 1.00 | 1.00 |
| 6 | 0.33 | 0.79 | 0.25 | 1.00 | 1.00 | nan | 0.71 | nan | 0.74 | 1.00 | 1.00 |

**Figure F.6:** Unity checks

## F.3. Parameter study - Part 3a

Table F.7 shows the settings of the ABC algorithm used for this part of the parameter study.

| Runs | Population number | Maximum evaluations | Limit |
|---|---|---|---|
| Pylon height | 38 | 1700 | 30 |
| Pylon shape | 38 | 1700 | 30 |
| Amount of cables | 38 | 1700 | 30 |

**Table F.7:** ABC settings

### Pylon height

**Optimisation settings**

Table F.8 shows that limits of the optimisation parameters. They were the same in all pylon height runs of this part of the parameter study.

| | Minimum | Maximum | Unit |
|---|---|---|---|
| Cable diameter | 40 | 110 | mm |
| Pylon dimension | 400 | 1000 | mm |
| Main beam height | 500 | 1000 | mm |
| Cross beam height | 300 | 500 | mm |
| Pylon shape | -3 | 3 | m |
| Amount of cables | 3 | 5 | - |

**Table F.8:** Limits optimisation parameters

**Optimisation results**

Figure F.7 shows the results by cycle of the runs with different pylon heights.
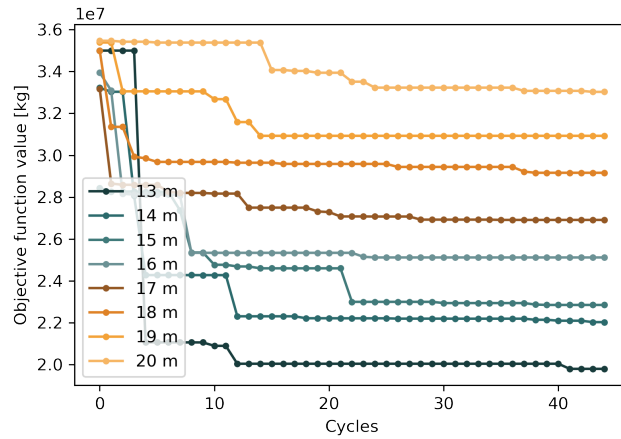
**Figure F.7:** Results by cycle - height runs

## Pylon shape

### Optimisation settings

Table F.9 shows that limits of the optimisation parameters. They were the same in all pylon shape runs of this part of the parameter study.

|  | Minimum | Maximum | Unit |
|---|---|---|---|
| Cable diameter | 40 | 110 | mm |
| Pylon dimension | 400 | 1000 | mm |
| Main beam height | 600 | 1000 | mm |
| Cross beam height | 300 | 500 | mm |
| Amount of cables | 3 | 5 | - |
| Pylon height | 11 | 17 | m |

**Table F.9:** Limits optimisation parameters

### Optimisation results

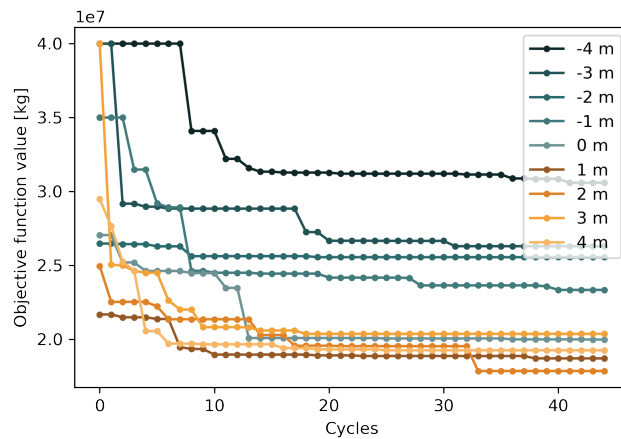Figure F.8 shows the results by cycle of the runs with different pylon shapes.



**Figure F.8:** Results by cycle - shape runs

## Amount of cables

**Optimisation settings**

The limits of the optimisation parameters were changed according to the expected outcome of the optimisation. They are shown in table F.10.

|  | Amount of cables | Minimum | Maximum | Unit |
|---|---|---|---|---|
| Cable diameter | all | 40 | 110 | mm |
| Pylon dimension | all | 400 | 1000 | mm |
| Main beam height | 2 | 500 | 1200 | mm |
|  | 3 - 6 | 500 | 1000 | mm |
| Crossbeam height | all | 300 | 500 | mm |
| Pylon shape | all | -3 | 3 | m |
| Pylon height | all | 11 | 17 | m |

**Table F.10:** Limits optimisation parameters

**Optimisation results**

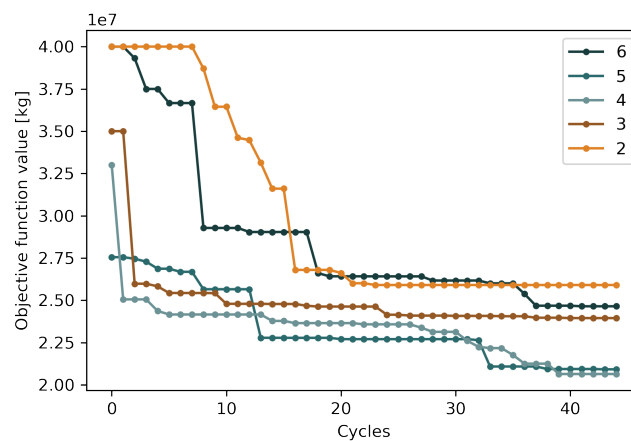Figure F.9 shows the results by cycle of the runs with different amounts of cables.



**Figure F.9:** Results by cycle - cable runs

## F.4. Optimisation study taking into account dynamic behaviour

**Optimisation settings**

The optimisation settings are shown in table F.11. Since the final run had more constraints, the maximum amount of evaluations was somewhat higher than the basic run. The parameter limits of both runs are shown in table F.12.

|  | **Population size** | **Maximum number of evaluations** | **Limit** |
|---|---|---|---|
| Basic run | 40 | 6500 | 35 |
| Final run | 40 | 8000 | 35 |

**Table F.11:** Optimisation settings

|  | Run | Minimum | Maximum | Unit |
|---|---|---|---|---|
| Cable diameter | Basic | 50 | 120 | mm |
|  | Final | 70 | 120 | mm |
| Pylon dimension | all | 5000 | 1000 | mm |
| Main beam height | all | 600 | 1000 | mm |
| Cross beam height | all | 300 | 500 | mm |
| Amount of cables | all | 3 | 5 | - |
| Pylon height | all | 11 | 17 | m |
| Pylon shape | all | -3 | 3 | m |

**Table F.12:** Limits optimisation parameters

## Results by cycle

Figure F.10 shows the results by cycle for the two optimisation runs. It shows that the increased number of maximum evaluations helped finding a better solution.
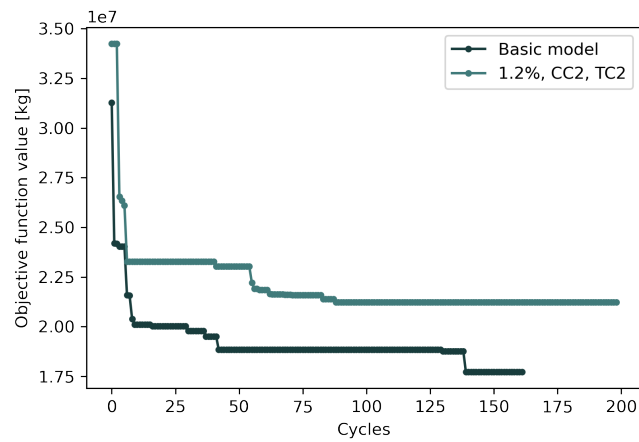


**Figure F.10:** Results by cycle

# G

# Initial runs and verifications

In this appendix the initial runs and some sensitivity studies and investigations about the influence of certain assumptions on the model are presented.

## G.1. Initial runs parameter study

As explained in section 4, the Artificial Bee Colony (ABC) optimisation algorithm needs a couple of preset values, namely the population size, the maximum number of evaluations and a limit. Next to that, limit values for each design parameter (chapter 6) need to be chosen. To find good presets for the optimisation algorithm and to catch potential flaws in the model, a set of initial runs was carried out. A *good* setup in this thesis is defined as a setup that yields an optimised solution in a reasonable amount of time.

12 initial runs were carried out; 4 models with 3 cables, 4 models with 4 cables and 4 models with 5 cables. The lower and upper limits of the optimisation parameters of these runs are shown in table G.1. These limits were based on some tests to ensure reasonable UCs could be obtained.

| Design parameters | Min | Max | Unit |
|---|---|---|---|
| Cable diameter | 30 | 80 | mm |
| Pylon dimension | 800 | 1200 | mm |
| Main beam height | 600 | 1000 | mm |
| Cross beam height | 350 | 500 | mm |

**Table G.1:** Design parameters initial runs

The presets of the ABC algorithm are shown in table G.2. Slight variations in the population size and limit are made, while the maximum number of evaluation increases in each set of runs. The increase in time is mainly correlated to the increase in maximum evaluation. The differences in time with the same presets are caused by two factors. The first is the total amount of GSA models made and analysed in a run. This number varies because only design variants that are potentially better than ones previously found are modelled and analysed. The second is the amount of activity on the laptop, while running the models. The more other programs are running, the slower the run. The last column shows whether or not shear deformation was taken into account. This was added once noted that this was not taken into account by default in GSA.

In figures G.1, G.2 and G.3, the progression of the objective function per cycle is shown for the runs with 3, 4, and 5 cables. A cycle is an iteration of the ABC algorithm, with an amount of evaluations that is equal to the population size. In some cases, the results of the first (few) cycle(s) were a factor 100 higher than the end result, which means the solver has not found a solution with UCs below 1. To ensure the graph is still readable, these results have been changed to a lower number. The graphs show that in most cases a higher maximum number of evaluation gives a better end result. One exception is run 26_1, that according to this pattern should have resulted in the lowest objective function value. Another exception is run 24_1, that has a higher end-result than the run with the smallest amount of evaluations. This might be due to the fact that the pylon opening parameter was increased from 3.3 to 4 meter and that shear deformation was introduced.

| Amount of cables | Code | Population size | Maximum number of evaluation | Limit | Time | Shear deformation |
|---|---|---|---|---|---|---|
| 3 | 22_1 | 30 | 600 | 40 | 02:15 | no |
| 4 | 22_2 | 30 | 600 | 40 | 02:25 | no |
| 5 | 22_3 | 30 | 600 | 40 | 03:30 | no |
| 3 | 23_2 | 35 | 700 | 40 | 03:33 | no |
| 4 | 23_1 | 35 | 700 | 40 | 05:44 | no |
| 5 | 22_4 | 35 | 700 | 40 | 03:30 | no |
| 3 | 25_1 | 35 | 2000 | 30 | 07:30 | yes |
| 4 | 24_1 | 35 | 2000 | 30 | 05:33 | yes |
| 5 | 23_3 | 35 | 2000 | 30 | 07:17 | yes |
| 3 | 26_1 | 35 | 2500 | 30 | 07:24 | yes |
| 4 | 27_1 | 35 | 2500 | 30 | 07:35 | yes |
| 5 | 28_1 | 35 | 2500 | 30 | 07:09 | yes |

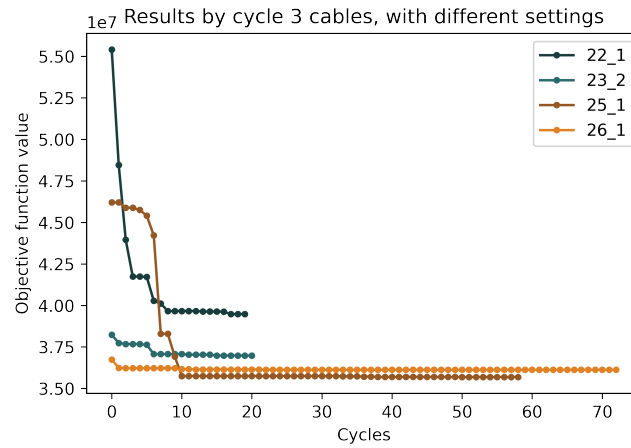**Table G.2:** ABC settings initial runs



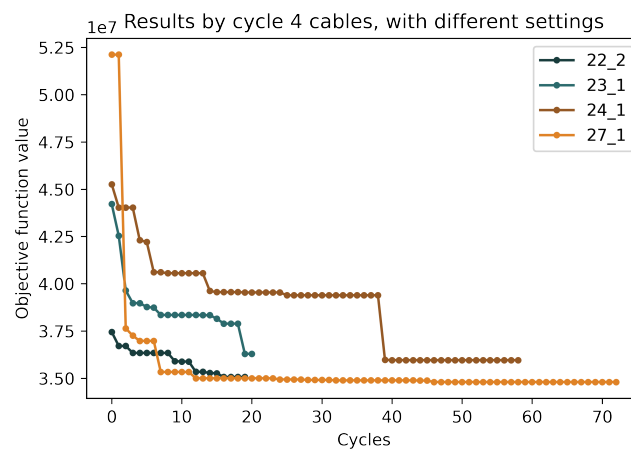**Figure G.1:** 3 Cables, different settings



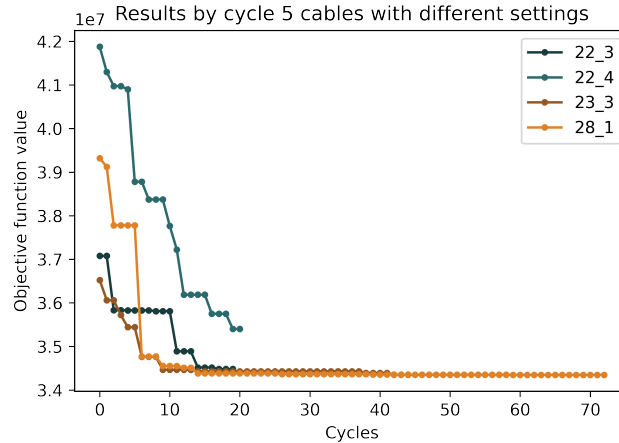**Figure G.2:** 4 Cables, different settings

**Figure G.3:** 5 Cables, different settings

From these runs, several conclusions were drawn with regards to the settings of the ABC. A result was accepted when there was no improvement for at least 10 cycles. Moreover, some runs have been done twice to check if it got the same result. Also, the parameter results of the runs were inspected to check if they behave as expected. For the parameter studies, a population size of 35, a limit of 30 and a maximum number of evaluation of 1500 were selected. Based on the initial runs, these settings were expected to give reasonable results. In the parameter studies with variable optimisation parameters and the final optimisations, the maximum number of evaluations was increased to 1700 and 2000 because the amount of optimisation parameters was higher (6 and 7 respectively).

## G.2. Model improvements

After the initial runs, the following changes have been made. Some of them are explained in more detail in the sections below.

- The support condition of the pylons was changed from clamped to hinged, because it was found that all existing bridges with timber pylons have hinged supports.
- Global deflection was added as a static check.
- Some attempts have been made to reduce the computation time.
- The limits of the variables were changed to a smaller range so that good results could be found more quickly.
- The distance between the deck and the first crossbeam of the pylon was increased, because with the distance of these runs it would be impractically small.
- The wind load in x-direction was included.

**Pylon support**
In the initial runs the pylons were clamped at the bottom. This was a mistake since it is more realistic to model hinged support conditions for timber pylons. Therefore, the support condition was changed to a hinge and the influence on the model was investigated. The unity check for pylon buckling increased by 22%. This is the result of decreased moments and an increased buckling length (from 0.7 times the length to the full length, see figure G.4. The change in moment lines is shown in figure G.5. The other change in the behaviour of the bridge was the mode shapes. The frequency of the first mode (a lateral mode) decreased by 31% and new types of pylon modes occurred in the frequency range of pedestrian loading, an example of which is shown in figure G.6. Pylon modes that curved around the y-axis were found in models with clamped support conditions too, but with a significantly higher natural frequency.
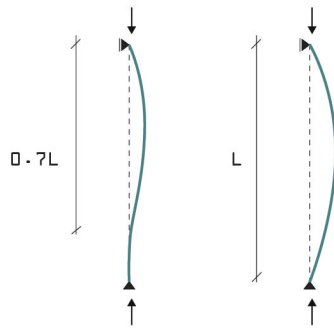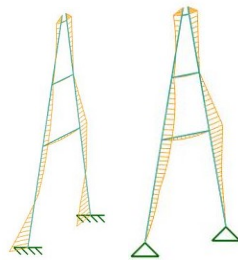
**Figure G.4:** Buckling length



**Figure G.5:** Moment lines under self-weight with clamped and hinged pylon supports
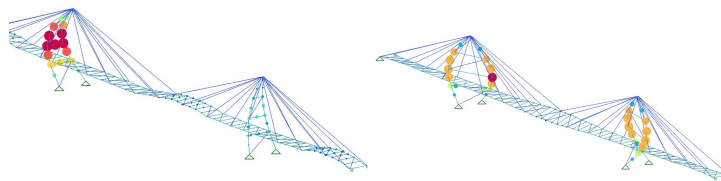


**Figure G.6:** Pylon vibratin modes

**Deflection**

In the initial runs, SLS requirements for deflection were not taken into account. When checking if this was an acceptable simplification, it turned out it was not because the maximum deflections in the optimised models were around 1 meter. There are no strict requirements about the maximum deflection, however 1 meter was considered outside reasonable limits. The EN1995-2-2 recommendation for maximum deflection is $1/200$ times the span, this would imply a maximum deflection of 550 mm. In the design of the DSB the requirement for maximum deflection was based on the *profielvrije ruimte*, the space under the bridge that should be free for ships to pass through during normal use. This implied a maximum deflection of 500 mm. Since in the design of this thesis, a camber is not taken into account, it was decided to commit to the maximum deflection recommended by the EN1995.

**Computation time reduction**

After the initial, runs some efforts have been made to decrease the computation time. The first is the way information about the model is handed over from GSA to the python script. Initially, a *.gwa* file was made for each model, containing all information about the model, such as the geometry and the materials. Since only the information about the nodes and the elements were needed for processing the results, some tests were done to investigate if the run time would decrease when only *.csv* files with information about the nodes and the elements were saved. On a total of around 30 seconds, this saved approximately 6 seconds.

The second way to reduce the computation time was to save less results (displacements, stresses) per element. Initially, 5 values per element were given; the values at the end, and 3 values at 25%, 50%

and 75% of the element length. Since the middle values hardly differed from the values at the ends, they were excluded from the output files. This resulted in approximately a 1 second improvement.

Finally, the amount of combination cases was reduced from 12 to 5. To find out which combinations could be excluded, the governing combinations of some optimised models were collected. The studies of all heights, shapes and amount of cables were taken into account to ensure the right decision could be made. From this, 6 governing cases were extracted, namely C2, C5, C6, C8 and C9. This resulted in a time saving of approximately 2 seconds.

## G.3. Verifications

**Element size**

As explained in chapter 5, the following aspects need to be taken into account when choosing the element size for beam elements. For bar elements this is not relevant since they always have the length of the member. First of all the accuracy of the results; halving the element size should not lead to significant changes in the results. Secondly the computational cost; both the time for running the analysis and saving the outputs increase exponentially when increasing the amount of elements. Thirdly, for finding reliable results in a modal analysis it is important to have approximately 10 nodes in each wave of a mode shape. And finally it is common practice in bridge modelling to have one element between each point where members meet.

A balance needed to be found between the first two and the last two considerations. As a starting point, the element size was set to 3 metres, which is the maximum distance between two crossbeams and therefore the maximum possible element size of the main girders. The highest amount of mode shape waves in a mode with a frequency relevant for human-induced vibrations, is around 3. This means that there are approximately 35 nodes per belly, which fulfills the requirement. Next, models with element size of 2 metres and 1 metre were run. The element size of the cross beam and the steel beams was kept constant at 0.5 times the width of the deck. The unity checks (UCs) and maximum accelerations are compared in figure G.7 and the run time is compared in figure G.8. It can be seen that the UCs do not change, but that the time for running the model increases when decreasing the target element size, see figure G.8. Therefore it was decided to take an element size of 3 metres for the main girders and the pylons.
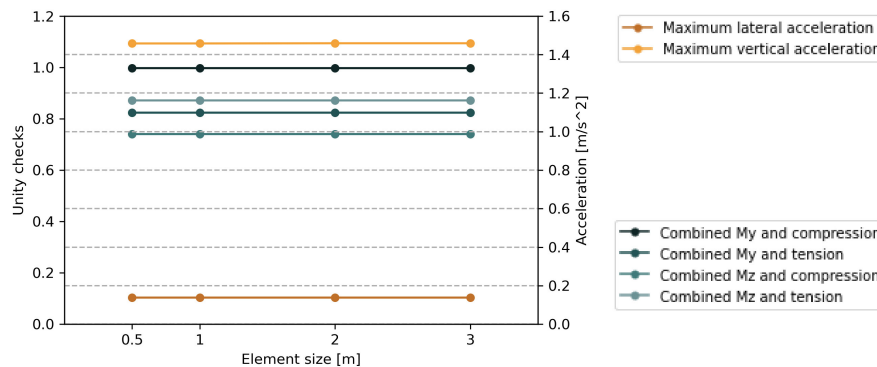


**Figure G.7:** UCs of the main beam and the maximum accelerations for different element sizes
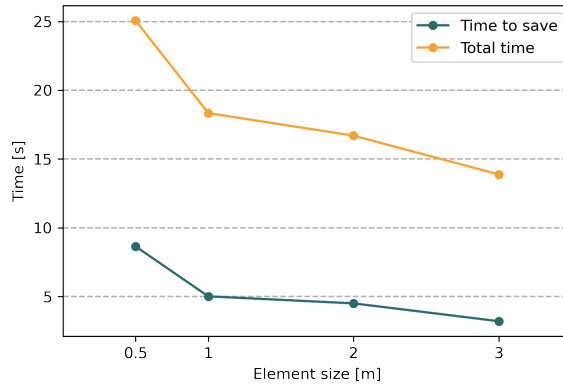
**Figure G.8:** Influence of the element size on the time to save results and the total time to create and analyse a model

**Lateral stiffness**

Since according to Arup experience, lateral modes are often governing the dynamic behaviour, it was suggested to make a design without lateral modes in the range that can be excited under pedestrian loading, namely 0.5 to 1.2 Hz. With the chosen deck design, the diameter of the bracing in the deck was deemed to have the biggest influence on the lateral stiffness of the deck, associated with the lateral modes. Therefore it was tested whether the bracing diameter could be increased until the lowest lateral mode had a natural frequency of more than 1.2 Hz. To this end, a design variant with 4 cables, a pylon height of 20 m and a pylon shape of 3 meters was taken and the bracing diameter was varied from 35 mm up til 115 mm. The results are shown in figure G.9. The figure shows that in this model, the goal of having no lateral modes in the range between 0.5 and 1.2 Hz can be met when the bracing diameter is 105 mm or higher. Since this is a very unrealistic dimension for a bracing rod in a pedestrian bridge, it was concluded that for this type of deck the goal could not be met.
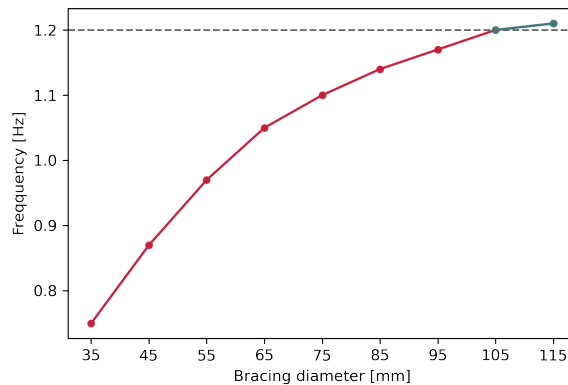


**Figure G.9:** Influence of the bracing diameter on the lateral stiffness

# G.4. Initial runs optimisation study

This section provides information about the initial runs of the optimisation study. A set of initial runs was carried out in the optimisation study, before reliable results were found. The initial runs failed to obtain reliable results, but helped understanding the problem and finding good settings for the runs used in the results. An optimised model in which dynamic behaviour was not taken into account was compared to models in which dynamic behaviour was included in the optimisation process.

**Optimisation settings**

The runs were done with different combinations of damping values, traffic classes and comfort classes. These are shown in tables G.3, G.4 and G.5.

| Damping value [%] | Traffic class | Comfort class | |
| --- | --- | --- | --- |
| | | Set 1 | Set 2 |
| 1.7 | 2 | 2 | 3 |
| 1.5 | 2 | 2 | 3 |
| 1.2 | 2 | 2 | 3 |
| 0.9 | 2 | 2 | 3 |
| 0.7 | 2 | 2 | 3 |

**Table G.3:** Runs with different damping values

| Traffic class | Comfort class | Damping value [%] |
| --- | --- | --- |
| 1 | 2 | 1.7 |
| 2 | 2 | 1.7 |
| 3 | 2 | 1.7 |

**Table G.4:** Runs with different traffic classes

| Comfort class | Damping value [%] | Traffic class |
| --- | --- | --- |
| 1 | 1.2 | 2 |
| 2 | 1.2 | 2 |
| 3 | 1.2 | 2 |

**Table G.5:** Runs with different comfort classes

The optimisation settings of the ABC algorithm are shown in table G.6.

| | Population size | Maximum number of evaluations | Limit |
| --- | --- | --- | --- |
| Basic run | 39 | 2000 | 30 |
| Different damping values (CC2) | 39 | 2000 | 30 |
| Different damping values (CC3) | 39 | 2000 | 30 |
| Different traffic classes | 39 | 2000 | 30 |
| Different comfort classes | 40 | 2200 | 30 |

**Table G.6:** Optimisation settings

**Results by cycle**
Figure G.10 shows the results by cycle for runs with different damping values. Note that the results of the first cycles have been adjusted to improve the readability of the graphs. The runs with comfort class 2 are shown left, those with comfort class 3 are shown on the right side. The figures indicate that the results might not be sufficiently optimised since not all lines are stable before the run ends and since the final don't follow the expected trend based on the amount of damping.
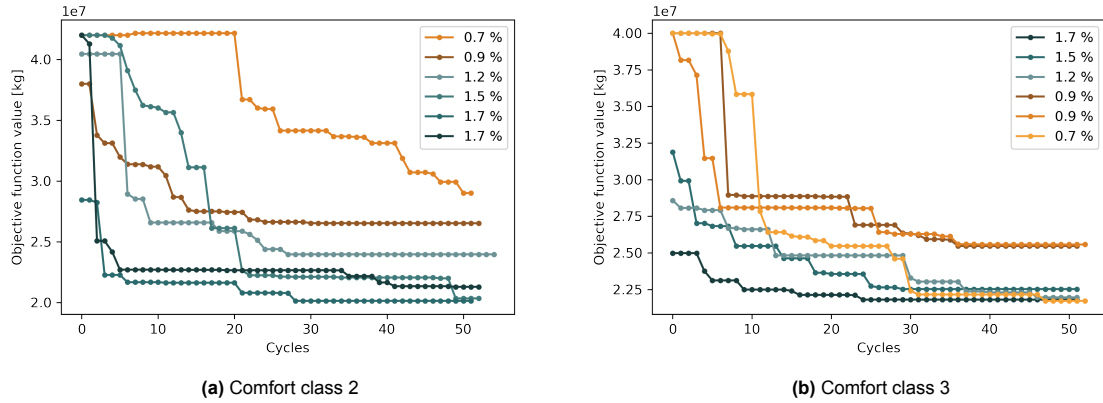
**(a)** Comfort class 2

**(b)** Comfort class 3

**Figure G.10:** Results by cycle - Different damping values

Figure G.11 shows the results by cycle for runs with different traffic classes (1, 2, and 3) and different comfort classes (2 and 3). The attempt to find a model that meets the limits of comfort class 1 was made too, but failed with the set optimisation settings and limits. In figure G.11b, a run where dynamic behaviour was not taken into account is shown in red. The fact that the final result is higher than a run with constraints based on dynamic behaviour, indicates that the run has not found a sufficiently optimised solution.



**(a)** Different traffic classes

**(b)** Different comfort classes
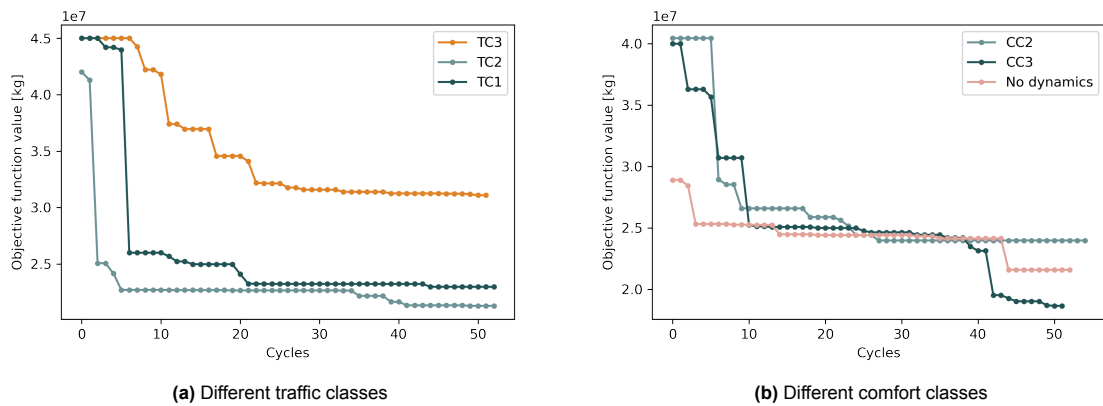
**Figure G.11:** Results by cycle

**Parameter results**

The figures below show parameter values of the different runs. The colours are added to help observing which values are highest and lowest. Red indicates the highest value of a column, green the lowest. The parameters do not follow a clear pattern.

| Comfort class | Traffic class | Damping | Result | Cable diameter [mm] | Pylon dimension [mm] | Main beam height [mm] | Cross beam height [mm] | Cable number | Pylon height [m] | Pylon shape [m] |
|---|---|---|---|---|---|---|---|---|---|---|
| n.a. | n.a. | n.a. | 21572074 | 84 | 671 | 748 | 401 | 4 | 13.9 | 1.0 |

**Figure G.12:** Result final optimisations - Basic run without taking into account dynamic behaviour

120

| Damping value | Comfort class | Traffic class | Result | Cable diameter [mm] | Pylon dimension [mm] | Main beam height [mm] | Cross beam height [mm] | Cable number | Pylon height [m] | Pylon shape [m] |
|---|---|---|---|---|---|---|---|---|---|---|
| 0.017 | 2 | 2 | 19070713 | 95 | 650 | 725 | 377 | 5 | 12.5 | 1.2 |
| 0.017 | 2 | 2 | 20144427 | 87 | 660 | 712 | 440 | 5 | 13.3 | 0.8 |
| 0.017 | 2 | 2 | 21300549 | 85 | 670 | 766 | 399 | 5 | 13.5 | 0.2 |
| 0.015 | 2 | 2 | 20347493 | 107 | 670 | 738 | 408 | 5 | 12.6 | 1.8 |
| 0.012 | 2 | 2 | 23973076 | 100 | 702 | 661 | 407 | 5 | 15.3 | -0.3 |
| 0.009 | 2 | 2 | 26532589 | 120 | 702 | 1031 | 401 | 4 | 14.1 | 2.0 |
| 0.007 | 2 | 2 | 29008762 | 107 | 743 | 924 | 379 | 5 | 15.3 | -1.3 |

**Figure G.13:** Result final optimisations - Different damping values

| Damping value | Comfort class | Traffic class | Result | Cable diameter [mm] | Pylon dimension [mm] | Main beam height [mm] | Cross beam height [mm] | Cable number | Pylon height [m] | Pylon shape [m] |
|---|---|---|---|---|---|---|---|---|---|---|
| 0.017 | 3 | 2 | 21803295 | 81 | 672 | 806 | 379 | 5 | 13.5 | 1.4 |
| 0.015 | 3 | 2 | 22522534 | 82 | 673 | 895 | 405 | 5 | 13.2 | 2.6 |
| 0.012 | 3 | 2 | 18461604 | 111 | 640 | 856 | 400 | 4 | 11.0 | -0.3 |
| 0.009 | 3 | 2 | 25461604 | 104 | 754 | 803 | 416 | 5 | 12.6 | -1.1 |
| 0.009 | 3 | 2 | 25566499 | 69 | 708 | 735 | 400 | 4 | 16.0 | 0.7 |
| 0.007 | 3 | 2 | 21717387 | 97 | 698 | 766 | 407 | 4 | 12.3 | 0.8 |

**Figure G.14:** Result final optimisations - Different damping values

| Traffic class | Damping value | Comfort class | Result | Cable diameter [mm] | Pylon dimension [mm] | Main beam height [mm] | Cross beam height [mm] | Cable number | Pylon height [m] | Pylon shape [m] |
|---|---|---|---|---|---|---|---|---|---|---|
| 1 | 0.017 | 2 | 22986922 | 78 | 688 | 744 | 402 | 4 | 14.4 | -0.5 |
| 1 | 0.017 | 2 | 19817965 | 113 | 673 | 825 | 376 | 5 | 11.0 | 0.5 |
| 2 | 0.017 | 2 | 20144427 | 87 | 660 | 712 | 440 | 5 | 13.3 | 0.8 |
| 3 | 0.017 | 2 | 31096523 | 99 | 731 | 1087 | 376 | 5 | 16.2 | -2.1 |

**Figure G.15:** Result final optimisations - Different Traffic Classes

| Comfort class | Traffic class | Damping | Result | Cable diameter [mm] | Pylon dimension [mm] | Main beam height [mm] | Cross beam height [mm] | Cable number | Pylon height [m] | Pylon shape [m] |
|---|---|---|---|---|---|---|---|---|---|---|
| 1 | 2 | 0.012 | Failed | Failed | Failed | Failed | Failed | Failed | Failed | Failed |
| 2 | 2 | 0.012 | 23973076 | 100 | 702 | 661 | 407 | 5 | 15.3 | -0.3 |
| 3 | 2 | 0.012 | 18641604 | 111 | 640 | 856 | 400 | 4 | 11.0 | -0.3 |

**Figure G.16:** Result final optimisations - Different Comfort Classes